Reliability Enhancements for Real-Time Operations of Electric Power Systems

by

Xingpeng Li

A Dissertation Presented in Partial Fulfillment
of the Requirements for the Degree
Doctor of Philosophy

Approved November 2017 by the
Graduate Supervisory Committee:

Kory Hedman, Chair
Gerald Heydt
Vijay Vittal
Jiangchao Qin

Arizona State University
December 2017

ABSTRACT

The flexibility in power system networks is not fully modeled in existing real-time contingency analysis (RTCA) and real-time security-constrained economic dispatch (RT SCED) applications. Thus, corrective transmission switching (CTS) is proposed in this dissertation to enable RTCA and RT SCED to take advantage of the flexibility in the transmission system in a practical way.

RTCA is first conducted to identify critical contingencies that may cause violations. Then, for each critical contingency, CTS is performed to determine the beneficial switching actions that can reduce post-contingency violations. To reduce computational burden, fast heuristic algorithms are proposed to generate candidate switching lists. Numerical simulations performed on three large-scale realistic power systems (TVA, ERCOT, and PJM) demonstrate that CTS can significantly reduce post-contingency violations. Parallel computing can further reduce the solution time.

RT SCED is to eliminate the actual overloads and potential post-contingency overloads identified by RTCA. Procedure-A, which is consistent with existing industry practices, is proposed to connect RTCA and RT SCED. As CTS can reduce post-contingency violations, higher branch limits, referred to as pseudo limits, may be available for some contingency-case network constraints. Thus, Procedure-B is proposed to take advantage of the reliability benefits provided by CTS. With the proposed Procedure-B, CTS can be modeled in RT SCED implicitly through the proposed pseudo limits for contingency-case network constraints, which requires no change to existing RT SCED

tools. Numerical simulations demonstrate that the proposed Procedure-A can effectively eliminate the flow violations reported by RTCA and that the proposed Procedure-B can reduce most of the congestion cost with consideration of CTS.

The system status may be inaccurately estimated due to false data injection (FDI) cyber-attacks, which may mislead operators to adjust the system improperly and cause network violations. Thus, a two-stage FDI detection (FDID) approach, along with several metrics and an alert system, is proposed in this dissertation to detect FDI attacks. The first stage is to determine whether the system is under attack and the second stage would identify the target branch. Numerical simulations demonstrate the effectiveness of the proposed two-stage FDID approach.

ACKNOWLEDGMENTS

The work presented in this dissertation is sponsored by three projects: 1) “Robust Adaptive Topology Control” under the Green Electricity Network Integration program funded by Advanced Research Projects Agency - Energy (ARPA-E) under the United States (U.S.) Department of Energy (DOE); 2) “Stochastic Optimal Power Flow for Real-Time Management of Distributed Renewable Generation and Demand Response” under the Network Optimized Distributed Energy Systems Program funded by ARPA-E; and 3) “A Verifiable Framework for Cyber-Physical Attacks and Countermeasures in a Resilient Electric Power Grid” funded by the National Science Foundation, a United States government agency.

I am very grateful for the instructions and support from my PhD supervisor Dr. Kory Hedman who is also the chair of my doctoral dissertation defense committee. During the years working with him, I have gained extensive research experience and broadened my horizon in the power system area. I am also very grateful to other committee members: Dr. Gerald Heydt, Dr. Vijay Vittal, and Dr. Jiangchao Qin.

To my friends and fellow researchers, I thank you for all kinds of support you provide. I would also like to thank my parents for the strong support I have been receiving for years. Their support paves the road to a promising future for me.

TABLE OF CONTENTS

Page

CHAPTER Page

CHAPTER Page

CHAPTER Page

CHAPTER Page

LIST OF TABLES

Table Page

Table Page

Table Page

Table Page

LIST OF FIGURES

Figure Page

Figure Page

NOMENCLATURE

Abbreviations

ACOPF	AC optimal power flow.
AGC	Automatic generation control.
ALB	Alert level associated with the metric branch overload risk index.
ALC	Comprehensive alert level for detecting whether the system is under cyber-attack.
ALE	Alert level associated with the metric enhanced malicious load deviation index.
ALM	Alert level associated with the metric malicious load deviation index.
BORI	Branch overload risk index.
CAISO	California Independent System Operator.
CBCE	Closest branches to contingency element.
CBVE	Closest branches to violation element.
CE	Complete enumeration.
CI	Comprehensive false data injection cyber-attack index.
CPU	Central processing unit.
CSCED	Corrective security-constrained economic dispatch.
CTS	Corrective transmission switching.
DCOPF	DC optimal power flow.
DOE	Department of Energy.
EDM	Enhanced data mining.

EMLDI	Enhanced malicious load deviation index.
EMS	Energy management system.
ERCOT	Electric Reliability Council of Texas.
E-SCED	Enhanced security-constrained economic dispatch.
FDI	False data injection.
FDID	False data injection detection.
FDPF	Fast decoupled power flow.
FERC	Federal Energy Regulatory Commission.
ISO	Independent System Operator.
IT SCED	Intermediate-time security-constrained economic dispatch.
LMP	Locational marginal price.
LP	Linear programming.
LODF	Line outage distribution factors.
MLDI	Malicious load deviation index.
NERC	North American Electric Reliability Corporation.
MISO	Midcontinent Independent System Operator.
NYISO	New York Independent System Operator.
ISO-NE	Independent System Operator New England.
OPF	Optimal power flow.
OTDF	Outage transfer distribution factors.
OTS	Optimal transmission switching.
PI	Pareto improvement

PJM	PJM Interconnection.
PSCED	Preventive security-constrained economic dispatch.
PSO	Particle swarm optimization.
PTDF	Power transfer distribution factors.
QP	Quadratic programming.
MIP	Mixed integer programming.
MILP	Mixed integer linear programming.
RDM	Regular data mining.
RTCA	Real-time contingency analysis.
RT SCED	Real-time security-constrained economic dispatch.
RTD	Real-time dispatch.
RTD-CAM	Real-time dispatch/corrective auction mode.
RTED	Real-time economic dispatch.
RTO	Regional Transmission Organization.
RTUC	Real-time unit commitment.
SE	State estimation.
SCUC	Security-constrained unit commitment.
SCED	Security-constrained economic dispatch.
SMLDI	System-wide malicious load deviation index.
TS	Transmission switching.
TVA	Tennessee Valley Authority.

Sets

C	Critical contingencies.
C_s	Critical contingencies under system scenario *s*.
D	Loads.
D(n)	Loads that locate at bus *n*.
D(k)	Loads that are critical to branch *k*.
DN	Non-positive loads.
DP	Positive loads.
DV	Virtual loads.
G	Generators.
G(n)	Generators that locate at bus *n*.
GD	Generators that are dispatchable.
I	Interfaces.
IKM(0)	Interfaces lines that are under monitor for base case.
IKM(c)	Interfaces lines that are under monitor for contingency case *c*.
IM(0)	Critical interfaces that are under monitor for base case.
IM(c)	Critical interfaces that are under monitor for contingency case *c*.
K	Branches.
KA	Branches that have the top ten values for malicious load deviation index.
KM(0)	Branches that are under monitor for base case.
KI(i)	Branches that form the interface *i*.
K(n-)	Branches with bus *n* as from-bus.

$K(n+)$	Branches with bus *n* as to-bus.
$KM(c)$	Branches that are under monitor for contingency *c*.
N	Buses.

Parameters

b_{mn}	Susceptance of the branch connecting bus *m* to bus *n*.
b_{mn0}	Total charging susceptance of a transmission connecting bus *m* to bus *n*.
$b_{mn0,m}$	Magnetizing susceptance at the terminal *m* of the transformer connecting bus *m* to bus *n*.
$b_{mn0,n}$	Magnetizing susceptance at the terminal *n* of the transformer connecting bus m to bus *n*.
$BS_{g,i}$	Breadth of segment *i* for unit *g*.
$C_{g,i}$	Cost for segment *i* of unit *g*.
CSR_g	Spinning reserve price for unit *g*.
g_{mn}	Conductance of the branch connecting bus *m* to bus *n*.
LL_{k0}	Initial loading level of branch *k* in the base case.
LL_{kc0}	Initial loading level of branch *k* under contingency *c*.
$LimitA_k$	Normal thermal limit in MW for branch *k* in SCED.
$LimitC_{kc}$	Emergency thermal limit in MW for branch *k* under contingency *c* in SCED.
$Limit_i$	Total flow limit in MW for interface *i* in SCED.
$Limit_{ic}$	Total flow limit in MW for interface *i* under contingency *c* in SCED.
$LODF_{k,c}$	Line *c* outage distribution factor on line *k*.

MRR_g	Energy ramp rate (MW/minute or p.u./minute) for unit g.
$n(d)$	Bus where load d locates.
$n(k-)$	From-bus of branch k.
$n(k+)$	To-bus of branch k.
N_1	The limit of an l_1-norm constraint.
ND_k	Number of loads that are critical to branch k.
NS_g	Number of cost segments for unit g.
nSS	The number of sub-segments for a slope segment of unit slope cost curve.
$OTDF_{n,k,c}$	Outage transfer distribution factor from bus n to line k when line c is outage.
Pct	Threshold (a percent number) for determining base-case monitor set.
$PctC$	Threshold (a percent number) for determining contingency-case monitor set.
P_c^0	Active power of the contingency generator c in the pre-contingency situation.
P_d	Target/forecasting active power of load d at the end of a SCED period.
P_{d0}	Initial active power of load d at $t = 0$ or at the beginning of a SCED period.
$P_{d0,ISO}$	Measurement of load d at $t = 0$.
P_{d-}	Actual load d at $t = -T_{ED}$.
PF_PD_{shed}	A fix penalty factor for variable $p_{d,shed}$ and $p_{d,shed,c}$.

P_g^0	Active power of unit g in the pre-contingency situation.
P_{g0}	Initial output of unit g.
$P_{g,max}$	Maximum output for unit g.
$P_{g,min}$	Minimum output for unit g.
P_{k0}	Initial active flow on branch k flowing out of from-bus in SCED.
$P_{k0,from}$	Initial active power on branch k flowing out of the from-bus.
$P_{k0,ISO}$	Measurement of active flow on branch k at $t = 0$.
$P_{k0,to}$	Initial active power on branch k flowing out of the to-bus.
$P_{k,c,0}$	Initial active flow on branch k under contingency c flowing out of from-bus in SCED.
$P_{kc0,from}$	Initial active power on branch k flowing out of from-bus under contingency c.
$P_{kc0,to}$	Initial active power on branch k flowing out of the to-bus under contingency c.
P_{k-}	Actual active flow on branch k at $t = -T_{ED}$.
$P_{k+,SCED}$	Active flow on branch k at $t = T_{ED}$, determined by SCED that runs at $t = 0$.
$PTDF_{n,k}$	Power transfer distribution factor from bus n to line k.
$PTDF_{n(d),k}$	Power transfer distribution factor from load d to line k.
$Q_{k0,from}$	Initial reactive power on branch k flowing out of the from-bus.
$Q_{k0,to}$	Initial reactive power on branch k flowing out of the to-bus.

$Q_{kc0,from}$	Initial reactive power on branch *k* flowing out of from-bus under contingency *c*.
$Q_{kc0,to}$	Initial reactive power on branch *k* flowing out of the to-bus under contingency *c*.
$RateA_k$	Normal thermal limit in MVA for branch *k* in power flow calculations.
$RateC_k$	Emergency thermal limit in MVA for branch *k* in power flow calculations.
r_{mn}	Resistance of the branch connecting bus *m* to bus *n*.
$sign(P_{k0})$	1 if actual flow direction is from from-bus to to-bus; -1 if actual flow direction is from to-bus to from-bus.
$S_{k0,from}$	Initial complex power on branch *k* flowing out of the from-bus.
$S_{k0,to}$	Initial complex power on branch *k* flowing out of the to-bus.
$S_{kc0,from}$	Initial complex power on branch *k* flowing out of from-bus under contingency *c*.
$S_{kc0,to}$	Initial complex power on branch *k* flowing out of the to-bus under contingency *c*.
SR_a	Spinning reserve requirement for area *a*.
SRR_g	Spinning ramp rate (MW/minute or p.u./minute) for unit *g*.
t_m	Transformer tap ratio at terminal *m*.
T_{ED}	Look-ahead time for SCED, or the time length of a SCED period.
T_{SR}	Time for spinning reserve requirements.
V_{max}	Maximum limit of voltage magnitude.

V_{min}	Minimum limit of voltage magnitude.
X_k	Reactance of branch *k*.
x_{mn}	Reactance of the branch connecting bus *m* to bus *n*.
y_{mn}	Admittance of the branch connecting bus *m* to bus *n*.
z_{mn}	Impedance of the branch connecting bus *m* to bus *n*.
v_{kc}	The violation on branch *k* under contingency *c*.
$v_{kc,CTS}$	The violation on branch *k* under contingency *c* with corrective transmission switching action implemented.
α_k	Phase angle of branch *k*; 0 if the branch is not a phase shifter.
Δbi	The initially selected breadth of a sub-segment for a slope segment of unit slope cost curve.
Δs	The actual breadth of each sub-segment for a slope segment of unit slope cost curve.

Variables

$AvgLMP$	Average locational marginal price over all buses in the system.
$AvgLMP_{cg}$	Average of congestion component of locational marginal price over all buses in the system.
CCR_{CTS}	Congestion cost reduction.
c_n	Change in phase angle at bus *n* due to attack.
$CngstCost$	Total congestion cost over the entire system.
$CngstRvn$	Total congestion revenue over the entire system.
D_{CTS}	Average depth of switching solutions.

$EMLDI_k$	The enhanced malicious load deviation index of branch *k*.
E_p	Parallel efficiency (a percent number).
F_{gc}	Participation factor of unit *g* under a generator contingency *c*.
F_τ	Cumulative distribution function of variable τ.
$GenCost$	Total generator cost over the entire system.
$GenRent$	Total generator rent over the entire system.
$If_{d,k}$	Influential factor for branch *k* due to the change in load *d*.
$Indictr_{d,k}$	1 if significant change in load *d* decreases the absolute flow on branch *k*; 0 if the change in load *d* is trivial; -1 if significant change in load *d* increase the absolute flow on branch *k*.
$L_{CTS,c}$	The location of the switching solution in the candidate list for contingency *c*.
$LdPaymt$	Total load payment over the entire system.
$LMP_{cg,n}$	Congestion component of locational marginal price at bus *n*.
LMP_n	Locational marginal price at bus *n*.
LMP_s	System-wide locational marginal price.
L_S	Load shift factor.
$GenRvn$	Total generator revenue over the entire system.
N_c	Total number of critical contingency.
$MLDI_k$	The malicious load deviation index of branch *k*.
M_c	Total number of critical contingencies for which at least a beneficial switching solution exists.

$p_{d,shed}$	Shedded active power for load *d*.
$p_{d,shed,c}$	Shedded active power for load *d* under contingency *c*.
p_g	Total output of generator *g*.
P_g^c	Active power output of unit g under generator contingency c for generator contingency analysis.
$p_{g,c}$	Total output of generator *g* under contingency *c* for SCED.
$p_{g,i}$	Output on segment *i* for generator *g*.
PI_n	Active power injection at bus *n*.
p_i	Total flow for interface *i*.
$p_{i,c}$	Total flow for interface *i* under contingency *c*.
p_k	Power flow on branch *k*.
$\tilde{p}_k$	Cyber flow on branch *k*.
$p_{k,c}$	Flow on branch *k* under contingency *c*.
P_{mn}	Active power flowing from bus *m* to bus *n*.
P_{nm}	Active power flowing from bus *n* to bus *m*.
Q_{mn}	Reactive power flowing from bus *m* to bus *n*.
Q_{nm}	Reactive power flowing from bus *n* to bus *m*.
S_n	Speedup achieved with parallel computing.
$S_{p,max}$	Maximum possible speedup achieved with parallel computing.
sr_g	Spinning reserve that generator *g* provides.
T_n	Computational time of parallel computing with *n* threads.
T_s	Computational time of the sequential program.

v_{c0}	Total violations in the post-contingency situation.
v_{c1}	Total violations in the post-switching situation for contingency *c*.
V_m	Voltage magnitude at bus *m*.
V_n	Voltage magnitude at bus *n*.
θ_{mn}	Phase angle difference across the transmission connecting bus *m* and bus *n*.
$\theta_{mn,s}$	Phase angle setting of the phase shifting transformer connecting bus *m* and bus *n*.
θ_n	Actual phase angle at bus *n*.
$\tilde{\theta}_n$	Cyber phase angle at bus *n*.
θ_s	Phase angle difference of the phase shifter transformer connecting bus *m* to bus *n*.
$\delta_{n(k-)}$	Phase angle of bus $n(k-)$.
$\delta_{n(k-),c}$	Phase angle of bus $n(k-)$ under contingency *c*.
$\delta_{n(k+)}$	Phase angle of bus $n(k+)$.
$\delta_{n(k+),c}$	Phase angle of bus $n(k+)$ under contingency *c*.
η_{CTS}	Average violation reduction in percent.
w_c	Probably of contingency *c*.
α	The number of scenarios for which the same contingency is identified as a critical contingency, used for analyzing the enhanced data mining method.

τ	The probability of a contingency being identified as a critical contingency, used for analyzing the enhanced data mining method.
γ	The number of scenarios where at least a beneficial CTS solution exists for a critical contingency, used for analyzing the enhanced data mining method.
β	The probability that at least a beneficial CTS solution exists for an identified critical contingency, used for analyzing the enhanced data mining method.
φ	The number of switching actions in the candidate list, obtained from the enhanced data mining method, for a critical contingency.
$\Delta\tilde{p}_d$	The malicious deviation of load *d*.
Δp_k	The difference between the post-attack actual and cyber power flows on branch *k*.

1. INTRODUCTION

A power system is an electrical network of interconnected elements that are used to generate, transmit, and consume electric power. It consists of, but not limited to, generators, loads, transmission lines, transformers, phase shifters, circuit breakers, and shunts. High voltage direct current lines may exist in some power systems.

The prime function of an electrical network is to transmit and distribute power. The voltage level varies from several hundred volts to around one thousand kilovolts (kV). A power system network can be divided into two portions: a high-voltage level transmission subsystem and a low-voltage level distribution subsystem.

The asset value of infrastructure in the North American power system represents more than 1 trillion United States (U.S.) dollars. The electricity grid of the United States contains over 360,000 miles of transmission lines including around 180,000 miles of high-voltage lines and connects to over 6,000 power plants in 2012 [1]. Reference [1] also reports that: 1) in 2011, the global power generation capacity, which grows by 2% annually, is about five trillion watts; 2) the two countries that have the largest generation capacity are the United States and China, each of which accounts for approximately 20% of the world's total installed capacity; 3) the generation capacity in China will increase by about 3% per year through 2035 while the capacity growth in the United States is less than 1% during the same period.

Only 10% of the energy consumption in America was used to produce electricity in 1940; this percentage increased to 25% in 1970 and it was around 40% in 2003 [2]. This implies the efficiency of electricity as a source for supplying energy is increasing.

As introduced in [3], 56% of the electricity generated in the United States in 2012 was provided by coal-fired power plants and nuclear power plants.

There are more than 3,100 electric companies, utilities, and regulation organizations in the United States. For instance, Federal Energy Regulatory Commission (FERC) regulates interstate transmission networks and energy markets [4]; North American Electric Reliability Corporation (NERC) ensures the reliability of the power systems in North America by developing reliability standards [5].

Independent System Operators (ISOs) were created under FERC Order 888 and Order 889. The goal of the ISOs is to meet the requirements of providing unbiased open access to transmission. Subsequently, FERC issued Order 2000 that presents the requirements to be a Regional Transmission Organization (RTO). Voluntary formation of RTO was encouraged by FERC to manage the regional transmission network [6]. The ISOs/RTOs in the United States include California ISO (CAISO), New York ISO (NYISO), ISO New England (ISO-NE), Midcontinent ISO (MISO), PJM Interconnection (PJM), Southwest Power Pool, and Electric Reliability Council of Texas (ERCOT). Note that ERCOT is governed by the Public Utility Commission of Texas rather than FERC.

1.1 Background

As energy cannot be economically stored on a large scale, electricity must be produced, transported, and consumed at the same time. Therefore, it is very challenging to maintain reliable real-time operations of power systems. Failure of any element may

have a negative effect on the normal operations of power systems. Hence, it is essential to improve power system security and reliability.

Power systems are built with some degree of redundancy due to concerns regarding power system security. In addition, a number of mandatory standards for power system reliability have been developed recently. Complying with these standards makes the system less susceptible. However, power systems are complex and dynamical in nature, which makes it hard to operate them properly. Uncertainty such as load fluctuation makes it more difficult to maintain power system security in real-time. Thus, power system real-time secure operations have gained increased attention. Operators are forced to make preventive adjustments in advance or take just-in-time corrective actions in order to maintain power system security in the event of a disturbance.

System security consists of three major functions [7], which includes:

- System monitoring,
- Contingency analysis,
- Security-constrained economic dispatch (SCED).

These are key functions of energy management systems (EMSs) used in modern power systems. The system monitoring function determines the system condition and provides a base for contingency analysis and security-constrained economic dispatch. Contingency analysis identifies potential post-contingency violations, which will be corrected by SCED.

The system monitoring function receives data from remote terminal units or local control centers and then performs state estimation (SE) to determine the real-time status

of the system, including bus voltage magnitude and angle. Thus, with this function, system operators will be informed immediately when branch overloads and voltage limit violations occur. It provides system operators with the actual real-time system condition, as well as a base case for other real-time applications.

Contingency analysis evaluates the impact of a potential contingency on system security. Contingency analysis when simulated in real-time is referred to as real-time contingency analysis (RTCA). With the results obtained from RTCA, the system can operate defensively in real-time. A contingency may cause serious consequences in a short time and operators may not have sufficient time to react to the contingency, prevent the situation from getting worse, and restore the system. Thus, the goal of RTCA is to enable system operators to be better prepared with pre-planned strategies to deal with potential critical contingencies.

SCED aims to provide a least-cost re-dispatch solution for online units while meeting the network constraints as well as other restrictions. When simulated in real-time, SCED is referred to as real-time SCED (RT SCED). Actual network violations obtained from state estimation or base-case power flow and potential post-contingency network violations obtained from RTCA will be sent to RT SCED as network constraints and are supposed to be eliminated with the new dispatch point obtained from RT SCED in the post-SCED steady state.

1.2 Motivation

Power system operations need to satisfy physical constraints such as Kirchhoff's laws and comply with reliability standards. Improper real-time operations may result in

system violations, islanding, irreversible damage to electrical equipment, and in the worst-case a blackout. Therefore, improving system reliability in real-time operations is very important. This dissertation focuses on reliability enhancements for real-time operations of electric power systems.

The ISOs typically use energy management systems to help system operators monitor and manage the system in real-time. Key functions of the EMS include system monitoring, RTCA, and RT SCED. System monitoring observes the system condition and provides a base case for all other real-time applications. RTCA identifies critical contingencies and the associated violations and forms network constraints for RT SCED. RT SCED produces a generation re-dispatch solution that would eliminate the actual base-case network constraints and the potential contingency-case network violations identified by RTCA and meet all the system requirements at least cost.

Electrical networks are built with some level of redundancy due to security concerns. They are traditionally considered as static assets in power system real-time operations. However, the flexibility in electrical network has not been fully utilized and reflected in existing operational tools. Prior research efforts have illustrated that transmission switching (TS) can provide a variety of benefits for power system operations. Transmission switching is a control strategy that switches a branch out of service to achieve a particular goal.

Though transmission switching has not been widely used as a regular strategy in reality, it is being used as an emergency corrective control scheme for some parties,

which is referred to as corrective TS (CTS). The switching actions are mainly determined based on ad-hoc methods and it is unclear how CTS would improve and fit in existing operational applications. In this dissertation, the reliability enhancements provided by CTS are investigated and a systematic procedure is proposed in order to integrate CTS into RTCA and RT SCED. The proposed integrating procedure will require minimal change to existing operational tools.

Given a base case, provided by the system monitoring function of EMS, RTCA will first execute and identify critical contingencies that are to be sent to the CTS routine. Several heuristic approaches are proposed to generate a ranked candidate switching list. Five beneficial switching actions, which would reduce or eliminate the post-contingency violations, are identified for each of those critical contingencies. Numerical simulations on three large-scale practical systems demonstrate the effectiveness of CTS. Simulation results also show that parallel computing can speed up the entire process including both contingency analysis routine and transmission switching routine.

Modeling CTS in RT SCED directly will largely increase the computational time, which makes it impossible for real-time applications. In this dissertation, a practical heuristic is proposed to capture the benefits provided by CTS in RT SCED, as a result of which existing RT SCED model can remain the same. With the proposed heuristic, the branch limits of the network constraints that are sent from RTCA to RT SCED would increase, which can then reduce congestion cost significantly and enable RT SCED to obtain a solution with a lower total cost. The increased limit is referred to as a pseudo limit; and a SCED with pseudo limits is referred to as an enhanced SCED (E-

SCED) in this dissertation. Simulation results demonstrate that the proposed E-SCED approach can reduce congestion cost significantly and the CTS actions identified for a critical contingency in the pre-SCED situation can still reduce the violations under the same contingency in the post-SCED situation.

As stated above, state estimation estimates the system condition and provides a starting point for RTCA and RT SCED. Thus, it is very important to ensure the correctness of state estimation. Bad data detection and identification can filter out large random measurement errors. However, malicious false data injection (FDI) cyber-attacks can bypass traditional bad data detection and cause branch overloads that are not observed by system operators. Thus, it is vital to develop a strategy that can effectively detect FDI attacks in real-time. Several metrics that monitor abnormal load deviations and flow changes are proposed in this dissertation. Qualitative analysis can be conducted with the proposed FDI cyber-attack alert system. A systematic two-stage FDID approach is proposed to determine whether the system is under attack and identify the target branch. Case studies validate the proposed metrics, alert system, and systematic two-stage FDID approach.

1.3 Summary of Contents

The rest of this dissertation is structured as follows. A thorough literature review is presented in Chapter 2. In this chapter, power flow studies are first presented, followed by a comprehensive introduction of contingency analysis. Then, a systematic review of past transmission switching research is presented, as well as a detailed review on economic dispatch and false data injection cyber-attack and detection. At the end of

this chapter, an overview of general parallel computing technology and its various applications in the power system area are presented.

Chapter 3 focuses on RTCA only. The RTCA model used in this dissertation is first introduced, followed by a discussion on the contingency list as well as the definition of critical contingencies. Case studies show that three large-scale practical systems are vulnerable to several contingencies. Parallel computing is also conducted to speed up the contingency analysis process.

In Chapter 4, the fundamentals of how transmission switching benefits the system are introduced and the metrics for defining a beneficial switching action are proposed. Heuristic algorithms are proposed to generate a list of candidate switching branches. Numerical simulations are then presented to demonstrate the effectiveness of CTS. It is shown that CTS is a promising strategy in industry. Parallel computing enhances this viewpoint by further reducing the solution time.

Chapter 5 first presents how the network constraints are obtained from RTCA and then introduces a typical RT SCED model used in industry. The procedure of considering CTS in RT SCED is described in detail. Multiple RT SCED models with different forms of network constraints are simulated and compared. With the most precise SCED model, the effects of CTS on SCED results are investigated. The benefits of CTS are also validated by running RTCA with a different base case representing the post-SCED situation. Case studies show that the congestion cost can be reduced significantly with CTS.

Chapter 6 studies cyber-physical system security. The effects of FDI attacks on power systems are examined and it is shown that FDI can result in physical flow violations. Several metrics are proposed in this chapter, as well as an FDI cyber-attack alert system. The proposed metrics can monitor malicious load deviations as well as suspicious flow changes. A systematic two-stage FDID approach is proposed to detect potential FDI attacks. Cases studies demonstrate the effectiveness of the proposed two-stage FDID approach.

Chapter 7 concludes this dissertation and potential future work is presented in Chapter 8.

2. LITERATURE REVIEW

2.1 Power Flow Studies

In power system engineering, a power flow study is the basis for steady-state analysis of the interconnected system. There are transmission system power flow studies and distribution system power flow studies. This dissertation only focuses on transmission system power flow studies. Thus, the system can be assumed to be three-phase balanced and only positive sequence network is modeled. Single-line diagrams and the per unit system are used to simply the analysis. The pi-equivalent circuit model is typically used to represent branches. Then, a power flow problem can be solved through computer programs under those assumptions and the information listed below will be reported:

- voltage magnitude and phase angle at each bus,
- active power injection and reactive power injection at each bus,
- active power flows and reactive power flows on each branch.

Two widely used models are the full AC power flow model and the simplified DC power flow model, which will be presented below. The power flow models are used for solving most problems in the power system domain. Hence, power flow studies are remarkably important for various power system applications including RTCA, RT SCED, and the proposed CTS. Note that RTCA and CTS implemented in this dissertation use the AC power flow model while RT SCED uses the DC power flow model. AC feasibility of the solutions obtained from RT SCED is verified through AC power flow simulations.

Fig. 2.1 shows the single-line diagram of a typical two-terminal circuit, which is an essential component of a transmission network. Note that P and Q denote active power and reactive power respectively. The power flowing out of one terminal does not equal to the power flowing into the other terminal because of the losses on the branch connecting those two buses, which means that $P_{mn} \neq -P_{nm}$ and $Q_{mn} \neq -Q_{nm}$. The branch power flow equations are shown below,

$$P_{mn} = V_m^2 g_{mn} - V_m V_n (g_{mn} \cos\theta_{mn} + b_{mn} \sin\theta_{mn}) \tag{2.1}$$

$$Q_{mn} = -V_m^2 \left(b_{mn} + \frac{b_{mn0}}{2}\right) + V_m V_n (b_{mn} \cos\theta_{mn} - g_{mn} \sin\theta_{mn}) \tag{2.2}$$

where,

$$y_{mn} = g_{mn} + jb_{mn} = \frac{1}{z_{mn}} = \frac{r_{mn} - jx_{mn}}{r_{mn}^2 + x_{mn}^2} \tag{2.3}$$

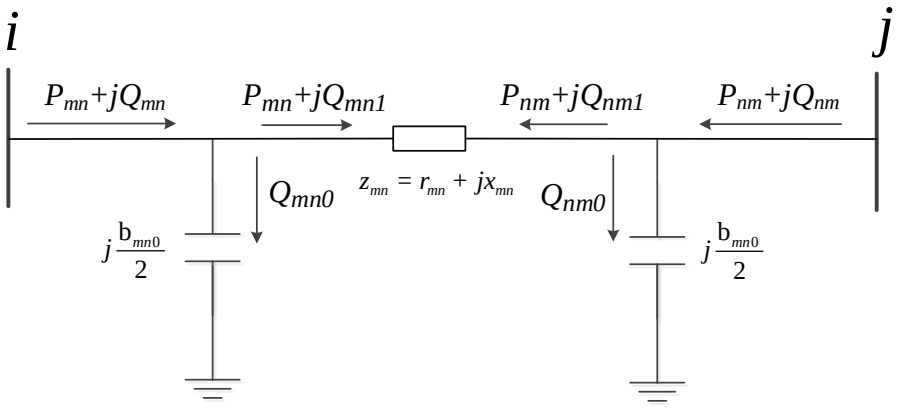

Fig. 2.1 Single-Line Diagram of a Two-Terminal Circuit.

Fig. 2.2 shows a single-line equivalent diagram of a transformer. A transformer is typically represented by a pi-equivalent circuit and an ideal transformer. The tap ratio is t_m for bus m and is one for the nominal end n. $b_{mn0,m}$ and $b_{mn0,n}$ are the magnetizing susceptances. In this dissertation, they are set equal for simplification. The power flow equations for transformers can be derived by replacing V_m with V_m/t_m and replacing

$b_{mn0}/2$ with $b_{mn0,m}$ in the transmission power flow equations (2.1) and (2.2). For a phase shifting transformer, an extra modification is to replace θ_{mn} with $\theta_{mn} - \theta_{mn,s}$, where $\theta_{mn,s}$ is the phase angle setting of this phase shifting transformer.

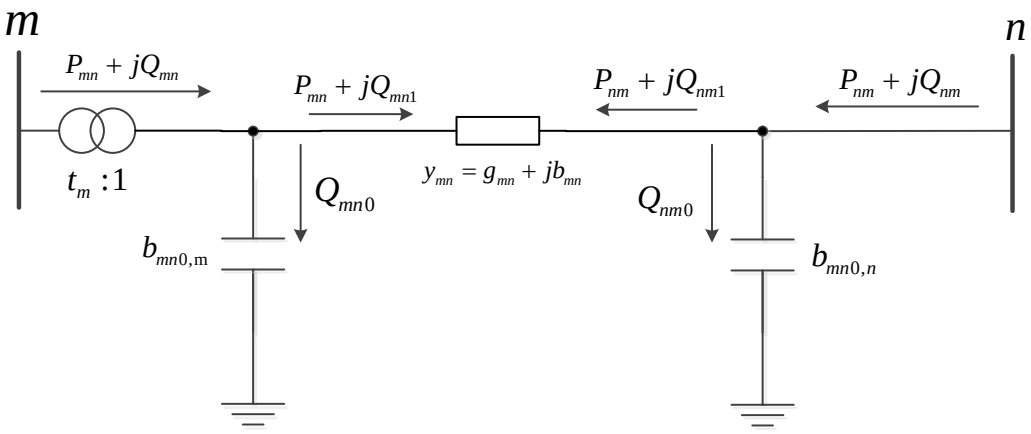

Fig. 2.2 Single-Line Equivalent Diagram of a Transformer.

2.1.1 AC Power Flow

A number of different AC power flow algorithms have been developed in the literature [8]-[9]. Several well-known iterative approaches include Gauss-Seidel method, Newton-Raphson method, and fast decoupled power flow **(**FDPF) method. There are three basic types of buses: PV buses, PQ buses, and slack buses.

A PV bus is a bus that has the capability of controlling its voltage magnitude and it is usually a generator bus or a bus whose voltage magnitude is controlled by nearby generators or other devices such as switched shunts and static VAR compensator. A PQ bus is typically a load bus or a connection bus. A slack bus should be a bus where there is a large amount of generation capacity. For some power flow algorithms including the Newton-Raphson method, a normal assumption is that the slack bus is used to balance

the generation and demand. A slack bus is also referred to as the swing bus, angle reference bus, or just $V\theta$ bus.

In a power flow study, the voltage magnitude and voltage angle at a slack bus are fixed; the active power and voltage magnitude at PV buses remain the same; and the active power and reactive power at PQ buses are fixed. The generator reactive power output Q will adjust automatically to maintain the voltage set point. In reality, the reactive power output Q has its minimum limit and maximum limit. Therefore, a PV bus may have to switch to a PQ bus when the Q at that bus reaches its limit. Another strategy for not violating generators' reactive power limits is to adjust the voltage set values at the PV buses when the associated reactive power capacity constraints are violated [8].

Gauss-Seidel Method

The Gauss-Seidel approach was the first method to solve the power flow problem on digital computers [8]. Although each iteration of this approach is fast, it is slow overall since it typically takes many iterations before it converges with the desired accuracy. It may fail to converge when the system contains negative reactance branches (compensated transmission lines). The determination of the initial point is critical for the algorithm convergence.

Newton-Raphson Method

The robust and reliable Newton-Raphson approach is widely used in practice for solving the power flow problem. The key of this approach is to create the Jacobian matrix based on the nodal power mismatch functions; then a set of linear equations are solved simultaneously to obtain an updated solution. This process repeats itself until

the specified stopping criteria are satisfied or the maximum number of iterations is reached. State variables have to be updated between each iteration, as well as the Jacobian matrix. The converged solution may be different with different starting points.

Fast Decoupled Power Flow

The fast decoupled power flow algorithm is developed based on the Newton-Raphson method. The Newton-Raphson method is robust but it may be slow as the Jacobian matrix has to be updated per iteration, which accounts for a significant percent of the total computational time.

Considering the fact that transmission branches typically have high reactance-to-resistance (*X/R*) ratios, the Newton-Raphson method can be simplified to accelerate convergence. One popular simplified method is the fast decoupled power flow method, which was originally proposed in [9] in 1974. Therefore, another term for FDPF is the Stott decoupled power flow method, named after the first author of [9]. After FDPF was first proposed, it has been further enhanced to make the algorithm more robust.

The assumptions of standard FDPF method include that 1) the interaction between active power and voltage magnitude is neglected, 2) the interaction between reactive power and voltage angle is neglected, and 3) the angle difference across a branch is small enough such that the associated cosine value can be assumed to be one. Assumptions 1) and 2) are based on engineering experience and observations: the voltage magnitude would not be significantly affected by the active power and the voltage angle will not change much due to change in reactive power.

The power flow converges when both the active power unbalance and the reactive power unbalance of each bus are less than the predefined tolerances. Though the tolerances for active power convergence and reactive power convergence are usually set to the same values, they do not have to be identical.

The above standard FDPF method is called the XB method. Another similar method is known as the BX method. The BX method may have a better convergence performance than the XB method when the system contains transmission lines with low X/R ratio [10]. The Jacobian matrix of the FDPF approach is constant. Thus, the calculation and factorization of the constant Jacobian matrix are conducted only once at the beginning of the algorithm and they can be directly used by all following iterations. Therefore, the FDPF approach can reduce the computation time per iteration. However, more iterations may be required to reach the desired precision.

The FDPF approach also uses the Newton's method. The difference between the FDPF and Newton-Raphson methods is that their correction equations are different. The Newton's method is used in the FDPF approach to solve two sets of equations with reduced dimension while the Newton-Raphson method solves the correction equations with full dimension.

2.1.2 DC Power Flow

Though a full AC model based power flow study is accurate, it is complex and hard to solve due to its non-linearity and non-convexity characteristics. When reactive power and voltage magnitude are not of concern, an approximate DC model can be used for

solving power flow problems. The simplification of an AC model into a DC model is illustrated below.

First of all, reactive power is ignored in the FDPF approach. Furthermore, with the assumption that voltage magnitude has little effect on active power, the voltage magnitude of each bus is simply set to one. Then, the simplified transmission power flow equation is as follows,

$$P_{mn} = \frac{\theta_{mn}}{x_{mn}} \tag{2.4}$$

The DC power flow model can be used to obtain information regarding the active power and voltage angle in high-voltage transmission networks. By using the approximate DC model instead of the accurate AC model, the non-linearity and non-convexity of the AC model can be avoided. Therefore, the DC model is widely used in many areas such as transmission expansion planning, maintenance scheduling, day-ahead unit commitment, and real-time economic dispatch (RTED).

Note that the branches of a distribution network typically do not have high ratio *X/R*. As a result, the DC model may not be accurate for a distribution network. It is worth mentioning that this DC power flow model is used to model an alternating current network rather than a direct current network.

2.1.3 Linearized AC Power Flow

Though the DC power flow model is widely used in the electric power industry, especially in the energy markets areas, it is not as accurate as the AC power flow model [11]. Hot-start α-matching and h-matching power flow methods can provide much more precise results in comparison with cold-start DC power flow method [11]-[12].

However, those methods do not capture the information about reactive power and voltage magnitude. Linearized AC power flow models can incorporate reactive power and voltage magnitude while the linear character remains. Reference [13] proposes a linearized AC power flow model, which is faster than the full AC power flow model and can capture reactive power and voltage magnitude information that are ignored in the DC power flow model. A piecewise linear AC power flow model is proposed in [14] to speed up the process of power networks islanding.

2.2 Contingency Analysis

There are two types of outage in power systems: planned outage and unplanned outage. Planned outage is typically preventive maintenance or replacement for power system elements. It ranges from several minutes to months. Regular maintenance can largely extend the lifetime of an equipment, which can reduce the investment cost. An unplanned outage normally means the failure of elements in real-time. A forced outage is unpredictable and may seriously jeopardize the system security. Thus, an unexpected outage is also referred to as a contingency. This dissertation will focus on the unplanned outage - contingency only.

In general, a contingency is the loss or failure of a single element or multiple elements of a power system. An element of a power system usually refers to a major electrical equipment such as a transmission line. The system can be considered to be secure under a particular contingency if it does not create any major problem.

There are two types of violations, branch thermal limit violation (flow violation) and bus voltage limit violation (voltage violation). Flow violation occurs when the flow

on a branch exceeds its capacity rating. Voltage violation includes under-voltage violation when the voltage magnitude is less than V_{min} and over-voltage violation when the voltage magnitude is greater than V_{max}. Typically, V_{min} is set to 0.9 and V_{max} is set to 1.1. For systems that requires a tight voltage range, V_{min} and V_{max} can also be set to 0.95 and 1.05 respectively.

Contingency analysis can be conducted either in real-time or day-ahead. Day-ahead contingency analysis evaluates the effect of contingency on system reliability and identifies active network constraints for day-ahead scheduling. It may help quickly identify the critical problems in real-time. Real-time contingency analysis reports the consequences of contingencies that may occur in a very short time, which allows operators to react quickly to the unexpected outages by using pre-determined recovery strategies. This dissertation only focuses on real-time contingency analysis.

RTCA is an essential application in the EMS of modern power systems. The goal of RTCA is to analyze the system static security under each potential contingency, which will be reported to the system operators in real-time. RTCA can identify the critical contingencies and the associated violations. Thus, RTCA enables system operators to make corrective control plans in advance for handling post-contingency violations when a critical contingency actually occurs, or to preposition the system to eliminate those potential post-contingency violations. Therefore, RTCA is very important for power system real-time secure operations and, thus, it is worthwhile to investigate RTCA in this dissertation. RTCA on three large-scale real power systems are simulated and analyzed in Chapter 3.

2.2.1 Contingency Types

There are two basic types of contingency, single-element contingency and multiple-element contingency. A single-element contingency includes a generator contingency or a branch contingency. It is also referred to as the widely used term *N*-1. A multiple-element contingency is a simultaneous failure of multiple elements, which can be denoted by *N*-*m*. It can be a simultaneous failure of a generator and a branch, two branches, two generators, or three or more elements. Note that the probability of a multiple-element contingency is extremely low.

To be specific, the term branch in this dissertation includes transmission line, transformer, and phase shifter. A phase shifter is a special type of transformer that can create a phase angle shift and control the flow of active power.

Contingency analysis has been traditionally limited to *N*-1 level due to the computational complexity and low probability of simultaneous failures. In this dissertation, only single-element contingency is studied. Contingency analysis estimates the impact of potential near-future contingencies on power system security: if a contingency occurs, what the results could be and whether the system can withstand this contingency.

Branch contingency is much more common than generator contingency. When a branch is out of service and disconnected from the rest of the network, the flow on that branch becomes zero and the flows on nearby branches may change significantly. As a result, branch overloads and bus voltage violations may occur under a branch contingency.

If generation re-dispatch is not conducted for a generator contingency, all the generation loss would have to be picked up only by a slack bus, which is impractical. Thus, generation re-dispatch is required. Adjustments of generation can be determined with a set of generator participation factors as well as optimization-based methods. Normally, four options are available to calculate the participation factors that can be calculated based on:

- available capacity,
- capacity,
- reserve,
- or inertia.

In reality, when a generator outage occurs, there would be a power imbalance issue between total demand and total generation. This will cause a frequency drop and all other generators will immediately increase their outputs based on their inertia and then reposition their dispatch points due to droop control when governors start to react. System operators can perform generation re-dispatch for a generator contingency. However, it is worth noting that there is very limited time for operators to re-dispatch generation to pick up the loss of a generator and recover the frequency back to its normal range. Therefore, due to the computational complexity, no optimization method is involved for any of the above participation factor based re-dispatch algorithms, which are very fast and can be used to perform generation re-dispatch in real-time. In this dissertation, available capacity based participation factor is used to perform generation re-dispatch to resolve the power imbalance issue caused by a generator contingency.

2.2.2 Procedure

The procedure of contingency analysis is presented in Fig. 2.3. A base case power flow simulation is first performed to determine the pre-contingency system condition. Then, the base case solution including bus voltage magnitudes and bus voltage angles are used as the starting point of each contingency power flow simulation. In the case of a branch contingency, the active power outputs of generators will remain at the pre-contingency level except for the generators at the slack bus, which is assumed to pick up the change in losses. However, in the event of a generator contingency, they may change significantly due to generation re-dispatch.

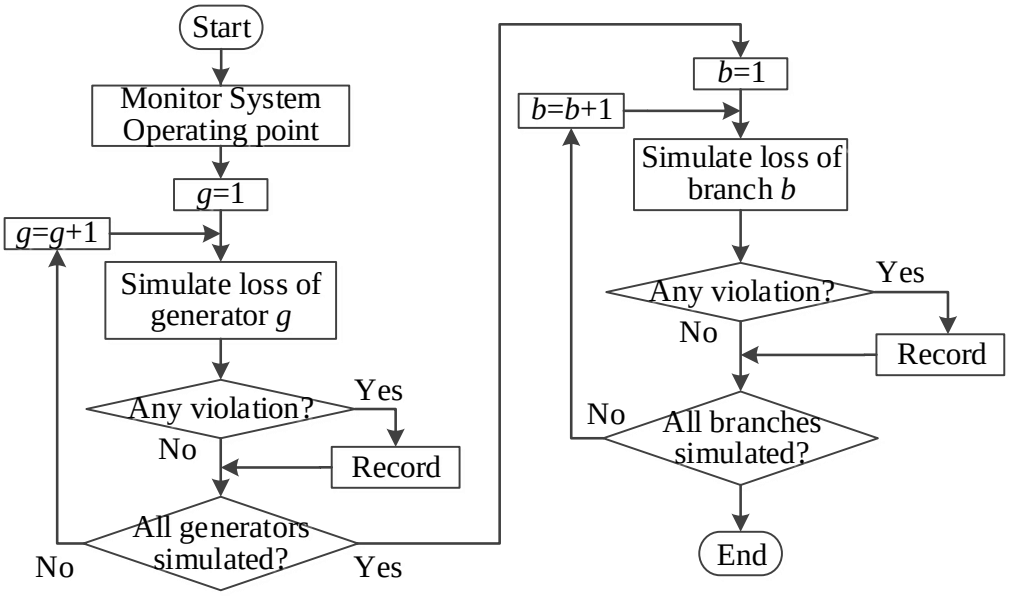

Fig. 2.3 Contingency Analysis Procedure.

After the base case power flow is solved, the first contingency in the contingency list will be simulated. This contingency is modeled by fully de-energizing the corresponding outaged element from the system. The power flow problem is then solved

again with the updated system model. The consequences of this contingency are evaluated by checking the bus voltages against the limits V_{max} and V_{min} and by checking branch flows against branch capacities. This evaluation process is referred to as limit checking.

After the simulation for the first contingency is completed, the system is reset to the original base case operating condition. Then, the second contingency in the contingency list is simulated and its impact is analyzed. This process repeats itself until all the remaining contingencies in the contingency list are examined. The identified critical contingencies and the associated potential post-contingency violations are recorded in this process.

As presented above, the contingencies are independent of each other. The order of contingencies in the contingency list does not affect the results. Therefore, it is concluded that contingency analysis is suitable for parallel computing.

2.2.3 Contingency List

Power systems are built with some level of redundancy that it can sustain a number of contingencies. However, it is improper and impractical that the redundancy can prevent all contingencies from causing system violations. The RTCA application may not be able to simulate all potential contingencies in a very limited time. Therefore, only a subset of contingencies may be modeled in practice.

Off-line analysis can be performed with historical data to determine the contingency list, which contains contingencies that may cause negative effects on system security and contingencies that correspond to a high probability of occurrence. Thus,

RTCA only simulates the contingencies in the contingency list that contains a subset of all potential contingencies, which would save a lot of solution time for RTCA. The contingency lists may be different for different system conditions. For example, the contingency list for a peak hour might be very different with the contingency list for an off-peak hour.

Note that DC power flow model based contingency analysis would take much less time than AC power flow model based contingency analysis. If voltage magnitude and reactive power are not of concern, the DC model based contingency analysis may be preferred. Moreover, the DC model based contingency analysis can be used as a screening process to reduce the contingency list for the full AC contingency analysis simulation. However, it is worth pointing out that the DC power flow model is not as accurate as the AC power flow model.

2.2.4 Results of Contingency Analysis

It is very important to analyze the results of contingency analysis as they expose the system vulnerabilities. Typically, contingency analysis will report a list of critical contingencies that may cause potential violations and a list of individual potential post-contingency violations. It may also report some statistics shown below:

- the total post-contingency violations per contingency,
- the number of buses with voltage violations,
- the number of branches with flow violations over all the contingencies,
- the number of contingencies that cannot converge, and

- the worst flow violation and the worst voltage violation among all the contingencies simulated.

2.2.5 Industry Practices

To ensure secure operations of power systems, ISOs have to comply with several reliability standards required by NERC. One of those standards is *N*-1 reliability that requires power systems to withstand the loss of one element. Thus, RTCA is conducted successively every several minutes at all ISOs. The implementation of contingency analysis could be different among different ISOs.

In MISO, the RTCA tool simulates more than 11,500 contingency scenarios every 4 minutes [15]. Data from state estimator are utilized and contingency analysis is performed by solving contingency power flows independently. All the potential flow violations and voltage violations are recorded, as well as the associated critical contingencies [16].

PJM runs a full AC contingency analysis to identify the contingencies that would cause violations in the system [17]. Approximately 6,000 contingencies are simulated every minute at PJM [17]. Though there is a list of all contingencies in the PJM database, not all contingencies in that list are evaluated at all times [18].

A two-phase procedure is used in ERCOT to perform contingency analysis [19]. A heuristic screening procedure is conducted in phase one to identify the most severe contingencies with respect to post-contingency violations. Then, in phase two, fast decoupled power flow based full AC analysis is then performed on the selected contingencies as well as those explicitly chosen in advance. ERCOT has approximately 3938

contingencies, including 3333 branch contingencies and 605 generator contingencies, modeled in its operations database in 2012 [20]. RTCA in the ERCOT system executes every five minutes [20].

The RTCA tool used in CAISO simulates about 2,200 pre-specified contingencies every five minutes [21]. It would report potential overload and voltage violation following contingency, which alerts the system operator to critical contingencies.

NYISO performs RTCA on pre-defined single and multiple contingencies, which would provide system operator with a list of potential transmission violations [22].

The contingency analysis software used in ISO-NE executes every six minutes automatically or upon demand [23]. RTCA would sort flow violations and voltage violations by the percent severity and provide system operator only with the critical constraints of which the associated post-contingency flow is over 90% of the emergency limit [24].

2.2.6 Post-contingency Violation Management

Contingencies may result in system security violations such as voltage limit violations and branch overloads. It would further weaken the system if the right corrective actions are not implemented. For instance, a cascading failure or cascading outage may occur and cause system blackouts. Therefore, managing post-contingency violations is essential for the system secure operations.

For each critical contingency that would cause potential post-contingency violations, appropriate corrective actions should be determined in advance to ensure system

security in case a contingency actually occurs. A number of approaches are available to handle these violations. Some approaches are listed below:

- Economic dispatch,
- Committing fast-start units,
- Transformer tap adjustment,
- Phase shifter angle adjustment,
- Transmission switching,
- Load shedding.

The DC power flow based economic dispatch problem with additional network constraints can be solved to relieve flow violations. If fast robust algorithms and advanced computers are available, the AC power flow model based economic dispatch may also be used to relieve both flow violations and voltage violations. Committing fast-start units is an effective strategy but that may come with extra costs. Transformer tap adjustment and phase shifter angle adjustment are different approaches to mitigate violations. Transmission switching is also an effective way to reduce violations or even completely eliminate all the violations. Load shedding will always be the last option to resort due to the concern regarding economic loss.

The effect of transmission switching on post-contingency violation reduction is thoroughly investigated in this dissertation. Transmission switching is a low cost alternative in comparison to other corrective strategies presented above, which indicates transmission switching is a promising approach to relieve post-contingency violations.

2.3 Transmission Switching

It is very unlikely that a single network topology could be optimal for different operating hours or different system conditions. Network reconfiguration is a valuable strategy to build a smarter and more flexible power grid.

Traditionally, transmission network is considered as a static network for short-term operations of power systems. For example, the conventional economic dispatch or optimal power flow (OPF) model does not include the flexibility in transmission network. However, system operators are able to reconfigure the network in real-time and transmission switching can benefit the system in various aspects. Transmission switching that temporarily reconfigures the system network can be used to relieve branch overloads, eliminate voltage violation, reduce cost, and improve system reliability.

Redundancy of transmission networks is one of the reasons why there are flexibilities in the power system networks and why transmission switching can provide various benefits. Typically, transmission switching can provide more benefits for a meshed transmission network than a distribution network.

In this dissertation, the flexibility in transmission network is considered in RTCA and RT SCED via corrective transmission switching. With CTS, the violations reported from RTCA can be substantially reduced, which demonstrates the reliability benefits provided by CTS. Those reliability benefits can be translated into significant congestion cost reduction when CTS is considered in RT SCED. The reliability benefits with CTS are studied in Chapter 4 and the economic benefits with CTS are studies in Chapter 5.

A thorough literature review of transmission switching and network topology optimization is presented in [25]. Transmission switching can be used as a corrective strategy, a loss reduction method, and a congestion management tool. The existing industry practices are introduced in [25], as well as the benefits achieved with optimal transmission switching (OTS). The effect of TS on financial transmission rights markets is also analyzed.

Given a problem, the optimal solution with TS will be at least as good as the solution obtained without TS because the feasible set with TS is a superset of the feasible set without TS. A three-node system is used in [26] to illustrate the concept of TS. The applications of TS in various power system areas are introduced below.

2.3.1 TS in Unit Commitment

A formulation for co-optimizing unit commitment and transmission switching is presented in [27] to ensure *N*-1 reliability. Numerical studies show that the optimal network topology varies from hour to hour and that the optimal unit commitment solutions will be different. A decomposition method is proposed to reduce the computational burden. Another conclusion is that the need to start up a generator can be replaced by TS, which will translate into significant cost savings. For example, $120,000 can be saved with TS on the IEEE RTS96 test system in the time frame of one single day. It is also concluded that TS can benefit the system without jeopardizing the reliability.

In [28], TS is introduced in security-constrained unit commitment (SCUC) problem to relieve violations and reduce operation costs. Benders decomposition is used to divide the original complex problem into two simplified problems, unit commitment

master problem and TS sub-problem. Iterations between those two sub-problems are required. The proposed SCUC model with TS can be used for congestion management without causing additional cost [28].

Three algorithms for day-ahead corrective transmission switching are proposed in [29]. TS is incorporated in the *N*-1 contingency analysis model. The three approaches include 1) a mixed integer programming (MIP) in which the status of transmission line is represented by binary variables, 2) a heuristic based MIP in which only one switching action is allowed per iteration, and 3) a greedy algorithm. The most accurate MIP model is very hard to solve. On the contrary, the heuristic based MIP and the greedy algorithm are less complicated and relatively easy to solve. Numerical simulations show that the greedy algorithm can provide quality solutions with less solution time as compared to the other two approaches.

2.3.2 TS in Optimal Power Flow

A novel formulation for determining both the optimal transmission topology and the optimal generation dispatch is proposed in [30]. Numerical simulations on the standard IEEE 118-bus test case show that system operation cost can be reduced by 25% by optimizing the network topology. It is also observed that a switching action aiming for cost saving does not necessarily have a negative impact on reliability [30]. Reference [31] presents how network topology changes would affect energy markets. Simulation results indicate that topology changes for cost reduction typically result in lower load payments and higher generation rents. It is illustrated in [32] that incorporating transmission switching in the system dispatch application can reduce cost while the system

N-1 reliability still remains. With the *N*-1 DC optimal power flow (DCOPF) model, 15% savings are obtained through TS. Both [30] and [32] use the same IEEE 118-bus test system.

Although co-optimization of network topology and unit generation could achieve significant reduction in congestion cost, its MIP model is not solvable within a reasonable time even for moderate-scale systems. A shift factor based MIP model with TS was presented in [33]. A branch outage can be simulated with the original topology by using flow-cancelling transactions approach. The complexity of this problem highly depends on the numbers of switchable lines, monitored lines, and contingencies. The proposed shift factor based MIP formulation is more compact and more scalable than the conventional *B*-θ based MIP formulation and, thus, it is faster as verified by the simulation results. It would be more efficient when fewer constraints are explicitly enforced.

To solve optimal transmission switching problem efficiently, three different heuristics are proposed in [34], a DC heuristic with DCOPF, a DC heuristic with AC optimal power flow (ACOPF), and an AC heuristic with ACOPF. Case studies show that the two ACOPF based heuristics provide similar solutions while the results obtained by the DCOPF based heuristic are very different.

Heuristic policies based integration of TS in the OPF problem is discussed in [35]. A general algorithm structure is proposed in [35] and its objective is to determine the transmission topology in a reasonable time. Although the optimality is not guaranteed,

the proposed structure has the potential to attain high quality solutions for network topology and generations with a low computational effort. Simulation results on the IEEE 118-bus test system demonstrate the effectiveness of the proposed heuristic policies in terms of production cost reduction.

Based on the algorithm structure proposed in [35], three additional transmission switching policies are proposed in [36]: price difference, total cost derivative, and power transfer distribution factor (PTDF)-weighted cost derivative. These policies can provide production cost savings and maintain system reliability. The computational complexity of the proposed three policies is significantly lower than MIP-based approaches. The results show that the branches that the algorithm tends to switch are with low loading level, high degree of connectivity, and negative price differences.

Optimal transmission switching can reduce generation costs and the investment cost for implementing OTS is low. However, heavy computational burden is one obstacle to implement OTS. Two heuristics are developed in [37] to resolve this issue. They both rely on the line-ranking parameter derived from the optimal solution of a regular DCOPF problem. Case studies show that the proposed two heuristics are much faster than the previous methods in the literature while the cost reductions are similar.

Promising results are achieved in a reasonable time with the heuristics proposed in [35]-[37]. However, all of those heuristic approaches are based on the DC power flow model, which is an approximation of the accurate AC power flow model and may introduce errors. Extended from the DCOPF based heuristics proposed in [36] and [37], ACOPF based heuristics are proposed in [38]. Simulation results show that the DCOPF-

based heuristics may provide poor quality switching solutions that may even lead to cost increase. The ACOPF based heuristics have a better performance than DCOPF based heuristics at the cost of longer computational time. A conclusion made in [38] is that a good heuristic approach for practical application should be not only accurate but fast as well.

2.3.3 TS in Energy Markets

Transmission switching can be used to optimize transmission outages in a market environment [39]. Reference [40] demonstrates the economic value of transmission switching with the IEEE 73-bus (RTS96) test system. It is shown in [41] that OTS can improve economic dispatch not only on small test systems but also on large-scale ISO models.

Two novel concepts, just-in-time transmission and flowgate bidding, are presented in [42]. With just-in-time transmission, transmission elements that are switched off service per the optimal dispatch solution can be switched back into the system as needed. Branch flow is allowed to temporarily exceed the rated capacity for a penalty price, which is flowgate bidding. Simulation results on large-scale ISO systems demonstrate the effectiveness of those models.

2.3.4 TS in Expansion Planning

Transmission switching is not only able to provide benefits in short-term operation studies but also in long-term planning studies. It is shown in [43] that modeling transmission switching in system expansion planning can enhance the system security and reduce the total cost including the operation cost and investment cost.

2.3.5 TS in Load Shedding Recovery

A novel load shedding recovery control scheme through transmission switching is proposed in [44]. Following a critical *N*-1 or *N*-2 contingency, implementing transmission switching can reduce the amount of load that would be curtailed from the system. The system can return to an *N*-1 reliable state faster with TS.

2.3.6 TS in Congestion Management

The total congestion costs in the PJM system in 2013 increased by $147.9 million or 28.0% in comparison with the 2012 level $529.0 million [45]. Obviously, a tremendous amount of money has been wasted due to network congestion. Therefore, transmission congestion management is essential to operate power systems economically. As a corrective control scheme, transmission switching is able to relieve congestion or overloads.

With *N*-1 contingency criteria, transient stability, and voltage stability margin considered in [46], transient instability issues that exist in previous OTS methods can be resolved. It is also demonstrated that TS is an effective strategy to reduce congestion cost.

Congestion management with OTS is studied in [47]. Two different procedures are proposed for determining the best network topology with respect to security criteria. The first procedure models the TS problem with mixed integer linear programming (MILP). The second procedure employs an augmented genetic algorithm, which takes *N*-1 security constraints into account. Numerical simulations on the CIGRE sample 33-bus system and the 432-bus Extra High Voltage network of Italy show that solutions

obtained from those procedures are consistent while the deterministic procedure is twice as fast as genetic algorithm.

PJM has published a list of switching solutions that may reduce or even eliminate the violations [48]. Though this list is for informational purposes only, it indicates the importance of TS in congestion management. Those identified switching solutions are not guaranteed to provide benefits since the beneficial switching actions may vary based upon the system conditions. The implementation of the identified transmission switching solutions would be determined at the discretion of PJM operators. Therefore, a systematic methodology is desired to identify the beneficial switching solutions in real-time.

2.3.7 TS with Uncertainty

Recently, renewable energy sources including wind power are growing rapidly and the penetration level of renewables in power systems is increasing quickly. Thus, more attention have been paid on the system uncertainty. In addition, load profile cannot be precisely predicted, which also contributes to the system uncertainty.

Robust optimization can be used to handle the uncertainty. It is demonstrated in [49] that the switching solutions obtained from robust optimization will work for all possible system states. Given a pre-defined uncertainty set, TS can mitigate constraint violations. Simulation results show that TS does not necessarily degrade the system reliability and it may even benefit the system for achieving *N*-1 feasibility with uncertainty.

Implementing corrective switching might cause disconnection of wind farms that do not have the low voltage ride through function from the main grid. A methodology is proposed in [50] to determine feasible alternatives for eliminating violations in a reasonable time. Simulation results show that none of the switching variants would disconnect wind farms from the system even for the wind farms that are not equipped with low voltage ride through technology.

2.3.8 TS as a Corrective Mechanism

Transmission switching can benefit the system as a corrective control method in emergency situations. A strategy for evaluating switching actions is proposed in [51]. This strategy maximizes the minimal system security margin. An algorithm that combines line switching, bus-bar switching, and shunt switching is proposed to relieve overloads and voltage violations that are caused by system faults. Simulation results verify that the proposed corrective switching algorithm can effectively relieve system violations. Note that switching action can be implemented on different types of elements such as shunt and transmission line. However, this dissertation only focuses on transmission switching.

A greedy algorithm is proposed in [52] to improve the computational performance for the TS problem. A priority list of candidate switching lines is generated based on sensitivity. This heuristic is tested with various types of contingencies including *N-1* events, *N-m* events, and cascading events. Numerical simulations show that the proposed heuristic is able to provide quick TS solutions for load recovery by improving the deliverability of reserve. The computational complexity of the TS problem can be

reduced with the proposed heuristic by transforming a MILP problem to a linear programming (LP) problem. Therefore, it is possible to implement the proposed TS heuristic in real-time. Another advantage of greedy algorithm is that it scales well for large-scale systems while quality solutions would still be obtained.

2.3.9 Industry Practices

Though studies on transmission switching in the literature started in 1980s [53]-[55], TS has not been extensively used in industry today. The main concerns of implementing TS include reduction of system security margin, instability issue due to discrete switching actions, and long computational time required to solve the TS problems. However, with fast development of power engineering, optimization, and computer science technologies, those concerns and hurdles will be addressed eventually. Prior efforts in the literature have demonstrated that switching a line off service does not necessarily adversely affect the system and can benefit the system in various aspects.

Transmission switching has gained a lot of attention recently. The hardware to implement TS is mainly circuit breakers that already exist in contemporary power systems. The only requirement for implementing TS is to develop a decision support tool that can provide operators with beneficial switching solutions. Moreover, switching a line out of service should be fast enough for TS to be considered as a promising strategy in real-time operations. As switching actions would degrade circuit breakers and reduce their lifespan, it would be practical if TS is used as a corrective method or an emergency control scheme. Since the probability of the contingency is low, CTS would rarely need to be implemented. Thus, circuit breaker degradation due to CTS is minor.

In May 2009, as a result of the outages in the high voltage transmission system, significant congestion costs occurred for multiple days until CAISO was able to identify a TS action to relieve the congestion [56].

As documented in ISO-NE operating procedure No. 19 - Transmission Operation [57], TS is a viable option under both normal and emergency operating conditions and can be used to relieve transmission constraints.

PJM lists switching solutions as corrective actions in response to several specific contingencies [58]. In 2012, PJM took several high-voltage lines out of service as a corrective action in response to Superstorm Sandy to alleviate over-voltage problems [44]. Note that the system had already lost multiple high voltage transmission assets when TS was implemented.

Though there are several instances where TS is implemented in practice to accomplish particular objectives, the decisions are predominantly made based on lookup table methods or ad hoc procedures that may require operators' personal judgment. Such empirical methods or offline analysis will limit operators' capability of fully utilizing the flexibility provided by TS. As a result, the utilization of TS is limited in practice. Therefore, accurate, fast, and systematic approaches are desired and essential for the implementation of TS in industry.

2.4 Economic Dispatch

Economic dispatch determines the optimal outputs of a fleet of generating units to meet system demands with the least cost. As NERC requires bulk electric systems to

be able to withstand the loss of a single element and meet specific performance requirements [59], security constraints should be considered in economic dispatch. Economic dispatch that considers system security requirements is known as security-constrained economic dispatch.

There are two basic types of SCED: day-ahead SCED and real-time SCED. Day-ahead SCED is a multiple-period SCED that executes subsequent to the complete of the SCUC that determines units' commitment status for each hour. RT SCED is typically a single-period SCED that focuses on a short-term ranging from 5 minutes to 15 minutes. Note that day-ahead SCED and RT SCED are LP problems. This dissertation focuses on RT SCED.

As described in Chapter 1, RT SCED is a major EMS function for power system operations. For a real power system, SCED runs consecutively in real-time. Generally, SCED is an optimization process that aims to provide the least cost generation that meets all the operation and reliability constraints.

The system load profile changes constantly over time and would deviate from the forecast. As a result, the scheduled generator dispatch solution may not be optimal in terms of total system operation cost for the next SCED period. In addition, the uncertainty such as load fluctuation may cause unexpected violations, which would jeopardize the system reliability. Therefore, SCED that can effectively relieve system violations with the least cost is used as a regular mechanism for real-time operations of power systems in industry [60]-[61]. SCED can also be used to determine the energy prices in real-time markets [62]-[63].

As an essential module of EMS, RT SCED is studied in Chapter 5 of this dissertation. Procedure-A is first proposed to connect traditional RTCA and RT SCED, which is consistent with existing industrial practice. Then, Procedure-B is proposed to utilize the flexibility in transmission network. In Procedure-B, CTS is considered in SCED implicitly which requires no change to existing operational tools.

2.4.1 SCED with Renewables

Recently, with the advancement on the techniques for renewable energy sources, the penetration of renewables into power systems has increased significantly. Some renewables like wind power and solar power cannot be fully controlled. For instance, the generation from wind power largely depends on wind speed. Thus, they are also referred to as variable renewables. As the percent of variable renewables in power supplies has increased to a significant level, it is very important to consider the uncertainty of variable renewables in SCED.

As stated in [64], the conventional economic dispatch approach may not be able to properly accommodate the economic implication of power systems with significant level of penetration of renewables with high variability. Thus, [64] proposes an optimization model that can capture the variability cost of renewables by using the "best-fit" participation factors. Simulation results on two test cases demonstrate the effectiveness of the proposed approach as compared to the traditional method.

A stochastic look-ahead economic dispatch model and uncertainty response concept are proposed in [65] to manage uncertainty at the near-real-time stage. Scale reduction approaches and a hybrid parallel computing architecture are developed to speed

up the solution time. Case studies on a practical 5889-bus system illustrate the effectiveness of the proposed approach.

To address the challenges posed by integrating renewables into power grids, a stochastic decomposition framework for multiple timescale economic dispatch is proposed in [66]. The proposed framework determines the generation of slow-response resources hourly ahead, which allows slow-response resources to adjust in time; it also determines the generation of fast-response resources at a smaller sub-hourly timescale, which allows the system can better handle the variable RES. Simulations results demonstrate the effectiveness of the proposed framework by considering sub-hourly dispatch.

2.4.2 Decentralized SCED

For large-scale practical power systems, solving a centralized SCED directly might not be computationally efficient. Therefore, decentralized SCED may be an alternative in the case that centralized SCED does not solve efficiently. Another advantage of decentralized SCED is that it requires minimal information exchanged between different areas and, thus, it can help protect the privacy of each area.

A consensus algorithm based distributed economic dispatch approach that considers the effect of transmission losses and generator limits is proposed in [67]. The two consensus algorithms use different strategies to ensure power balance. Simulation results demonstrate the effectiveness and scalability of the proposed approach.

A decentralized and self-organizing economic dispatch approach is developed in [68]. Weighted averages of variables are used to obtain the economic dispatch solutions. Simulation results demonstrate the effectiveness of the proposed approach.

A multiple-stage decentralized approach is proposed to solve the economic dispatch problem in [69]. With a deterministic method, it consists of two stages; however, a third stage is required to obtain the final solution if a nondeterministic method is applied. The proposed approach can incorporate transmission losses and can be adapted for solving both convex and non-convex economic dispatch problems. Numerical studies on three cases verify the advantages of the proposed approach.

A decentralized dynamic multiplier-based Lagrangian relaxation approach is proposed in [70] for solving multi-area economic dispatch problem. The proposed method can solve to the global optimality faster and reflect the marginal cost change due to variation of power exchange level. Case studies performed on three systems show that the proposed method can significantly benefit large-scale multi-area power systems.

2.4.3 SCED with Automatic Generation Control

SCED dispatches generation in a timeframe of 5 minutes to 15 minutes. However, load demand fluctuates in seconds. To better resolve load variation and frequency deviation, automatic generation control (AGC) is employed to control frequency and maintain the system power balance in real-time. It is worth noting that the requirements for a unit to provide AGC service or regulation reserve are very strict and only a small subset of units are qualified as AGC service providers. Thus, coordination of AGC and SCED can better ensure sufficient regulation reserve in real time.

A distributed approach is proposed in [71] to enable each generator to re-dispatch its output independently. The proposed formulation combines economic dispatch and

AGC. Numerical simulations show that the proposed method can correct for frequency deviations using the aggregate power imbalance only.

The coordination between AGC and economic dispatch is studied in [72]. The traditional AGC is improved by using a distributed approach that combines economic dispatch with AGC. A hybrid of traditional AGC and the economic AGC is also studied. In this hybrid method, the power exchanges between different areas are fixed while the generators within their own areas can be re-dispatched. Case studies show that the hybrid AGC performs the best and it requires only local information.

An extensive model that accounts for inter-temporal coupling between multiple timescales is proposed in [73]. The proposed integrated model consists of SCUC, SCED, and AGC. It can model the interaction between different timescales and can better handle the variability and uncertainty of variable generations such as wind units.

2.4.4 SCED with Demand Management

Traditionally, loads are treated as fixed and uncontrollable in SCED. However, flexible demands are increasing. Some flexible demands can be directly curtailed by system operators at the cost of providing extra credits for the customers that participate the load shedding incentives program. Therefore, it is very important to capture demand management in SCED. As the shares of renewables in power supplies increase, demand side management can benefit the system by providing tertiary reserve capacity [74].

As stated in [75], many utilities opt to curtail load rather than bring additional expensive units online during peak-load periods. The authors of [75] argue that direct

control mechanism is more promising for real-time economic dispatch than price response mechanism as price signals cannot be used for services in real-time.

The value of demand response can be estimated with a production cost model such as a SCED model [76]. The work presented in [76] investigates the effects of demand response on ancillary service and shows that demand response can contribute to meeting the system ancillary service requirements.

2.4.5 Industry Practices

Economic dispatch was applied to adjust the outputs of online units as early as 1930s and it was initially solved by hand [77]. The classical AC OPF formulations was first developed in 1962 by Carpentier [78]. Even though the problem has been formulated for over 50 years, a fast, robust and reliable technique has not been developed to solve it due to its non-linearity, non-convexity, and large-scale features. As a result, the industry still uses a simplified linearized DC power flow model as described in Section 2.1.2. There are two DC power flow models: PTDF model and B-θ model. Typically, the PTDF model is used in industry rather than the B-θ model.

PJM

PJM real-time dispatch package has two main applications: intermediate-time SCED (IT SCED) and RT SCED. IT SCED performs resource commitment over four intervals corresponding to a look-ahead period of about 2 hours [79].

RT SCED does not change units' status and it dispatch online units in a single look-ahead period of 15 minutes. RT SCED runs about every 5 minutes or upon demand whenever operators believe re-dispatch is needed. The solutions obtained from RT

SCED have to be approved by operators before they are sent to generators. For each RT SCED run, three scenarios are solved independently. Those three scenarios are known as base scenario, high scenario, and low scenario [80]. The base scenario data are from EMS. The other two scenarios are biased against the base scenario. Compared to the base scenario, high scenario has a higher amount of load while low scenario has a lower amount of load. RT SCED co-optimizes energy, reserves, and regulation simultaneously [81].

IT SCED does not directly send signals to generators. However, it provides a 2-hour look-ahead dispatch trajectory and guides RT SCED [82]-[83]. IT SCED can also report potential warning information such as shortage of generation capacity to system operators so that they can take actions in advance.

It is worth noting that the RT SCED software used at PJM will only provide a basis for the locational pricing calculator engine which determines the locational marginal price (LMP). Locational pricing calculator runs exactly every 5 minutes [81].

MISO

The RT SCED tool used by MISO dispatches the energy and operating reserve to meet the forecasted energy demand and operating reserve requirements [84]. SCED executes continuously on a 5-minute periodic basis and the interval of its single look-ahead period is 5 minutes. RT SCED starts solving the problem five minutes before the start of the RT SCED target interval or 10 minutes prior to the end of the RT SCED dispatch interval. In other words, if the target interval of RT SCED is from t to (t + 5 minutes), then, RT SCED starts solving at the time of (t – 5 minutes).

Similar to PJM, the RT SCED application of MISO also uses an LP solver. Its objective is to minimize the total dispatch cost that excludes commitment costs such as start-up costs and no-load costs; because commitment costs are sunk costs for RT SCED [85].

ISO-NE

ISO-NE uses the unit dispatch system to perform SCED, which produces desired dispatch points for the generators in its territory. They have to be approved before they are sent to the generators. The desired dispatch points will refresh periodically on a 5-minute basis [86] as SCED executes every 5 minutes [87].

The single time-interval SCED of ISO-NE jointly optimizes energy and reserves and typically looks 15 minutes ahead [86], [88]-[89]. It uses an incremental linear-optimization method to minimize the cost and produces dispatch instructions for dispatchable resources. Real-time unit commitment (RTUC) is performed automatically every 15 minutes or manually on demand. The commitment status of fast start units in the approved RTUC scenario will be passed to the unit dispatch system that either uses RTUC recommendations or just ignores it [90].

NYISO

The real-time applications of NYISO include real-time commitment, real-time dispatch (RTD), and real-time dispatch/corrective auction mode (RTD-CAM) [91]. Similar to the IT SCED of PJM, real-time commitment is also a multi-period security-constrained unit commitment that minimizes the total production cost and co-optimizes

energy and reserves. Real-time commitment evaluates the system over a period of 2 hours and 15 minutes with intervals of 15 minutes.

RTD executes every 5 minutes and looks about an hour ahead [91]. It is essentially RT SCED. RTD-CAM overrides the regular RTD and executes on demand as determined by operators. Note that RTD-CAM may commit extra resources. RTD is a multi-period dispatch process that simultaneously co-optimizes energy and reserves without involving commitment decisions [92]. The objective function of RTD includes incremental energy cost. The solution for the first 5-minute look-ahead interval is immediately passed to the units while the solutions for other intervals are just for advisory purpose.

Security assessment is triggered periodically on a minute basis. It will provide a list of transmission constraints that will be reviewed for operations and would be sent into RTD as inputs.

CAISO

As a component of the Market Analysis Engine of CAISO, SCED is used to determine the dispatch base points of participating generators [93]. The main applications in the real-time market of CAISO include hour-ahead scheduling process, short-term unit commitment, real-time unit commitment, real-time economic dispatch, real-time contingency dispatch, and real-time manual dispatch [94].

Short-term unit commitment looks at least 3 hours ahead and commit short and medium start units for reliability purpose. RTUC looks 1 to 2 hours ahead and commit only fast and short start units. Though short-term unit commitment executes hourly

while RTUC runs every 15 minutes, they are both multi-period optimization processes with 15-minute intervals.

RTED performs generation re-dispatch to balance energy and normally executes on a 5-minute basis. However, under certain situations, real-time contingency dispatch and real-time manual dispatch would replace RTED and execute upon demand.

RTED uses SCED as the optimization engine to determine the least cost 5-minute dispatch solutions that meet the units and transmission constraints within CAISO territory. RTED is a multi-period optimization process that co-optimizes energy and ancillary services [95]. Only the dispatch solution associated with the first 5-minute interval will be implemented. RTED also calculates LMP for market financial settlement. The fixed time delay between the start time of each RTED run and the start time of the corresponding RTED target interval is set to 5 minutes. The time delay accounts for RTED computational time, operator approval time, and communication time [96].

ERCOT

In ERCOT, SCED determines the least-cost dispatch of all generating units to meet the short-term load forecast. SCED is scheduled to execute every 5 minutes in the ERCOT nodal market [97] and solves for a single interval of 5 minutes [98]-[99]. SCED can also be executed by ERCOT operators or other ERCOT systems [100]. It is interesting that the SCED used in ERCOT is a quadratic programming (QP) problem due to the fact that the cost function for the ERCOT system is quadratic [98]-[99].

In ERCOT, the SCED application typically minimizes the total real-time dispatch cost and determines the optimum generation dispatch while reliability constraints are

satisfied. The outputs of SCED also include LMP [101]. Energy and ancillary services are co-optimized for available resources in the day-ahead markets of ERCOT. However, currently, there is no co-optimization for the real-time markets [102]-[103]. Note that real-time co-optimization is considered as a new initiative to improve the ERCOT real-time markets [102].

The SCED application used by ERCOT runs twice per cycle. The two executions of SCED per cycle can reduce market power and ensure competition [100]. The first SCED execution observes the limits of competitive constraints only and determines reference LMPs; the second SCED execution observes the limits of all constraints and uses the adjusted energy offer curve based on the results of the first SCED execution. SCED produces LMPs as well as the price of system-wide reserves. Real-time contingency analysis identifies a list of constraints that will be sent to SCED and then SCED will re-dispatch generation to resolve the constraint violations [104].

Comparison

The RT SCED tools used by various ISOs are similar to each other but they still have some different features. A comparison between various ISOs' RT SCED applications is presented in Table 2.1. Normally, all six ISOs listed in Table 2.1 automatically run RT SCED every 5 minutes. Four ISOs implement a single time-interval RT SCED; however, the RT SCEDs used by the other two ISOs (NYISO and CAISO) look multiple intervals ahead but only implement the solution associated with the first interval. The actual dispatch signals sent to generators are for the next 5 or 15 minutes for all ISOs. All ISOs except ERCOT co-optimize energy and reserves in real-time operations

or RT SCEDs. The RT SCED model used in ERCOT is a QP problem due to the fact that the cost functions in the ERCOT markets are quadratic. PJM, MISO, and ISO-NE execute RT SCED with LP solvers while it is not very clear what formulations are used to model the SCED problems in NYISO and CAISO. To follow the most widely used features in industry, the SCED implemented in Chapter 5 of this dissertation is a single 15-minute interval LP based SCED that co-optimizes energy and reserves.

Table 2.1 Comparison between Various ISOs' RT SCED Applications

ISO	Execution cycle (minutes)	Single period or multiple periods	Only implement the solution of first period	Interval of the first period (minutes)	Look-ahead interval (minutes)	Co-optimize energy and reserve	Model
PJM	5	single	NA	15	15	Yes	LP
MISO	5	single	NA	5	5	Yes	LP
ISO-NE	5	single	NA	15	15	Yes	LP
NYISO	5	multiple	Yes	5	~60	Yes	Unknown
CAISO	5	multiple	Yes	5	Unknown	Yes	Unknown
ERCOT	5	single	NA	5	5	No	QP

NA denotes not applicable and "Unknown" means the associated information is not available publicly.

2.5 False Data Injection Attacks

In the EMS of modern power systems, state estimation executes regularly in real-time and serves as a core function in EMS for monitoring system condition. State estimation can effectively estimate the system status with the data transmitted from remote terminal units or local control centers through a communication network. As many applications such as RTCA and RT SCED rely on state estimation, it is critical to ensure the results of state estimation are accurate. Traditional bad data detection in state estimation can detect random bad data that are introduced by large measurement errors. However, recent efforts in the literature show that power system state estimation is

subject to false data injection attack [105]-[123]. A biased system condition caused by an FDI attack may mislead system operators to take incorrect actions which may cause severe violations or damage to power systems. Thus, a detection method that can efficiently detect FDI attacks is essential to enhance reliability of power system real-time operations.

2.5.1 FDI Attacks

FDI attack on power system state estimation has gained significant attention since it was first proposed by Liu in [105]. Both random FDI attacks and targeted FDI attacks are investigated and case studies show both attacks can change the DC state estimation results in an unobservable manner. Even if the attacker only has access to a specific subset of meters or can only compromise a limited number of meters, the proposed FDI attack can still efficiently launch an attack that will bypass the DC state estimation [105]. This proposed FDI attack is extended by the same authors to a generalized FDI attack [106]. The attack vector and attack impact are further analyzed and more detailed results are presented in [106].

Two regimes of attacks, a strong regime and a weak regime, are presented in [107]. The strong regime attack has access to a sufficient number of meters and can launch unobservable attacks. For the weak regime attack, unobservable attacks cannot be launched due to the fact that only a limited number of meters are under attackers' control. A generalized likelihood ratio detector is proposed in [107] to detect the weak regime attack.

A graph theory based algorithm is proposed in [108] to identify the locations where attackers can attack with the least-number measurements to keep the attack from being detected by AC state estimation. Hacking the least-number measurements would require minimal efforts of attacker to conduct an attack. Thus, the locations identified by the proposed algorithm would be the system vulnerabilities and may need more protection due to potential FDI attacks.

It is shown in [109] that attacker is capable of conducting an unobservable attack to power systems by introducing false measurements only within a subgraph that is determined by the subgraph algorithm proposed in [108]. An unobservable attack may result in a false estimated system state and mislead operators to take actions that could cause damage to the physical system. Simulation results also show that DC model based attacks can be easily detected by AC state estimation while AC model based attacks are unobservable.

Reference [110] extends [109] to investigate the physical consequences of false data injection attacks on power system state estimation. In the proposed FDI attack approach, a bi-level optimization is first conducted to determine the values of the state variables associated with the attack subgraph, which can result in the maximum physical flow on a target branch; then, those values are used to calculate the false measurements that can bypass AC state estimation. Numerical simulations demonstrate the proposed unobservable attack can cause physical overloads that may result in system damage or even outages.

Though the FDI attack approach proposed in [110] can launch an attack that is unobservable to system operators and causes branch overloads, it cannot converge for the IEEE-118 test system in a reasonable time [111], which indicates it does not scale. Therefore, three computationally efficient algorithms are proposed in [111] to speed-up the solution time and provide boundaries on system vulnerability. In addition to the three algorithms presented in [111], reference [112] proposes a Benders' decomposition based algorithm that can also solve large-scale systems in a reasonable time. In [112], vulnerability assessments are performed and conclude that there is a positive correlation between the level of congestion and the level of vulnerability.

Though references [109]-[112] show that the unobservable FDI attack approach can physically overload a branch, they all assume that the attacker has knowledge of the entire network topology, branch parameters, and generator parameters, status, and cost functions. However, all this information is actually very hard to obtain. Therefore, an FDI attack model with limited information is proposed in [113]. Simulation results demonstrate that the proposed attack model can launch successful attacks with limited local information. Built upon [113], [114] proposes an FDI attack model that uses even less information than [113]. The information used in this proposed FDI attack model is strictly limited to the attack sub-network only. The information outside the attack sub-network are estimated with measurements within the attack sub-network. Simulation results illustrate that the proposed attack model with information only from the attack sub-network can launch a successful attack.

As illustrated in [105]-[114], attacker can compromise system state through FDI attack. Furthermore, attacker can also launch topology attack. In [115], state-preserving topology attack is investigated and an algorithm is proposed to determine the minimal attack sub-network. With the proposed algorithm, state-preserving topology attack can change the topology without being detected and thus is unobservable.

Built upon [115], a systematic malicious state-and-topology attack strategy is proposed in [116]. This topology attack changes both the state data and topology data of a sub-network in order to cover a physical topology attack, which is taking a single or multiple branches out of service physically. Numerical simulations show that the proposed state-and-topology attack can cause physical branch overloads and the successful rate of such attacks is very high, which indicates that the system is vulnerable to the proposed state-and-topology attack.

2.5.2 FDI Attack Detection

As introduced above, recent work [105]-[116] demonstrates that power systems are subject to FDI attacks which are unobservable and can cause severe physical consequences. Therefore, it is very important to develop effective approaches to detect FDI attacks.

In [117], a specific set of measurements are selected and protected in order to detect the FDI attack that is proposed in [105]. Two approaches, brute-force search and protecting basic measurements, are proposed to strategically identify the smallest set of measurements that need to be protected from being manipulated.

Random bad data injection and stealth bad data injection are discussed in [118]. Random bad data injection can be identified and will not bypass state estimation. However, state estimation cannot detect stealth bad data injection. Thus, a detection method against stealth bad data injection is proposed in [118]. This proposed defense strategy conducts real-time statistical analysis on a sequence of data and minimizes the detection delay while enforcing the error probability constraints. Numerical simulations demonstrate that the proposed defense strategy can detect a stealth data injection attack in real-time at the minimum cost of delay.

As attacker is typically restricted to a small sub-graph, injected false data is sparse in the temporal measurements matrix. In addition, intrinsically, the dimensionality of temporal measurements of power grid states is low [119]. Based on these two facts, a novel FDI attack detection mechanism is proposed in [119]. Two different methods, nuclear norm minimization and low rank matrix factorization, are used in this detection mechanism to separate the nominal power grid states and the anomalies. Numerical simulations demonstrate the effectiveness of the proposed mechanism.

A real-time mechanism is proposed in [120] to detect FDI attack on power system state estimation. Potential anomalies can be identified by evaluating spatiotemporal correlation between system states. The proposed detection mechanism consists of three phases, spatial-pattern recognition and temporal-pattern-consistencies evaluation, trust-based voting, and system condition inference. Simulation results demonstrate that the proposed FDI attack detection mechanism can provide an accurate and reliable solution.

A novel FDI attack detection method is proposed in [121] with the assumption that the probability distributions derived from measurement variations among adjacent time steps should be consistent or similar. The distance between two probability distributions, which is calculated by Kullback-Leibler distance, should be small under normal condition but can be very large under an FDI attack. Numerical simulations demonstrate that the proposed approach can detect most of the attacks by tracking the dynamics of measurement variations.

Based on the generalized likelihood ratio, a new centralized sequential detector is proposed in [122] to efficiently detect FDI attacks. The proposed detection approach can scale with the number of measurements in the system. In addition, a distributed sequential detector that employs the adaptive level-triggered sampling technique is proposed for wide-area monitoring in power systems. Simulation results demonstrate the effectiveness of the proposed centralized and distributed FDI detectors.

A least-budget defense strategy is proposed in [123] to protect power system state estimation against FDI attacks. The behavior of a rational attacker is first formulated, followed by the investigation of how the attacker and defender interact with each other. Selection of the meters that need to be protected is formulated as a mixed integer nonlinear programming problem. Benders' decomposition is applied to efficiently solve this meter selection problem. Numerical simulations demonstrate that the proposed approach can achieve quality solutions in a reasonable time.

2.6 Parallel Computing

As the rapid development of computer technology, computers with multiple cores are easily available today. High performance computing employs multiple threads to run computationally heavy programs such as weather forecasting [124]. With the high performance computing techniques, a problem can be divided into separate sub-problems that will be solved simultaneously with multiple processes. High performance computing has gained a lot of attention since it can significantly reduce the solution time. Another commonly used term for high performance computing is parallel computing.

Based on memory access pattern, there are basic two types of parallel platforms: shared memory and distributed memory. For shared memory based parallel computing, the memory of a single computer can be accessed by each thread and all threads share the same memory. For distributed memory based parallel computing, the memory accessed by each thread is private to itself and cannot be accessed by other threads.

A number of tools that provide user-friendly interfaces have been developed to support parallel programming. It makes parallel programming attainable for real-world applications. Some popular parallel computing tools include Pthreads [125], Message Passing Interface [126], MPJ Express [127]-[128], Compute Unified Device Architecture [129], and Coarray [130].

There is a tradeoff between the costs and benefits of implementing parallel computing. The costs include the added programming difficulty, new classes of bugs in a parallel program, and expensive hardware. In general, small-scale problems are not

worth the effort for implementing parallel computing. For computationally intense applications, the benefits may outweigh the costs as the solution time can be significantly reduced.

2.6.1 Motivation of Parallelism

Though parallel programming is much more complex to implement than sequential programming and it is harder to maintain parallel programs than sequential programs, parallel computing is gradually gaining popularity. A variety of reasons for using parallel computing are listed below:

- Sequential program is not able to fully use the computer resources with multiple central processing units (CPUs).
- A number of standardized parallel libraries are available, which makes the implementation of parallel programming easier.
- There is a need to solve large-scale computationally expensive problems in a limited time window. With the speed-up benefit provided by parallelism, it becomes possible for solving computationally challenging problems in real-time.
- Computers with multiple cores can be easily obtained.
- The cost of cluster, large parallel platform, keeps decreasing while the quality keeps increasing.
- Multicore systems with parallel computing can break the bottleneck caused by the limited efficiency improvement of one single CPU.

Thus, parallel computing is implemented in this dissertation to speed-up the solution time for contingency analysis and corrective transmission switching since both of them are parallelizable and easily to implement.

It is worth mentioning that there may be some serial sections that cannot be divided into sub-tasks in a parallel program. In addition, certain problems are very hard to parallelize and have to be solved sequentially.

2.6.2 Amdahl's Law

The concept of speedup that could be achieved by parallel computing is defined as the equation given below,

$$S_n = T_s/T_n \tag{2.5}$$

where, n denotes the number of threads; T_s denotes the computational time of the sequential program; and T_n denotes the computational time of the parallel program with n threads.

It is intuitive that the serial sections of a parallel program will pose a limit to the efficiency of the parallel effectiveness. This is expressed by Amdahl's Law [131], which denotes the maximum possible speedup $S_{p,max}$ that could be achieved with n threads, as given by the equation below,

$$S_{p,max} = \frac{1}{(1-p)+p/n} \tag{2.6}$$

where p is the proportion of the program for which the code can be parallelized. For example, if p=8/9, then the maximum speed-up is 9 no matter how many threads/CPUs are used. Application of Amdahl's Law is to decide whether parallelization is worthwhile. Ideal linear scale may occur when the speedup is n with n threads, i.e. S_n=n.

However, serial sections of a program are obstacles to achieve it. It is important to recognize the performance bottlenecks of parallel computing in each specific problem. They may vary for different applications.

Though Amdahl's Law determines maximum speed-up, it is very difficult to achieve the maximum speed-up in reality due to the following possible reasons:

- parallel tasks are not evenly assigned to each thread,
- cost of communications and synchronizations between threads,
- cost of invoking and killing threads,
- cache availability and memory availability.

Another metric to measure the effectiveness of parallel computing is the parallel efficiency as defined below,

$$E_p = \frac{S_p}{p} = \frac{T_s}{pT_p} \tag{2.7}$$

A strategy that may increase parallel efficiency is using *n*-1 CPUs where *n* is the number of CPUs on a single computer while one CPU is kept idle to deal with the regular tasks of operating systems.

2.6.3 Parallel Computing in Power Systems

Parallel computing can significantly reduce the computational time as compared to sequential simulations. Thus, parallel computing techniques are applied to solve the computationally expensive problems in power systems.

A parallel particle swarm optimization (PSO) algorithm is developed in [132] to solve the OPF problem. Numerical studies show that solution time of the PSO algorithm can be reduced with parallel computing while quality solutions retain. Another parallel

computing based PSO algorithm is developed to solve the dynamic optimal reactive power dispatch problem [133]. It is divided into several independent sub-problems that can be solved simultaneously. Simulation results show that parallel computing achieves significant reduction in solution time.

A transient stability-constrained unit commitment model is presented in [134]. In this model, transient stability constraints are incorporated in the unit commitment problem. Thus, transient stability-constrained unit commitment is a very intensive problem. Parallel computing is conducted to speed up the solution time and simulation results demonstrate the effectiveness of parallel computing.

Transient stability-constrained optimal power flow can minimize the total cost while maintaining the stability performance. However, Transient stability-constrained optimal power flow is a very complex and intensive problem. To deal with this difficulty, a two-level parallel reduced-space interior point method is proposed in [135]. Case studies indicate that the proposed two-level method can obtain quality solutions and convergence properties while computational time is largely reduced. A hybrid dynamic optimization approach is proposed in [136] to solve stability-constrained optimal power flow problem. It is shown that the efficiency and scalability of the proposed approach can be improved with parallel acceleration.

A transient stability analysis application using parallel computing runs in real-time at PJM [137]-[138]. This application can complete the simulation every 7 minutes per circle on the large-scale practical PJM system that has about 15,000 buses and around 3,000 generators. In each circle, about 1,000 contingencies are simulated.

As described in Section 2.3, transmission switching can benefit the system in various aspects such as cost reduction. Quality solutions can be obtained even with a single switching action. The process to investigate each single switching action is independent. Thus, parallel computing can be used to develop a scalable TS algorithm. With parallel computing, it is possible to implement advanced transmission switching algorithms in real-time. For instance, a parallel implementation of three TS algorithms is presented in [139].

3. REAL-TIME CONTINGENCY ANALYSIS

Flow violations and voltage violations can compromise secure operations of power systems and cause system damage. It is worth noting that even if no violation exist in the base case, severe violations may still be observed when contingencies occur. In addition, contingencies may have negative impact on system stability. Therefore, power systems are subject to contingencies and it is very important to conduct real-time contingency analysis to identify critical contingencies that would cause violations.

As an essential EMS function, real-time contingency analysis runs a series of power flow studies simulating each contingency in the contingency list and determines the critical contingencies and the associated flow violations and voltage violations, which allows operators to be aware of the potential system vulnerabilities beforehand. Thus, with RTCA, operators can make corrective control schemes such as the proposed CTS strategy in advance and implement them to handle post-contingency violations only when a critical contingency actually occurs; alternatively, operators can also proactively adjust the system to eliminate those potential post-contingency violations.

To determine the system vulnerabilities and examine the performance of the proposed CTS strategy for post-contingency violation management, RTCA is first performed and the results are analyzed in this chapter; then, the proposed CTS technique to handle the potential post-contingency violations is studied in the next chapter.

An assumption made in this dissertation is that all elements are equipped with protection devices. Thus, an element that is under contingency would be completely deenergized and removed from the system.

Most of the work presented in this chapter and the next chapter have been done as a part of the project, “Robust Adaptive Topology Control”, under the Green Electricity Network Integration program funded by Advanced Research Projects Agency - Energy under U.S. DOE.

3.1 Modeling

OpenPA version 1 [140] is used as the AC power flow solver in this dissertation. It is an open-source tool written in Java and it was initially developed in 2013. It does not have the capability of enforcing the generator reactive power limits. However, the author of this dissertation has implemented that functionality in this tool. Note that switched shunts and transformer taps are fixed in the fast decoupled power flow algorithm implemented in this tool. This tool also assumes that the contingency element is isolated from the main grid and is entirely removed from the system model.

In the case of a branch contingency, it is assumed that all generators remain at the same generation level as the pre-contingency condition. The change in losses is reflected by the slack bus.

In the case of a generator contingency, it is not practical to pick up the entire generation loss only by the slack bus. Thus, a simple fast participation factor based approach is used in this dissertation to re-dispatch the generations after a generator contingency. Due to data availability, inertia and reserve are not used to calculate the participation factors. The upper limit of generator’s active power may be violated if a capacity based participation factor is implemented. Therefore, as shown in (3.1) and (3.2),

an available capacity based participation factor is implemented in this dissertation to perform generation re-dispatch after a generator contingency,

$$F_{gc} = \frac{P_{g,max} - P_g^0}{\sum_{\forall g, g \neq c}(P_{g,max} - P_g^0)} \tag{3.1}$$

$$P_g^c = P_g^0 + P_c^0 F_{gc} \tag{3.2}$$

where F_{gc} is the participation factor of unit g under generator contingency c; P_g^0 is the active power output of unit g in the pre-contingency state; P_c^0 is the MW output of the contingency generator c in the pre-contingency state; and P_g^c is the active power output of unit g under generator contingency c in the post-contingency situation. Note that this method can be easily modified to consider generator ramping limits or use other participation factors.

3.2 Contingency List

For a large-scale system, there could be thousands of possible contingencies. As introduced in Section 2.2.5, the ISOs only simulate selected contingencies. However, to provide a comprehensive study, all potential important contingencies excluding radial branches are simulated in this dissertation. The low-voltage network is usually referred to as distribution network or sub-transmission network, which is not a main concern to the ISOs. Thus, low-voltage (less than or equal to 70 kV) branches are not included in the contingency lists for ERCOT and PJM. Similarly, low-voltage branches and low-voltage buses are excluded in the monitored set for ERCOT and PJM. For a transformer, the voltage of high-voltage end is considered to be its voltage level in this dissertation.

A bus is defined as a one-bus-island if it connects to only one bus. In Fig. 3.1, load bus *m* is a one-bus-island since it only connects to bus *n*. If branch 1 experiences a forced outage, the flow on it in the pre-contingency situation will be entirely transferred to branch 2 in the post-contingency situation and no other network flow would change. If a contingency on branch 1 causes flow violation on branch 2, the only solution for reducing that violation is to shed the load at bus *m*; and transmission switching will not provide any benefit in this case. The main goal of this chapter and Chapter 4 is to investigate the potential benefits of corrective transmission switching in terms of post-contingency violation reduction. Therefore, the branches that connect to one-bus-islands are excluded in the contingency list in this dissertation.

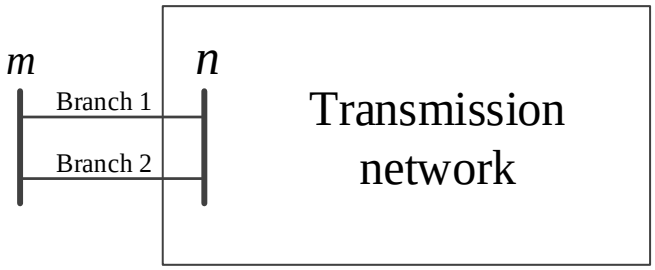

Fig. 3.1 Illustration of a One-Bus-Island.

3.3 Critical Contingencies

A contingency that does not cause any violation will not be considered as a critical contingency in this dissertation. It is not uncommon that a contingency only causes a very small amount of violations, which is negligible. Therefore, tolerances are used to determine the critical contingencies that would cause significant violations. A contingency is considered to be critical if it causes violations beyond the tolerances. In this dissertation, the tolerances are set to 5 MVA for flow violation and 0.005 per unit for

voltage violation. Both metrics are based on an aggregate level. To be more specific, only contingencies that cause a total flow violation greater than 5 MVA or a total voltage violation greater than 0.005 per unit will be considered to be critical. In this dissertation, the voltage upper limit and lower limit are set to 0.9 per unit and 1.1 per unit respectively.

3.4 Case Studies

Three large-scale real power systems are used for the studies in this chapter and Chapter 4. They are the Tennessee Valley Authority (TVA) system, the ERCOT system, and the PJM system. The computer platform used in Section 3.4 and Section 4.4 is a 64-bit Windows 7 Enterprise operating system that has four physical Intel(R) Core(TM) i7-3770 3.40 GHz CPUs. Each physical core can be hyper-threaded, which means that eight logical threads are available on that computer platform. The simulation for the TVA model and the ERCOT model are performed with one single thread via a sequential program, while the simulations for the PJM model are performed with six threads via a parallel program due to the computationally complexity of the PJM model.

The TVA cases are created based on the data provided for three days (72 hours) of September 2012. The modified TVA network contains about 1,800 buses and 2,300 branches and more detailed information can be found in [141]. The data received from ERCOT and PJM are the original EMS snapshots. Three snapshots of the ERCOT system and 167 snapshots of the PJM system are studied in this dissertation. No modification is made to those EMS real-time cases. The 167 snapshots of the PJM system represent the data of seven consecutive days, from July 14th (Sunday) to July 20th 2013, in

hourly resolution. The ERCOT system consists of around 6,400 buses and 7,800 branches. PJM is the largest system among those three systems and it contains about 15,500 buses and 20,500 branches. The details of those three systems are presented in Table 3.1. One difference between the TVA system and the other two systems is that the network topology is fixed for the TVA cases while it varies in different scenarios for the ERCOT system and the PJM system.

Table 3.1 Description of the Practical Systems

System	# of scenarios	Load (Real GW, Reactive GVAr)	# of buses	# of generators	# of branches	# of lines	# of transformers
TVA	72	~(24.0, 4.0)	~1,800	~350	~2,300	~1700	~600
ERCOT	3	~(56.9, 7.6)	~6,400	~700	~7,800	~6,150	~1,650
PJM	167	~(139.0, 22.4)	~15,500	~2,800	~20,500	~14,300	~6,200

Power flow convergence is a common technical hurdle that has received a lot of attention in the literature. This issue is beyond the scope of this dissertation and the contingency power flows that do not converge are simply ignored. It is worth mentioning that the divergence rate for the three practical systems is around 0.1%, which is very low and will not affect the statistical results and the associated conclusions in this dissertation.

Table 3.2 shows the cumulative statistical results of TVA, ERCOT, and PJM over all cases examined. The last row presents the cumulative results of those three systems. Over 1.5 million contingencies are checked for potential system vulnerabilities. Though less than 1% of the contingencies simulated cause network violations, the system security is still subject to a subset of contingencies.

Table 3.3 shows the average statistical results of TVA, ERCOT, and PJM over all cases examined. There are about 59, 13, and 48 critical contingencies per scenario on average for the TVA system, the ERCOT system, and the PJM system, respectively.

Table 3.2 Cumulative Statistics of Contingency Analysis

System	# of scenarios	# of contingencies simulated	# of contingencies not converged	# of contingencies that cause violations	# of critical contingencies
TVA	72	126,449	130	15,540	4,272
ERCOT	3	13,044	12	52	40
PJM	167	1,437,749	1,757	11,100	8,064
"*Sum*"	242	1,577,242	1,899	26,692	12,376

Table 3.3 Average Statistics of Contingency Analysis

System	# of scenarios	# of contingencies simulated	# of contingencies not converged	# of contingencies that cause violations	# of critical contingencies
TVA	72	1,756	1.8	215.8	59.3
ERCOT	3	4,348	4	17.3	13.3
PJM	167	8,609.3	10.5	66.5	48.3

3.5 Parallel Computing

The parallel computing tool used for the analysis in this dissertation is MPJ Express, an open source Java parallel computing library. The hardware used for the parallel computing simulations conducted in this section and Section 4.5 is cluster “cab” [142] at Lawrence Livermore National Laboratory.

Table 3.4 shows the average solution time with different threads for the contingency analysis simulations conducted on three large-scale practical systems. Note that simulations with less than 8 threads are not performed on the PJM system due to computational complexity. It is observed that as the number of threads increases, the solution time decreases as expected. The solution time for the TVA system comes down to 0.70 seconds with 128 threads as compared to 48.55 seconds for a sequential run with

a single thread. The sequential contingency analysis takes about 900 seconds for the ERCOT system, which is reduced to around 10 seconds by using parallel computing with 128 threads. For the PJM system, the solution time reduces to about two minutes with 128 threads from almost half an hour with 8 threads. Therefore, it demonstrates the effectiveness and efficiency of parallel computing for contingency analysis problem on the TVA, ERCOT, and PJM systems.

Table 3.4 Average Solution Time of RTCA with Different Threads

	Average solution time / s							
# of threads	1	2	4	8	16	32	64	128
TVA	48.55	24.54	12.72	6.88	3.67	2.00	1.11	0.70
ERCOT	898.84	454.82	231.12	122.69	62.96	33.04	17.56	10.09
PJM	NA	NA	NA	1633.76	855.72	444.75	233.78	128.41

NA: not applicable.

Fig. 3.2 shows the solution time of RTCA with different threads on the ERCOT system. It is obvious that the solution time decreases as the number of threads increases and it is very convincing that parallel computing can significantly relieve computational burden.

Overhead, the indirect or excess undesired computation time, would increase as the number of threads increases, which would result in reduction of parallel efficiency. As shown in Fig. 3.3, the parallel efficiency for contingency analysis decreases as the number of threads increases. However, the parallel efficiency is still very high (80%) with 128 threads, which indicates parallel computing for contingency analysis is worth implementing.

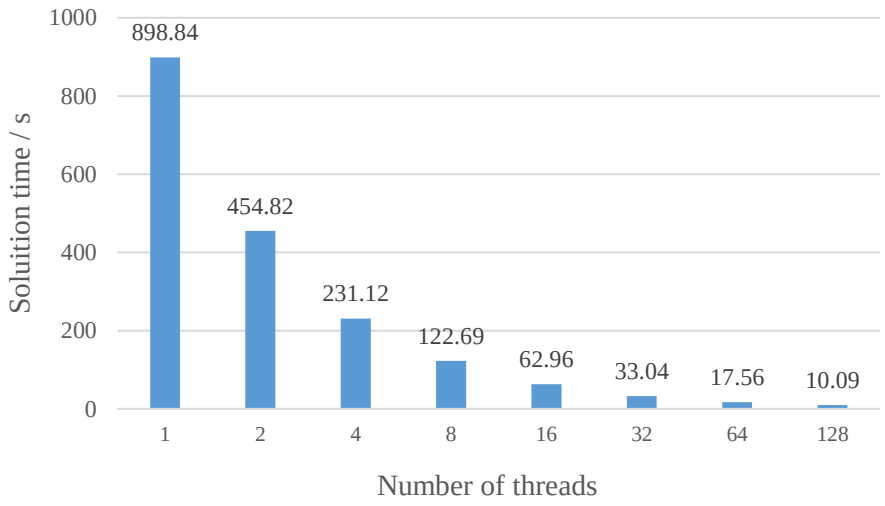

Fig. 3.2 Average Solution Time of RTCA on the ERCOT System.

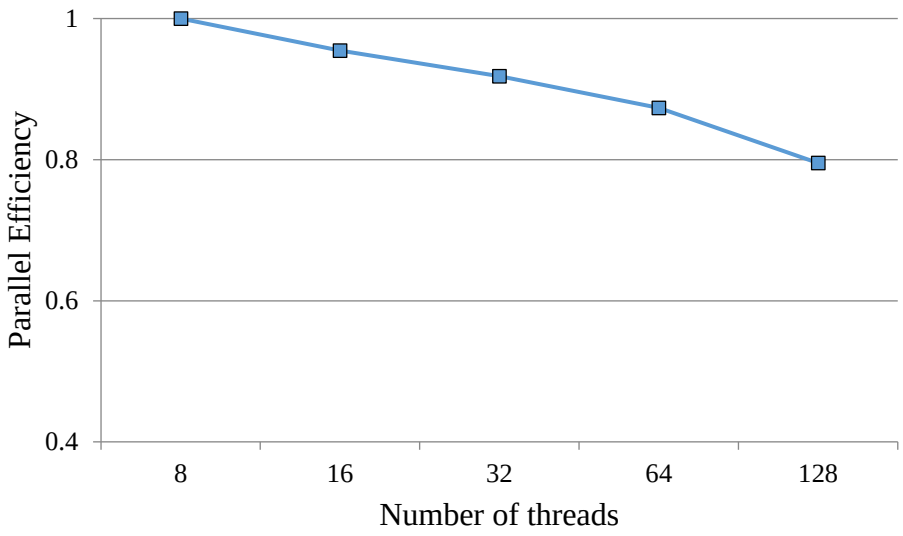

Fig. 3.3 Average Parallel Efficiency of RTCA on the PJM System.

3.6 Conclusions

In this chapter, traditional real-time contingency analysis is performed on three large-scale practical power systems, TVA, ERCOT, and PJM. The contingency list is first generated and, then, critical contingencies are identified by performing contingency analysis. Numerical simulations show that each system is vulnerable and the system security is subject to several critical contingencies. Since the simulation for each

contingency scenario is independent, parallel computing is implemented to speed up the RTCA process. In the next chapter, corrective transmission switching will be performed on those critical contingencies and the potential benefits, with respect to post-contingency violation reduction, that can be achieved with CTS will be investigated.

4. REAL-TIME CONTINGENCY ANALYSIS WITH CORRECTIVE TRANSMISSION SWITCHING

Failure of system elements may have negative effects on the power system security. Thus, real-time contingency analysis is essential to examine the system condition. With RTCA, the potential post-contingency violations would be identified and reported to system operators. Then, preventive and corrective strategies can be determined in advance to eliminate the system vulnerabilities. Transmission switching is proposed in this dissertation as a corrective strategy to reduce violations and maintain a reliable system.

In Chapter 3, it is assumed that the contingency element would be entirely removed from the system model. This assumption also holds for corrective transmission switching. A branch that is switched out of service is also modeled as fully de-energized with breakers at both ends of the branch opened.

Real-time contingency analysis is an essential module of modern energy management systems and is the key to foreseeing the potential post-contingency violation that may reduce system security margin as introduced in Section 2.2 and Chapter 3. Multiple traditional strategies such as economic dispatch are available to deal with post-contingency violations. However, they may be costly. Therefore, corrective transmission switching is proposed as an inexpensive alternative to the traditional corrective strategies. CTS is a switching action that temporarily reconfigures the network by taking a branch out of service shortly after a contingency occurs to achieve a particular goal, which is violation reduction in this dissertation.

The procedure for real-time contingency analysis with corrective transmission switching is illustrated in Fig. 4.1. The system condition in the pre-contingency situation, referred to as the initial point, is simulated by running a power flow program for the basic case. Contingency analysis is then performed to identify critical contingencies that would cause violations beyond the thresholds. Those identified critical contingencies are then examined by the corrective transmission switching routine. For each critical contingency, switching candidates in the CTS list will be enumerated and the top five beneficial switching solutions will be identified, which will provide system operators with choices. This process repeats until all critical contingencies are examined.

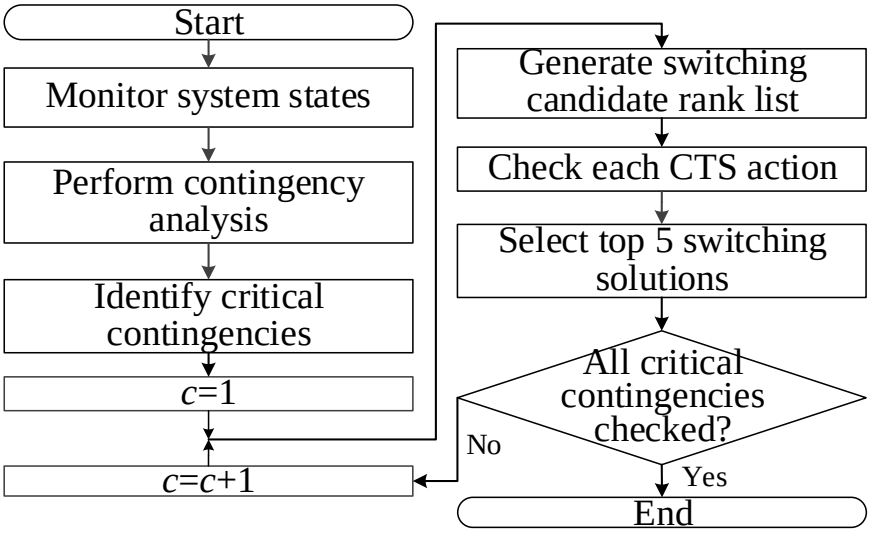

Fig. 4.1 Procedure of Contingency Analysis with Corrective Transmission Switching.

4.1 Concept of CTS

Transmission switching disconnects a transmission element out of service shortly after a contingency occurs to reduce violations. This is referred to as corrective transmission switching, which is the proposed approach for handling post-contingency violations. Note that only one corrective switching action will be implemented at a time.

This section will present the fundamentals on how corrective transmission switching functions as an effective corrective mechanism in terms of post-contingency violation reduction.

The voltage contours of the pre-contingency, post-contingency, and post-switching stages in Fig. 4.2 show that CTS fully eliminates all the voltage violations caused by a transmission contingency. The network shown in Fig. 4.2 is a 500 kV level portion of the TVA system, which is lightly loaded for this particular case. In the pre-contingency state, the line that is the CTS solution produces reactive power, which travels through the contingency line into the eastern area of this network. In the post-contingency state, more than the required reactive power has to stay in the affected area since the contingency line is no longer available to deliver the excessive reactive power out of this area, which leads to over-voltage violations. In the post-switching state, the source element producing the excessive reactive power, which is identified as the switching solution, is removed from the system; hence, all the over-voltage violations are eliminated.

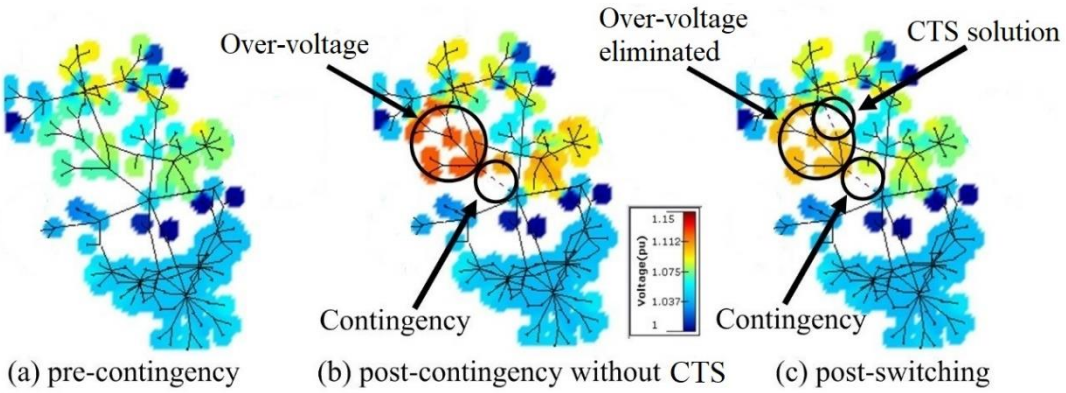

Fig. 4.2 An Example of Voltage Violations Fully Eliminated by CTS [141].

Fig. 4.3 shows an example in which CTS fully eliminates the flow violations caused by a transmission contingency. It is simplified from an actual example of the TVA system. The branch loading levels in the pre-contingency, post-contingency, and post-switching states are presented in Table 4.1. This example demonstrates flow violations can be eliminated with CTS.

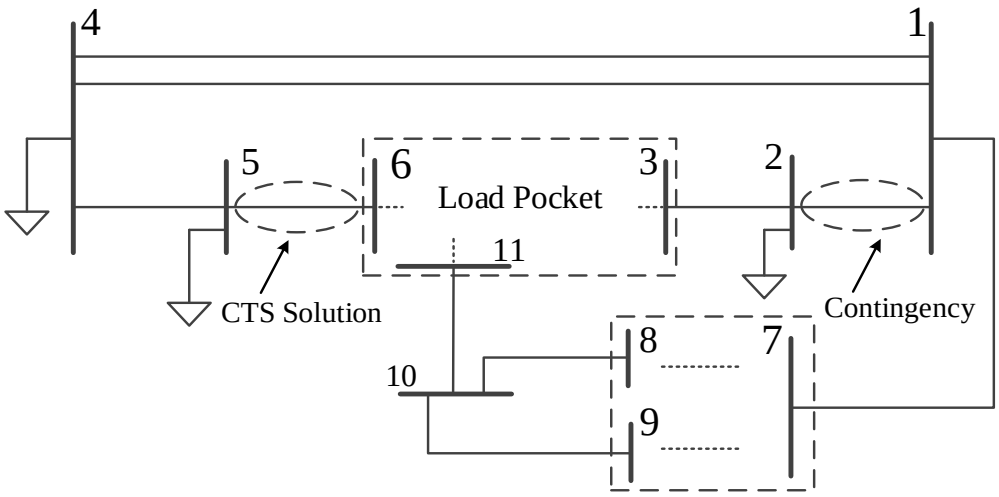

Fig. 4.3 An Example of Flow Violations Fully Eliminated by CTS.

Table 4.1 Branch Loading Levels in the Pre-Contingency, Post-Contingency, and Post-Switching States for the Example Shown in Fig. 4.3

Branch FromBus - toBus	Loading level		
	Pre-contingency	Post-contingency	Post-switching
1-2	44%	NA	NA
2-3	40%	-4%	-4%
1-4	74%	104%	46%
4-5	75%	122%	29%
5-6	49%	96%	NA
1-7	2%	7%	27%
8-10	26%	31%	45%
9-10	38%	46%	67%
10-11	9%	22%	56%

The two parallel lines connecting bus 1 and bus 4 are identical, which indicates that the power flows on them will be the same. The negative sign in Table 4.1 means the flows travel in the opposite direction of the reference direction. All branch flows are within the capacity limits in the pre-contingency state. In the post-contingency state, more power must travel through the path with bus 1, 4, 5, and bus 6 on it to serve the load pocket area, which causes overloads on line 1-4 and line 4-5. By simply switching line 5-6 out of service, the power can still be delivered to the same load pocket through other route while the post-contingency flow violations are eliminated. This particular case represents a total flow violation of 96.1 MVA which is fully eliminated with one single switching action and no additional violation is introduced.

Though the switching action significantly increases flows on lines 9-10 and 10-11 in the post-switching situation in this example, it may not cause a significant change in market settlement as CTS is proposed as a corrective action for contingency situations

only. The market settlement for emergency situations is different with the market settlement for normal situations. Manual adjustments may be involved and abnormal market results would be avoided.

4.2 Metrics

Two metrics, average violation reduction at an aggregate level and Pareto improvement (PI) at an elemental level, are proposed in this dissertation to determine whether a switching action is beneficial. Another metric, depth, is proposed to estimate the effectiveness of the proposed CTS algorithms. Note that depth will not be used to identify the beneficial CTS solutions.

4.2.1 Average Violation Reduction

Average of violation reduction in percent (average violation reduction) is proposed in this dissertation to investigate how much violation can be reduced with CTS. This metric measures the effectiveness of CTS at an aggregate level and is defined in (4.1),

$$\eta_{CTS} = \sum_{c=1}^{N_c} w_c (v_{c0} - v_{c1}) / v_{c0} \times 100\% \tag{4.1}$$

where, v_{c0} denotes the aggregate violation in the post-contingency situation under contingency c; v_{c1} denotes the aggregate violation in the post-switching situation under contingency c; w_c denotes the probability of contingency c; and N_c denotes the number of critical contingencies identified in the RTCA simulations.

Note that this metric can also be used to perform overall statistical analysis over multiple scenarios for the same system. For instance, N_c could be the total number of critical contingencies across the entire week with scenarios of hourly resolution and c is the index of critical contingency in the 167 scenarios simulated on the PJM system.

In this dissertation, for simplicity, it is assumed that the probabilities for each contingency are equal. Then, (4.1) can be replaced by (4.2) to calculate average violation reduction.

$$\eta_{CTS} = \frac{1}{N_c}\sum_{c=1}^{N_c}(v_{c0} - v_{c1})/v_{c0} \times 100\% \tag{4.2}$$

4.2.2 Pareto Improvement

Though the post-contingency violations may be reduced at an aggregate level by implementing a switching action, certain individual violations may increase or additional violations may be introduced. Therefore, analyzing the effect of CTS at an elemental level is also very important and Pareto improvement is proposed to investigate this issue. A switching action can be considered as a solution with Pareto improvement only when it does not cause any new violation and does not increase any existing post-contingency violation. A beneficial switching action with Pareto improvement can reduce the post-contingency violation at an aggregate level without causing additional violation on any element.

The proposed concept of Pareto improvement for CTS can be illustrated with Table 4.2. This table shows the results of four independent CTS solutions for the same contingency, which causes overloading violations on line 1 and line 2.

The first switching action can completely eliminate the violations on line 1 and line 2 at the cost of introducing an additional violation on line 3. Though the overall violation is reduced by 90%, it is not a solution that provides Pareto improvement due to the additional violation on line 3. The second CTS solution eliminates the flow violation on line 2 and does not cause any new violation; however, it increases the flow violation

on line 1 by 10 MVA, which means this solution also does not provide Pareto improvement. In the post-switching state with implementation of the third CTS solution, no flow violation exists; however, a new voltage violation introduced by CTS is detected. Hence, the third switching action will not be considered as a beneficial CTS solution when Pareto improvement is required. The last solution is the only CTS solution in this example that provides Pareto improvement. Though the flow violation on line 1 remain the same after implementation of this CTS action, the total violation is reduced and no additional violation is observed. Therefore, the fourth CTS action is a solution with Pareto improvement.

Table 4.2 Examples for Illustrating the Concept of Pareto Improvement for CTS

State	CTS Solution	Flow violation	Voltage violation
Post-contingency	NA	Line 1: 40MVA flow violation, Line 2: 60MVA flow violation, No flow violation on other lines.	No voltage violation
Post-switching	1	Line 3: 10MVA flow violation, No flow violation on other lines.	No voltage violation
	2	Line 1: 50MVA flow violation, No flow violation on other lines.	No voltage violation
	3	No flow violation	0.1 per unit over-voltage violation at bus 1
	4	Line 1: 40MVA flow violation	No voltage violation

Small amounts of additional violation beyond post-contingency violations after switching will be considered as noise and will not be considered as a violation of Pareto improvement. Thus, tolerances are used to measure PI. In this dissertation, the tolerance is 0.005 per unit for individual voltage violation and 5 MVA for individual flow violation. For instance, for the example shown in Table 4.2, if the flow violation on line 1 is just 41 MW for the second CTS solution, then, the second CTS action is considered to

be a beneficial solution that provides PI, since the additional 1 MW violation is within the tolerance and thus is ignored.

4.2.3 Depth

In this dissertation, depth is proposed to estimate the effectiveness of the proposed CTS algorithms. Depth is defined as the location of the identified beneficial switching action in the candidate list for a particular contingency. It is worth mentioning that depth is proposed to evaluate the efficiency of the proposed CTS algorithm rather than identifying a beneficial switching solution. The average depth can be calculated with the equation below,

$$D_{CTS} = \frac{1}{M_c}\sum_{c=1}^{M_c} L_{CTS,c} \tag{4.3}$$

where $L_{CTS,c}$ denotes the location of the CTS solution in the candidate list for contingency c and M_c is the number of critical contingencies for which at least a beneficial CTS solution exists.

4.3 Algorithms

Four heuristic algorithms are proposed in this dissertation to generate the candidate switching list. They are listed below.

- Closest branches to contingency element (CBCE),
- Closest branches to violation element (CBVE),
- Regular Data mining (RDM),
- Enhanced Data Mining (EDM).

The beneficial switching branches are typically very close to the contingency element or violation elements. Thus, two proximity based algorithms CBCE and CBVE

are proposed to create the candidate list. Inspired by the observation that the switching branches come from a small subset of branches, RDM is proposed to generate the candidate CTS list. Customizing the candidate switching list for different contingencies may substantially improve algorithm performance. Thus, EDM, an enhanced version of RDM, is developed. Complete enumeration (CE) is also implemented in this dissertation as a benchmark to gauge the performance of the proposed heuristics.

4.3.1 CBCE and CBVE

Theoretically, the CBVE method may have a more robust performance than the CBCE method. In the case of a branch contingency, the violations are very close to the contingency branch. The candidate list of switching lines generated by CBCE would be very similar to CBVE. Therefore, CBVE method would perform almost the same with CBCE method. In the case of a generator contingency, it is possible that the violations are far away from the contingency-generator since the generators including those that are far from the contingency are re-dispatched. This may cause violations that are not close to the contingency. In this case, the candidate list for CBCE may consist of branches that are not near the violations and CBCE may not be able to relieve the violation. Therefore, CBVE would perform better than CBCE. In this dissertation, the lengths of the candidate list for CBCE and CBVE are the same and each of the candidate list consists of exactly 100 branches.

The distance of one element to another element used by CBCE and CBVE is the number of branches in the shortest path connecting these two elements. The shortest path has the smallest sum of the weights of its constituent branches. In this dissertation,

the weights of all branches are equal. Therefore, neither the electrical distance in ohms nor the real distance in miles is involved. The proximity of two elements is only determined by the network topology, which makes it easy to implement the proposed algorithms CBCE and CBVE.

4.3.2 RDM

Data mining method shows that beneficial switching actions are limited to a subset of branches that can be determined by enumerating all possible switching actions on the historical real-time EMS data. The candidate CTS list for a particular scenario consists of the beneficial switching solutions identified in advance with other scenarios of the same system. Tolerances can be used to filter out the solutions that provide trivial benefits. Three different RDM methods with different tolerances are investigated in this dissertation. They are referred to as RDM1, RDM2, and RDM3. No tolerance is applied for RDM1; thus, even the CTS solution that provide negligible benefit will be listed as a beneficial candidate. RDM2 uses 5% as the tolerance so that only the solutions that provide more than 5% improvement will be considered as CTS candidates. RDM3 uses 10% as the tolerance; thus, the length of the candidate switching list for RDM3 is minimal, which would result in the least computational time.

The RDM method is examined only on the TVA system in this dissertation. Due to the fact that only a very small number of the ERCOT cases are available, it is not reasonable to conduct the RDM approach on the ERCOT system. The RDM algorithm is also not performed on the PJM system due to the following two reasons: 1) it is

extremely time-consuming to identify the beneficial CTS solutions by performing complete enumeration on all the 167 scenarios of the PJM system because of its large-scale feature and computational challenge; 2) PJM real-time data have different network topologies for different hours and it is extremely difficult to match the branch between different hourly scenarios given that only very limited data are available.

For the TVA system, there are three days' data or 72 cases that are divided into two categories, training set and test set. The training set contains two days' data while the test set contains the other day's data. CE is performed for each critical contingency on the training cases and identifies the beneficial switching actions; those identified switching actions form the candidate CTS list for the cases in the test set. Note that the candidate CTS list is the same for different critical contingencies.

4.3.3 EDM

The candidate list of the RDM approach contains the same set of switching actions for all the critical contingencies. However, this would unnecessarily make the list lengthy and inefficient since the beneficial switching solutions for a contingency may fail to reduce the violations caused by other contingencies.

A switching action that reduces the violation for a particular contingency in one scenario may also provide benefits for the same contingency under a different scenario but may not provide any benefit for other contingencies. Inspired by this idea, the EDM approach that uses different candidate switching lists for different contingencies is proposed. Similar to the regular data mining heuristic, the EDM heuristic is also a static

lookup table based approach. Though the switching list for each contingency is identified beforehand for both heuristics, EDM is much faster and more effective than RDM, since the candidate switching list for EDM is customized for each contingency and is much shorter than RDM.

PJM switching solutions as listed in [48] indicate that the beneficial switching solutions for the same contingency would probably remain the same even if load profile varies, which is consistent with the philosophy behind the proposed EDM approach.

The procedure for the EDM study in this dissertation consists of two stages. The first stage is to determine the candidate switching actions using historical data in the training set and the second stage is to investigate the performance of the EDM heuristic, with the candidate CTS actions identified in the first stage, on different cases in the test set.

Stage 1: Determination of Candidates CTS List

To illustrate the methodology of the proposed EDM heuristic, it is assumed that multiple historical scenarios of the system conditions are available, which is reasonable and practical for real power systems. These scenarios form the training set for determining the static lookup table offline. The associated procedure is described below:

1) For each scenario, RTCA is conducted to identify the critical contingencies.
2) For each critical contingency identified in step 1), complete enumeration of all switchable branches is performed to determine the best switching action.
3) By examining all historical scenarios, a lookup table consisting of beneficial switching solutions for the CTS application can then be created.

The lookup table contains the critical contingencies and the associated best CTS solutions identified from the scenarios in the training set.

Fig. 4.4 shows the flowchart of the proposed EDM heuristic for the CTS application. RTCA is conducted on the historical scenarios to identify critical contingencies with potential violations. All the identified critical contingencies are sent to the CTS routine along with all possible solutions in the candidate list. After this process is completed, the best CTS solutions for the same contingency in different scenarios can then form the candidate switching list for the test cases that will be examined in stage 2.

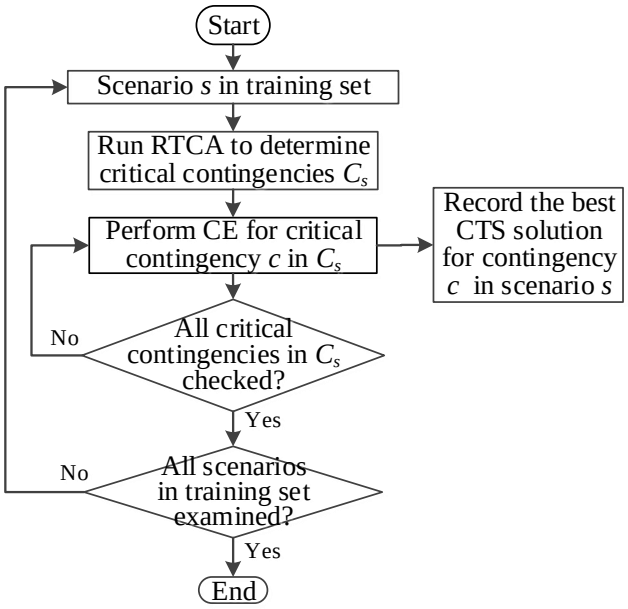

Fig. 4.4 Flowchart of the Proposed EDM Heuristic.

Stage 2: Performance of the proposed EDM heuristic

Stage 2 investigates the performance of the proposed EDM heuristic by examining the efficiency and effectiveness of the same CTS solutions, pre-determined for each critical contingency in stage 1, on cases that are different with the historical scenarios used in stage 1.

Similar to the RDM approach, only the TVA system is used to validate the effectiveness of the EDM approach in this dissertation. The first two days or 48 hours that represent the historical cases are used to determine the candidate switching list for each critical contingency identified on those cases, which corresponds to stage 1. Then, those pre-determined candidate lists are checked for the CTS performance on the remaining 24 cases in stage 2. The EDM heuristic that uses a candidate list without any tolerance for improvement is referred to as EDM1. Candidate list with a tolerance of 5% is referred to as EDM2, while the list for EDM3 corresponds to a tolerance of 10%.

4.3.4 Complete Enumeration

Complete enumeration is implemented in this dissertation to evaluate the effectiveness of the proposed heuristics. Complete enumeration can guarantee the optimal solution but that comes at the cost of a long solution time, which is not practical for real-time applications. Thus, it is only used to provide a basis for evaluating the proposed heuristics.

4.4 Case Studies

Numerical simulations are performed on the TVA, ERCOT, and PJM systems to demonstrate the effectiveness of the proposed CTS algorithms for relieving the post-contingency violations. The computer platform used in Section 4.4 is the same as the computer used in Section 3.4. The simulations on the TVA system and the ERCOT system are performed with only one single thread via a sequential program. Due to computationally complexity, parallel computing with six threads is applied to solve the PJM system.

Table 4.3 and Table 4.4 show the cumulative statistical results and the average statistical results respectively. The results are associated with the first best switching actions reported from the CBVE method without consideration of Pareto improvement. The first best switching action is defined as the solution that the associated violation reduction at an aggregate level is at least as good as the other candidates.

Table 4.3 Cumulative Statistics for the TVA, ERCOT, and PJM Systems

System	# of scenarios	# of critical contingencies	# of contingencies with violations fully eliminated by CTS	# of contingencies with partial violation reduced by CTS	# of contingencies with no violation reduced by CTS
TVA	72	4,272	427 (10.0%)	3,535 (82.7%)	310 (7.3%)
ERCOT	3	40	6 (15%)	27 (67.5%)	7 (17.5%)
PJM	167	8,064	2,684 (33.3%)	4,554 (56.5%)	826 (10.2%)
"*Sum*"	242	12,376	3,117 (25.2%)	8,116 (65.6%)	1,143 (9.2%)

Table 4.4 Average Statistics per Scenario

System	# of scenarios	# of critical contingencies	# of contingencies with violations fully eliminated by CTS	# of contingencies with partial violation reduced by CTS	# of contingencies with no violation reduced by CTS
TVA	72	59.3	5.9	49.1	4.3
ERCOT	3	13.3	2	9	2.3
PJM	167	48.3	16.1	27.3	4.9

The percentage values in the last column of Table 4.3 denote the ratios of critical contingencies where there is no beneficial corrective switching action to the total number of critical contingencies. They are just around 7%, 18%, and 10% for the TVA, ERCOT, and PJM systems respectively. The last row in Table 4.3 shows the statistics over the three systems. The overall percent of critical contingencies that have no beneficial CTS solutions is less than 10% among the three systems. The post-contingency violations can be completely eliminated for over 25% of the critical contingencies identified for those three practical systems.

Note that there is no minimum threshold used for identifying beneficial CTS in Table 4.3 and Table 4.4. Therefore, even the switching actions that provide negligible improvement are considered. With 5% and 10% as the thresholds for determining the beneficial CTS solutions, the associated results are shown in Table 4.5 and Table 4.6 respectively. With a threshold of 5%, the CTS solutions that provide less than 5% improvement will not be considered to be beneficial solutions and switching actions that provide more than 95% improvement will be considered as the solutions that can fully eliminate all the post-contingency violations. The statistics are calculated in the same manner for a threshold of 10%. As the threshold increases from 0 to 10%, the number of critical contingencies where the violations are fully eliminated with CTS increases, as well as the number of critical contingencies where there is no beneficial solution. Though the overall percent of critical contingencies for which at least a beneficial CTS solution exists drops to 61% with a threshold of 10%, the application of CTS for post-contingency violation reduction is still very promising.

Table 4.7 shows the average of violation reduction in percentage with CTS. The results correspond to the first best switching solutions reported by the CBVE method. The average reductions in flow violations are 40%, 53%, and 59% for the TVA, ERCOT, and PJM systems respectively and the average reductions in voltage violations are 36%, 12%, and 20% for those three systems respectively. Note that these statistics are associated with the solutions that do not enforce Pareto improvement. If the CTS solutions that do not provide Pareto improvement are ignored, only slight negligible differences will be observed in those statistics. This implies that most CTS solutions

can reduce the violations at an aggregate level while each individual element is not adversely affected.

Table 4.5 Cumulative Statistics per System with 5% Tolerance

System	# of scenarios	# of critical contingencies	# of contingencies with violations fully eliminated by CTS	# of contingencies with partial violation reduced by CTS	# of contingencies with no violation reduced by CTS
TVA	72	4,272	445 (10.4%)	2,962 (69.3%)	865 (20.2%)
ERCOT	3	40	9 (22.5%)	11 (27.5%)	20 (50.0%)
PJM	167	8,064	2,756 (34.2%)	2,049 (25.4%)	3,259 (40.4%)
"*Sum*"	242	12,376	3,210 (25.9%)	5022 (40.6%)	4144 (33.5%)

Table 4.6 Cumulative Statistics per System with 10% Tolerance

System	# of scenarios	# of critical contingencies	# of contingencies with violations fully eliminated by CTS	# of contingencies with partial violation reduced by CTS	# of contingencies with no violation reduced by CTS
TVA	72	4,272	458 (10.7%)	2,845 (66.6%)	969 (22.7%)
ERCOT	3	40	9 (22.5%)	8 (20.0%)	23 (57.5%)
PJM	167	8,064	2,802 (34.7%)	1,433 (17.8%)	3,829 (47.5%)
"*Sum*"	242	12,376	3,269 (26.4%)	4,286 (34.6%)	4,821 (39.0%)

Table 4.7 Average Violation Reduction with CTS per System

System	Average flow violation reduction		Average voltage violation reduction	
	Without Pareto improvement	With Pareto improvement	Without Pareto improvement	With Pareto improvement
TVA	40.0%	40.0%	36.2%	35.6%
ERCOT	53.1%	49.3%	12.3%	12.3%
PJM	59.3%	59.0%	19.5%	19.3%

4.4.1 TVA Cases

Table 4.8 lists the results of various CTS methods on the TVA system. Note that the results of the EDM heuristic are analyzed from a probabilistic view and are presented separately later in the same section.

Typically, it is expected that the CBCE method would perform similar to the CBVE method. However, this is not the case for the TVA system since the majority of critical contingencies are generator contingencies, which involve generation re-dispatch

throughout the entire network and cause violations that are far away from the contingency element. This is the main reason why the results obtained from CBCE and CBVE are so different. The CBVE method can reduce flow violations by 40%, which is very close to what CE achieves. For the voltage violation reduction, it achieves around 36% which is roughly 12% less than CE. However, the solution time for CBVE is less than 7% of the time that CE takes. The solution time for the CTS methods is averaged over all the scenarios simulated and it does not include the solution time for RTCA. To be consistent, the solution time for CTS is presented in the same manner throughout this dissertation.

Table 4.8 Results of Various CTS Methods on the TVA System

CTS methods	Average solution time (s)	Average flow violation reduction		Average voltage violation reduction	
		Without Pareto improvement	With Pareto improvement	Without Pareto improvement	With Pareto improvement
CBCE	166.7	15.6%	15.0%	31.8%	30.9%
CBVE	177.8	40.0%	40.0%	36.2%	35.6%
RDM1	201.9	40.6%	40.1%	48.1%	47.8%
RDM2	106.6	40.5%	40.0%	48.1%	47.7%
RDM3	98.3	40.5%	40.0%	48.0%	47.7%
CE	2585.3	40.8%	40.3%	48.2%	47.9%

Table 4.8 also presents the results obtained with the three RDM methods introduced in Section 4.3. The RDM methods achieve almost the same results with CE while the computational time is significantly reduced. The violation reductions with the three RDM methods are very similar. However, RDM3 is the fastest since it has the shortest list and it is 26 times faster than CE.

Table 4.9 shows the solution time of RTCA and various CTS methods on the TVA system. The solution time that CBVE takes is about 4 times longer than the computational time of RTCA while RDM3 takes just twice the time that is required for performing RTCA. It is worth noting that RDM3 is over 50 times faster than CE for the case that corresponds to the maximum solution time.

Table 4.9 Solution Time of RTCA and Various CTS Methods on the TVA System

	Solution time (s)		
	Average	Min	Max
RTCA	45.0	43.4	47.7
CTS - CBCE	166.7	16.6	346.4
CTS - CBVE	177.8	17.7	373.0
CTS - RDM1	201.9	17.9	464.2
CTS - RDM2	106.6	9.9	230.8
CTS - RDM3	98.3	9.7	207.0
CTS - CE	2585.3	208.5	10523.7

Table 4.10 presents the statistics for violation reductions corresponding to the 5 best switching solutions with the CBVE heuristic. It is observed that the results with and without enforcing Pareto improvement are very alike. This means that even if Pareto improvement is not a requirement, most of the identified beneficial switching actions do not cause any additional violation while the total violations are reduced. The average depth of the first best CTS solution for flow violation reduction is just 11, which demonstrates that the beneficial switching elements are located very close to the violation elements. For voltage violation, the average depths associated with the top 5 CTS solutions are similar and are around 40. This means that the heuristic algorithm CBVE performs in a more effective way on the TVA system for flow violation reduction as compared to voltage violation reduction.

Fig. 4.5 shows the flow violation reductions and voltage violation reductions that are associated with the top 5 CTS solutions identified by CBVE without imposing Pareto improvement. The average flow violation reduction and average voltage violation reduction are similar with the first best switching actions. However, the curve for voltage violation reduction is relatively flat while the flow violation reduction drops significantly as the rank of beneficial CTS solution decreases. Only top 2 CTS solutions identified for flow violation reduction provide improvement more than 15% while the fifth best CTS solution for voltage violation reduction can achieve over 15% improvement.

Table 4.10 Results of the 5 Best Switching Actions on the TVA System using CBVE

CTS	Average flow violation reduction				Average voltage violation reduction			
	Without Pareto improvement		With Pareto improvement		Without Pareto improvement		With Pareto improvement	
	Reduction	Depth	Reduction	Depth	Reduction	Depth	Reduction	Depth
1st Best	40.0%	11.0	40.0%	11.1	36.2%	46.1	35.6%	48.8
2nd Best	27.8%	23.9	27.7%	24.4	25.1%	46.1	24.8%	45.3
3rd Best	11.7%	54.0	11.7%	54.2	21.8%	39.3	21.6%	37.6
4th Best	8.6%	52.8	8.5%	52.9	19.5%	39.2	19.3%	38.8
5th Best	7.2%	47.8	7.2%	47.7	17.9%	39.9	17.7%	37.5

Analysis of Simulation in Stage 1 for EDM

With RTCA conducted on the scenarios of day 1 and day 2 for the TVA system, 153 different critical contingencies are identified. CE is performed on all 48 scenarios to determine the best CTS solutions for each critical contingency. The best CTS solutions for the same contingency under various historical scenarios in the training set form the candidate list for that contingency.

Random variable α is defined as the number of cases for which the same contingency is identified as a critical contingency. Table 4.11 presents the statistics for this

random variable. From this table, it is observed that most of the critical contingencies could cause violations for different system conditions corresponding to different historical cases. In other words, a contingency that causes violations in one scenario may also cause violations in other scenarios.

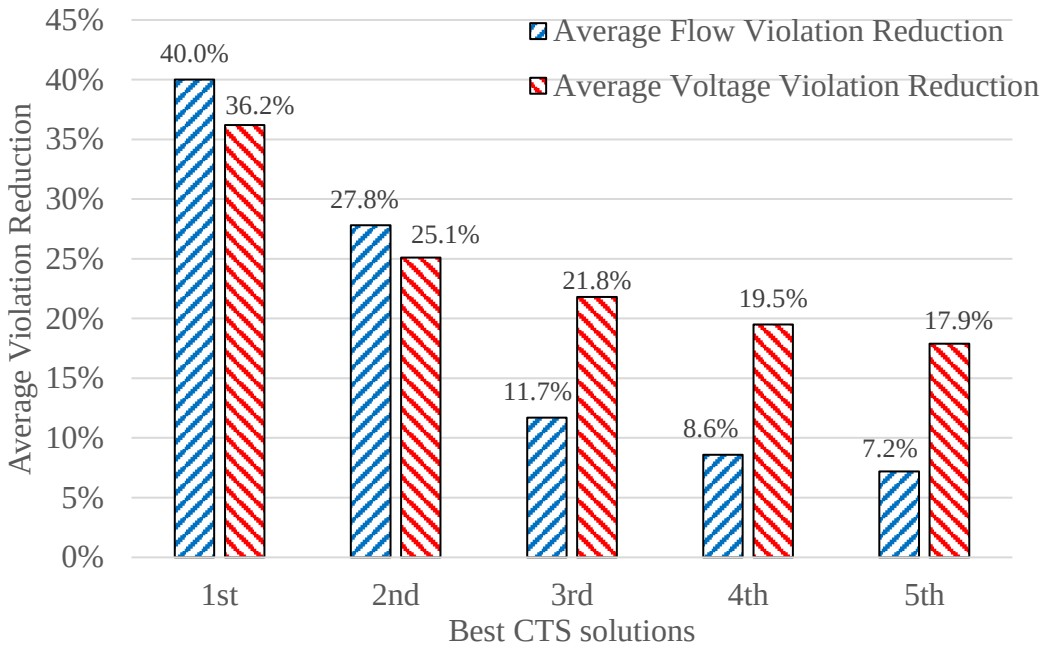

Fig. 4.5 Violation Reduction with the 5 Best Switching Actions Identified by CBVE on TVA.

Random variable τ is defined in (4.4). In (4.4), α_c is number of cases where contingency c is identified as a critical contingency and nT is the total number of cases examined in this stage. nT is 48 in this dissertation. Thus, τ denotes the probability of a contingency being identified as a critical contingency.

The statistics for τ is presented in Table 4.11. The maximum probability of a contingency being identified as a critical contingency is as high as around 90%. The average number of scenarios in which the same contingency will be identified as a critical contingency is 18.7 out of 48, corresponding to a probability of 39.0%.

$$\tau_c = \alpha_c / nT \tag{4.4}$$

Table 4.11 Statistics for Random Variables α and τ

	Max	Min	Median	Average	Standard deviation
α	43	1	20	18.7	11.1
τ	89.6%	2.1%	41.7%	39.0%	23.1%

Fig. 4.6 shows the cumulative distribution function F_τ of variable τ. It is observed that the probability of a contingency being identified as a critical contingency, among 153 identified critical contingencies obtained in stage 1, is primarily in the range between 20% and 80%.

To verify the idea that the beneficial CTS solutions for a contingency will also provide violation reduction for the same contingency in a different scenario of the system, two random variables γ and β are proposed. Random variable γ denotes the number of scenarios where a beneficial CTS solution exists for a critical contingency. Then β, as defined in (4.5), denotes the probability that at least a beneficial CTS solution exists for an identified critical contingency. The subscript c in (4.5) denotes critical contingency c.

$$\beta_c = \frac{\gamma_c}{\alpha_c} \times 100\% \tag{4.5}$$

Table 4.12 presents the statistics for random variable β. It shows that the probability of existence of beneficial CTS solutions for a critical contingency is extremely high. Even if 10% improvement is used as the tolerance for defining a beneficial switching action, on average, beneficial CTS solutions are still available to relieve violations caused by the same critical contingency for more than 80% of the scenarios.

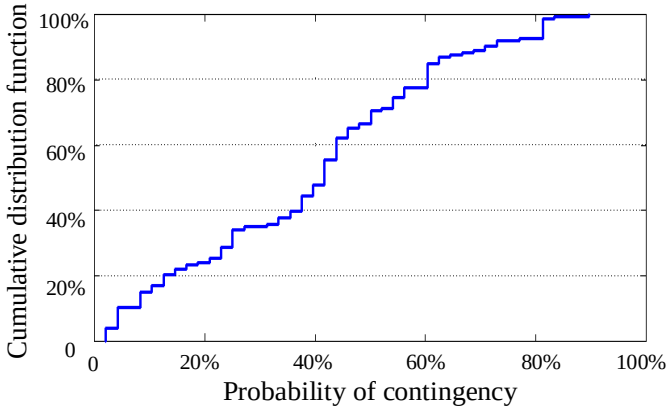

Fig. 4.6 Cumulative Distribution Function of Random Variable τ.

Table 4.12 Statistics for Random Variable β

Heuristic	Tolerance	Max	Min	Median	Average	Standard deviation
EDM1	0	100%	0	100%	97.1%	13.84%
EDM2	5%	100%	0	100%	86.6%	29.0%
EDM3	10%	100%	0	100%	83.5%	31.3%

Random variable φ is defined as the number of switching actions in the candidate list for a critical contingency. Table 4.13 presents the statistics for this random variable. The candidate list obtained from EDM is extremely short. The average length is just around two, which implies that the added computational time per contingency due to CTS is just the solution time that is needed to perform two power flow simulations.

There are 153 numbers in the sample space for each random variable α, τ, γ, β, and φ since there were 153 critical contingencies identified in stage 1.

Table 4.13 Statistics for Random Variable φ

Tolerance	Max	Min	Median	Average	Standard deviation
0	18	0	2	2.39	2.35
5%	6	0	1	1.66	0.99
10%	5	0	1	1.58	0.96

Analysis of Simulation in Stage 2 for EDM

Stage 2 aims to justify the proposed data-driven heuristic. Simulations were performed on the 24 hourly scenarios of day 3 for the TVA system to demonstrate the effectiveness of the proposed EDM approach. In this stage, RTCA is first conducted on the 24 scenarios in the test set from day 3. Overall, 152 critical contingencies that would cause network violations are identified. Among those critical contingencies identified in stage 2, 84.2% or 128 contingencies are found in the critical contingency list identified from the 48 scenarios of day 1 and day 2 in the training set. For each critical contingency in stage 2, only the beneficial switching actions identified in stage 1 for the corresponding contingencies are examined for the proposed EDM heuristic.

Table 4.14 presents detailed statistics of the results obtained from RDM, EDM, and CE methods respectively. The maximum, minimum, median, average, and standard deviation of the solution times per scenario for the different CTS methods are presented in Table 4.14. For both RDM and EDM approaches, as the tolerance for defining beneficial CTS solutions increases from 0% to 5%, the solutions time reduces by a large factor while the violation reductions stay almost the same; however, further increase in the tolerance from 5% to 10% only has a very small effect on the reduction in solution time.

Both voltage violation reduction and flow violation reduction are reported in Table 4.14. Both RDM and EDM methods are proven to be very effective as they provide almost the same violation reductions in comparison to the CE method. The violation reductions obtained by the proposed EDM heuristic is only around 1% lower than the

RDM and CE methods, while EDM achieves the results in much less solution time. EDM1 is around 20 times faster than RDM1 and EDM3 is over 10 times faster than RDM3. Moreover, EDM is over 200 times faster than the CE method. In conclusion, the proposed EDM heuristics provide near optimal solutions while adding the least overhead to the solution time for contingency analysis, which is very promising for real-time CTS applications.

Table 4.15 shows the average number of switching actions in the candidate list per contingency and the average solution time for the CTS routine per scenario. In Table 4.15, *nCTS* denotes the average number of switching actions per contingency; and T_1 denotes the average solution time of the CTS routine per scenario. It is observed that the solution time is linearly correlated with the number of switching actions in the candidate list. Obviously, one reason why EDM is much faster than RDM is that the candidate list of the proposed EDM approach is much shorter.

Table 4.14 Results of the TVA Cases in the Third Day

Methods	Solution times (s)					Violation reduction	
	max	min	median	average	std	Flow	Voltage
RDM1	464.2	22.1	208.7	219.5	161.4	39.77%	51.09%
RDM2	225.9	11.0	103.6	108.3	79.5	39.77%	51.07%
RDM3	200.7	9.7	90.9	96.1	70.8	39.76%	50.95%
EDM1	20.9	1.5	10.7	11.1	7.5	38.74%	50.24%
EDM2	18.0	1.4	9.1	9.6	6.5	38.73%	50.22%
EDM3	17.6	1.1	8.9	9.3	6.3	38.73%	50.03%
CE	9636.5	208.5	2003.5	2458.2	2316.9	39.77%	51.22%

Table 4.15 Comparison among a Variety of CTS Methods on the TVA Cases in the Third Day

	CE	RDM1	RDM2	RDM3	EDM1	EDM2	EDM3
nCTS	1528.9	145.0	64.0	55.0	2.4	1.7	1.6
T_1 (s)	2316.9	219.5	108.3	96.1	11.1	9.6	9.3

4.4.2 ERCOT Cases

Table 4.16 lists the results of various CTS approaches on the ERCOT system. CBVE provides almost the same performance with CBCE in terms of voltage violation reduction while it results in 10% more reduction in flow violation than CBCE. The violation reductions achieved through those two heuristics are very similar to that achieved with CE. However, the proposed heuristics are 47 times faster. Note that the solution time is the average solution time for the three available scenarios of the ERCOT system.

Table 4.16 Results of Various CTS Methods on the ERCOT System

CTS methods	Average solution time (s)	Average flow violation reduction		Average voltage violation reduction	
		Without Pareto improvement	With Pareto improvement	w/o Pareto improvement	w/ Pareto improvement
CBCE	245	40.8%	37.7%	12.1%	12.1%
CBVE	244	53.1%	49.3%	12.3%	12.3%
CE	11,505	53.3%	49.3%	14.3%	14.3%

Table 4.17 presents the average, minimum, and maximum solution times of RTCA and different CTS heuristics. The overall solution times of the CTS heuristics are found to be less than the time taken for RTCA since the number of critical contingencies that require CTS is smaller for the ERCOT system compared to the TVA system. The maximum solution time to find the CTS actions is close to 6 minutes even for the sequential implementation of the CTS heuristics. Note that the solution time of the proposed CTS heuristics highly depends on the number of the identified critical contingencies. If all contingencies in the contingency list are trivial, then CTS will not be implemented since there will be no network violation and the associated solution time for CTS will just be zero.

Table 4.17 Solution Time of RTCA and Various CTS Methods on the ERCOT System

	Average (s)	Min (s)	Max (s)
RTCA	766.7	575.3	784.9
CTS - CBCE	244.8	181.5	356.1
CTS - CBVE	244.2	184.7	349.6
CTS - CE	11504.7	8728.3	16733.8

Fig. 4.7 shows violation reductions with the 5 best switching actions identified by the CBVE algorithm on the ERCOT system. Pareto improvement is not imposed for the results shown in Fig. 4.7. All top 5 switching actions can reduce the flow violations significantly while the performance of CTS voltage violation reduction is less promising. The top CTS solutions can reduce the flow violations by 53.1% and even the fifth best CTS solutions can reduce the flow violations by 47.2% on average. As for voltage violation, the first best CTS solutions provide 12.3% improvement; however, the improvement provided by the second best CTS solutions is less than 10% on average and the fifth best switching actions provide only 2.8% improvement which is negligible.

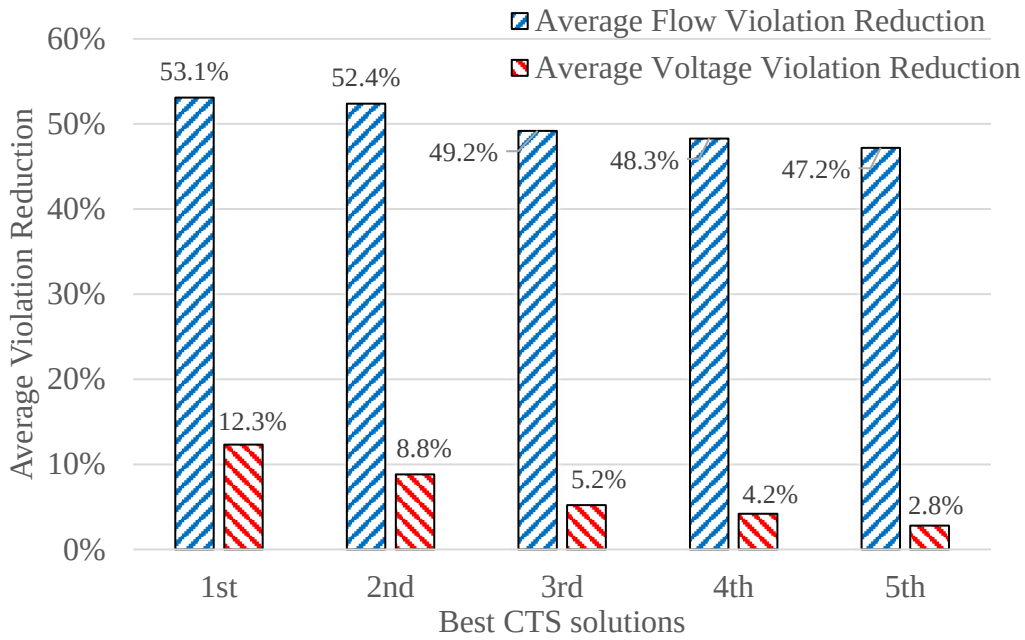

Fig. 4.7 Violation Reduction with the 5 Best Switching Actions on the ERCOT System.

4.4.3 PJM Cases

Due to large-scale feature of the PJM system, the solution time for simulating RTCA and CTS on the PJM system is significantly high. Thus, the PJM system is solved with parallel computing using six threads rather than one single thread.

Table 4.18 shows the results obtained with CBCE and CBVE on the PJM system. The flow violation reductions and voltage violation reductions achieved with CBCE and CBVE are very similar. The solution times presented in Table 4.18 do not include the time of RTCA and it is the average time over all 167 hourly scenarios. It is observed from Table 4.19 that the average, minimum, and maximum solution times of those two CTS heuristics are very similar.

Table 4.20 shows the statistics related to the 5 best switching actions identified by the CBVE heuristic. The reductions in flow violations for the first and fifth best CTS solutions are 59% and 46% respectively. However, for voltage violation, the reduction ranges from 20% to 6% for the top 5 CTS solutions. All top 5 switching solutions provide substantial reduction for flow violation while only top 3 switching solutions provide reduction more than 10% for voltage violation. The depths of the beneficial CTS solutions in the ranked candidate list are small for flow violation, which implies that the beneficial switching branches are very close to the violation elements. The depths of CTS that handles voltage violation are much larger than the depths of CTS that handles flow violation, which indicates that the proximity-based heuristic is more efficient for flow violation reduction than voltage violation reduction on the PJM system. The

violation reductions without Pareto improvement, obtained with CBVE, are presented in Fig. 4.8.

Table 4.18 Results of Various CTS Methods on the PJM System

CTS methods	Avg. solution time (s)	Average flow violation reduction		Average voltage violation reduction	
		Without Pareto improvement	With Pareto improvement	Without Pareto improvement	With Pareto improvement
CBCE	1592.6	61.6%	60.2%	19.1%	18.8%
CBVE	1611.8	59.3%	59.0%	19.5%	19.3%

Table 4.19 Solution Times of RTCA and Various CTS Methods on the PJM System

	Average (s)	Min (s)	Max (s)
RTCA	2617.3	2186.5	3100.1
CTS - CBCE	1592.6	236.9	3499.4
CTS - CBVE	1611.8	241.9	3441.1

Table 4.20 Results of the 5 Best Switching Actions on the PJM System using CBVE

CTS	Average flow violation reduction				Average voltage violation reduction			
	Without Pareto improvement		With Pareto improvement		Without Pareto improvement		With Pareto improvement	
	Reduction	Depth	Reduction	Depth	Reduction	Depth	Reduction	Depth
1st Best	59.3%	13.9	59.0%	14.4	19.5%	36.8	19.3%	37.6
2nd Best	57.7%	16.4	57.3%	16.7	14.6%	37.8	14.4%	38.1
3rd Best	52.6%	22.9	51.9%	23.7	11.5%	37.2	11.2%	37.9
4th Best	49.0%	26.5	48.7%	25.9	7.8%	39.9	7.7%	39.7
5th Best	46.3%	27.1	45.5%	27.4	6.4%	41.2	6.1%	41.4

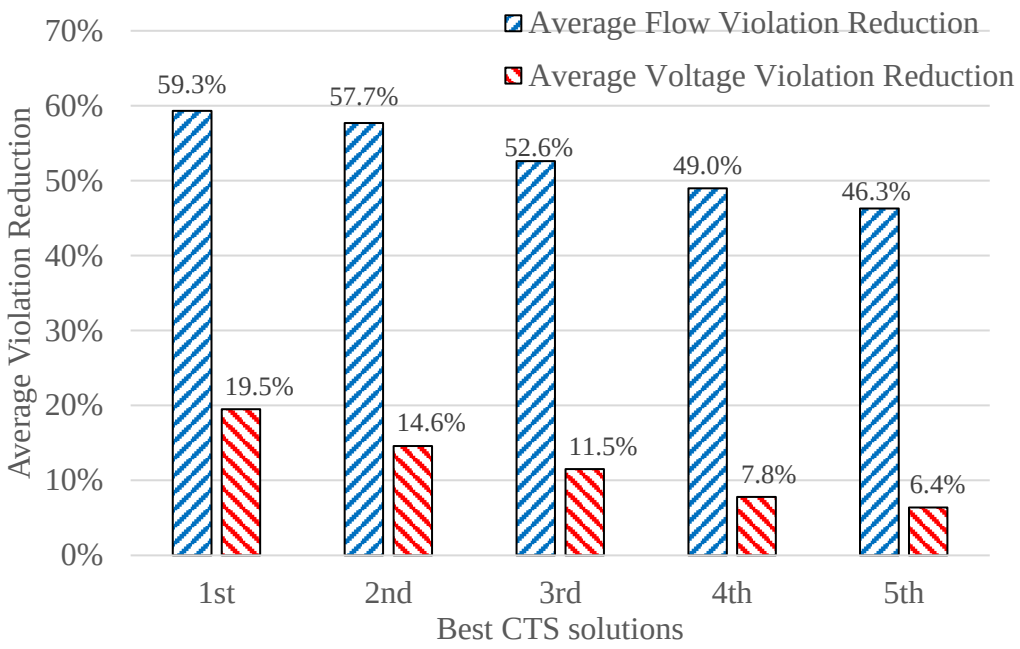

Fig. 4.8 Violation Reduction with the 5 Best Switching Actions on the PJM System.

For the PJM system, the simulation for CE can take an extremely long time even with 6 threads running in parallel. Therefore, CE is only performed on 6 selected scenarios out of 167 EMS snapshots. The 6 selected cases are hour 1, 5, 9, 13, 17, and hour 21 on day 1. They represent various system loading conditions for peak hours, off-peak hours, and shoulder hours.

Table 4.21 shows the statistics for results obtained from CBCE, CBVE, and CE on the selected scenarios of the PJM system. The heuristics achieve very similar results with CE in terms of violation improvement. However, the two heuristics are approximately 110 times faster than the complete enumeration.

Table 4.21 Results of Various CTS Methods on the PJM System for the Selected Hours

CTS	Average solution time (s)	Average flow violation reduction		Average voltage violation reduction	
		Without Pareto improvement	With Pareto improvement	Without Pareto improvement	With Pareto improvement
CBCE	872.3	62.1%	61.0%	19.4%	19.4%
CBVE	874.8	59.4%	59.4%	19.4%	19.4%
CE	96921.5	62.5%	62.5%	21.0%	20.4%

The results of the 5 best switching actions identified by CBCE, CBVE, and CE are presented in Table 4.22, Table 4.23, and Table 4.24 respectively. It is found that the statistics for reductions in violations achieved with CBCE, CBVE, and CE are very similar. This demonstrates the effectiveness of the proposed heuristic methods on the PJM system.

Table 4.22 Results of the 5 best CTS Solutions on the PJM System for the Selected Hours using CBCE

CTS	Average flow violation reduction				Average voltage violation reduction			
	Without Pareto improvement		With Pareto improvement		Without Pareto improvement		With Pareto improvement	
	Reduction	Depth	Reduction	Depth	Reduction	Depth	Reduction	Depth
1st Best	62.1%	12.2	61.0%	12.3	19.4%	31.3	19.4%	31.3
2nd Best	58.9%	15.5	58.6%	16.6	15.2%	34.8	15.0%	34.7
3rd Best	57.8%	21.1	57.7%	21.1	10.5%	32.4	10.4%	31.4
4th Best	50.2%	25.6	50.2%	24.5	7.1%	38.3	6.8%	39.6
5th Best	47.2%	24.6	47.2%	24.1	5.8%	39	5.7%	37.6

Table 4.23 Results of the 5 best CTS Solutions on the PJM System for the Selected Hours using CBVE

CTS	Average flow violation reduction				Average voltage violation reduction			
	Without Pareto improvement		With Pareto improvement		Without Pareto improvement		With Pareto improvement	
	Reduction	Depth	Reduction	Depth	Reduction	Depth	Reduction	Depth
1st Best	59.4%	11.4	59.4%	11.4	19.4%	31.1	19.4%	31.1
2nd Best	58.2%	13.8	58.2%	13.8	15.2%	34.9	15.0%	35.4
3rd Best	50.6%	18.6	50.6%	18.6	10.7%	32.0	10.4%	30.8
4th Best	48.1%	20.9	48.1%	20.1	7.2%	41.2	6.8%	40.7
5th Best	46.2%	22.7	46.2%	22.6	6.1%	34.9	5.7%	34.4

Table 4.24 Results of the 5 best Switching Actions on the PJM System for the Selected Hours using CE

CTS	Average flow violation reduction				Average voltage violation reduction			
	Without Pareto improvement		With Pareto improvement		Without Pareto improvement		With Pareto improvement	
	Reduction	Depth	Reduction	Depth	Reduction	Depth	Reduction	Depth
1st Best	62.5%	NA	62.5%	NA	21.0%	NA	20.4%	NA
2nd Best	61.3%	NA	60.9%	NA	17.8%	NA	17.0%	NA
3rd Best	60.2%	NA	59.5%	NA	12.9%	NA	12.7%	NA
4th Best	51.2%	NA	50.9%	NA	9.5%	NA	9.4%	NA
5th Best	49.1%	NA	49.1%	NA	7.9%	NA	7.7%	NA

NA means not applicable.

4.5 Parallel Computing

Since the candidate switching list contains only 100 branches for CBVE and CBCE, using more than 100 threads will be a waste of resources. Thus, up to 100 threads are used to investigate the efficiency of parallel computing with the proposed CBVE and CBCE heuristics.

Table 4.25 lists the average CTS solution time with various threads on the TVA, ERCOT, and PJM systems. To give a more intuitive understanding of how much time can be reduced with multiple threads, the average CTS solution time with different threads on the ERCOT system is shown in Fig. 4.9. It is clearly observed that the computing time decreases as the number of threads used increases. Note that the solution times shown in Table 4.25 and Fig. 4.9 are the average time over multiple scenarios for the same system and thus are the average CTS solution time per system rather than the average CTS solution time per contingency.

Table 4.25 Average CTS Solution Time per System with Different Threads

	Average CTS solution time per system / s							
# of threads	1	2	4	8	16	25	50	100
TVA	172.24	89.08	46.56	27.02	15.79	10.68	7.22	6.61
ERCOT	279.53	141.87	74.01	40.90	22.97	14.62	8.44	5.55
PJM	NA	NA	NA	999.46	565.90	322.94	172.70	96.18

NA: not applicable

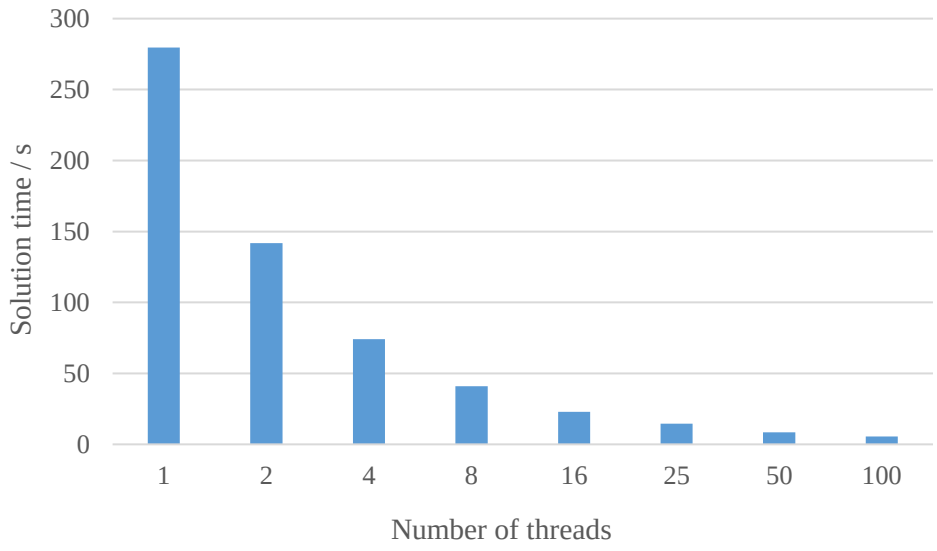

Fig. 4.9 Average CTS Solution Time per Scenario/Hour with Different Threads on the ERCOT System.

4.6 Conclusions

Violation reduction that can be achieved with CTS is studied in this chapter. Four heuristic based CTS algorithms are proposed to determine the candidate switching list. Numerical results on three large-scale practical systems demonstrate the effectiveness of CTS for reducing post-contingency violations in an AC setting.

Promising results on the TVA system are obtained from the data mining methods, RDM and EDM, in a reasonable solution time. All scenarios of the TVA system share the same network topology. Thus, the performance of data mining methods on dynamic network, for instance, caused by transmission maintenance outage, needs further investigations. Two other heuristic methods, CBCE and CBVE, have similar performance to complete enumeration on the ERCOT system and the PJM system. However, CBCE does not perform well on the TVA system while CBVE still shows a good performance. The reason is that generation re-dispatch is conducted throughout the entire system for

generator contingencies, which may cause violations that are far away from that the contingency-generator and the candidate list generated from CBCE may not benefit the system at all.

Complete enumeration is guaranteed to find the best solution. However, that comes with the cost of a long computational time, which is impractical. Overall, CBVE heuristic is considered to be the most efficient and robust CTS method among the proposed heuristics in order to provide valid solutions for reducing post-contingency violations.

Based on the analysis on three large-scale practical power systems, the beneficial switching solutions for flow violation reduction are typically found to be the overloaded branches, or the branches that are in parallel or on the same path with the overloaded branch. The reason for why CTS can reduce overloads without load shedding is that CTS reconfigures the transmission network and transfers the flows on overloaded branches to other paths that have extra available capacity. For voltage violation reduction, the identified CTS solutions typically carry a significant amount of reactive power or have shunts connected to it. Thus, switching those CTS actions can change the reactive power in the nearby area and, then change the voltage profile in the same area, which may reduce over voltage violations or under voltage violations.

5. REAL-TIME SECURITY-CONSTRAINED ECONOMIC DISPATCH WITH CORRECTIVE TRANSMISSION SWITCHING

Real-time security-constrained economic dispatch aims to provide the least cost dispatch solution for the online generating units while meeting all system requirements including network constraints. The system total operation cost includes energy cost and reserve cost. No-load cost is not considered in RT SCED as it does not affect the results at all. Typically, SCED uses the linearized DC power flow model rather than the AC power flow model due to concerns regarding computational complexity and algorithm convergence. In addition, RT SCED does not change generators' status and network topology. Thus, RT SCED is just a linear programming problem without any binary variables and thus can be solved to optimality quickly if it is feasible.

The system monitoring function of EMS performs state estimation with the data received from remote terminal units or local control center and determines the system condition in real-time. Then, base-case power flow and RTCA execute and provide a list of network constraints for RT SCED. This list of network constraints can be divided into two categories: base-case network constraints (actual network constraints) and contingency-case network constraints (potential network constraints). RT SCED considers those two categories of network constraints as well as other requirements in its linear optimization engine which will solve the associated problem and obtain a new set of dispatch points that meet all requirements with minimum cost.

It is worth noting that RT SCED is based on the DC power flow model while base-case power flow and contingency analysis use the full AC power flow model. Thus,

model conversion between RTCA and RT SCED is needed. This dissertation proposes Procedure-A for connecting RTCA and RT SCED. The proposed Procedure-A is implemented to mimic the industrial practice. Network constraints identified from base-case power flow and RTCA are modeled in RT SCED.

Several SCED models are proposed and compared. To evaluate the quality of solutions obtained from the different SCED models, SCED solutions are fed back to EMS and then, base-case AC power flow and full AC contingency analysis are performed again. The SCED model that has the best performance is selected. Simulation results demonstrate the effectiveness of the proposed Procedure-A. It is observed that the solution obtained from DC power flow model based SCED can pass AC feasibility check.

Due to network congestion, cheap generators may have to hold their power outputs, which would result in significant congestion cost. As demonstrated in Chapter 4, CTS can reduce post-contingency violations; in other words, CTS can relieve network congestions. Therefore, as an enhanced version of Procedure-A, Procedure-B is proposed to relieve congestions with CTS. With CTS, pseudo limits that are higher than the actual limits can be used for the network constraints in the SCED model. The SCED using pseudo limits in Procedure-B is referred to as enhanced SCED. With the use of pseudo limits in E-SCED, the reliability benefits provided by CTS can be translated into significant congestion cost savings due to substantially reduced need for expensive generation re-dispatch.

For solutions obtained from the proposed Procedure-B, branch overloads may be observed under some critical contingencies in the post-SCED stage; this is because

pseudo limits that are higher than actual limits are used for the contingency-case network constraints. However, the flow violations can be eliminated by implementing the CTS solutions identified in the pre-SCED stage. Simulation results demonstrate the effectiveness of the proposed E-SCED approach as well as the proposed Procedure-B.

Voltage violations are typically handled locally. Moreover, SCED does not consider voltage and reactive power. Therefore, in this chapter, RTCA focuses on flow violations only. In addition, RTCA used in this chapter is performed only on transmission contingencies, which is consistent with existing industrial practice.

5.1 EMS Procedures

This section presents the proposed Procedure-A and Procedure-B in detail. In the proposed Procedure-A, the network constraints formulated in DC model based RT SCED are determined from AC model based RTCA; Procedure-A can perform model conversion and connect RT SCED with the traditional RTCA. In fact, the proposed Procedure-A represents existing industrial practice. Based on Procedure-A, Procedure-B is proposed to utilize the flexibility in the transmission network. Procedure-B is a procedure for connecting SCED with CTS-based RTCA.

Procedure-A uses the actual limits, calculated by RTCA, to enforce network constraints while higher pseudo limits are used in Procedure-B, which is the main difference between Procedure-A and Procedure-B. The pseudo limits are determined by CTS-based RTCA. With the use of higher pseudo limits, the extra reliability provided by CTS can then be captured in SCED and be translated into economic benefits.

Theoretically, the proposed Procedure-A can be replaced by an AC power flow model based SCED model or ACOPF. However, AC based SCED is a non-linear and non-convex problem and is extremely difficult to solve for large-scale real power systems in a limited time. In addition, convergence and robustness are also big concerns. Therefore, the proposed Procedure-A, which is consistent with the industrial practice, is preferred.

Theoretically, instead of using pseudo limits in E-SCED of the proposed Procedure-B, CTS can be directly modeled in SCED and binary variables would be used to indicate the status of switching element, which will convert SCED from an LP problem into an MILP problem. This will cause a serious computational burden and substantially increase the solution time. Therefore, directly modeling CTS in SCED is impractical and Procedure-B with pseudo limits is preferred. In addition, the proposed Procedure-B requires no change to existing tools and the solution time for SCED will not change significantly.

Procedure-A and Procedure-B are presented in detail in Section 5.1.1 and Section 5.1.2 respectively. The detailed SCED mathematical models are presented in Section 5.2.

5.1.1 Procedure-A: SCED with RTCA

This section describes the proposed Procedure-A in detail. Fig. 5.1 illustrates the flowchart of the proposed Procedure-A representing existing industrial practice. As shown in Fig. 5.1, Procedure-A consists of four steps as listed below.

Step 1) Monitor system status.

Step 2) Perform base-case power flow and RTCA to determine the active network constraints for SCED.

Step 3) Run SCED with the network constraints identified in Step 2).

Step 4) Evaluate the SCED solutions.

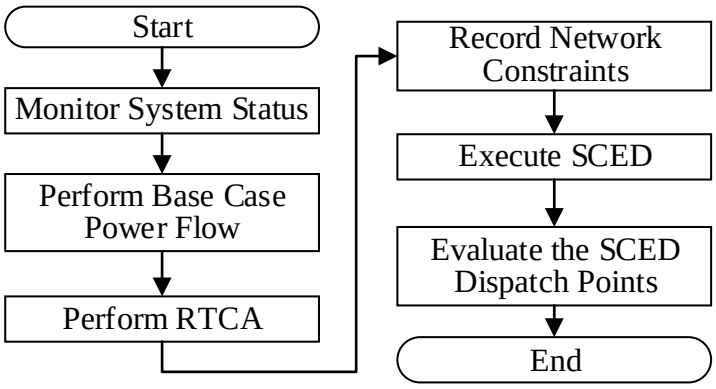

Fig. 5.1 Flowchart of the Proposed Procedure-A for Connecting SCED with RTCA.

With the data collected from local control centers and remote terminal units in real-time, state estimation is performed to determine the system status in Step 1). In Step 2), with the starting point determined in Step 1), base-case power flow and RTCA are performed sequentially; this step will identify the active network constraints that have to be enforced in SCED for secure operations of power systems. Then, the SCED that is subject to those active network constraints is solved and the optimal solution is reported to operators. The last step of Procedure-A evaluates the SCED solution by rerunning the base-case power flow and contingency analysis with the updated generators' outputs; the contingency list simulated in this step is the same with Step 2).

Determination of Network Constraints

Due to large-scale feature of real power systems, it is impractical to model all contingencies with all elements monitored in RT SCED. Thus, generation reserve is proposed and modeled in RT SCED aiming to have extra backup power for handling contingency in real-time and make sure the system is *N*-1 secure. However, reserve deliverability cannot be guaranteed due to congestion. Thus, extra network constraints are required to be enforced in RT SCED. With a limited number of extra network constraints modeled in SCED, it can still be solved within a short timeframe and be employed in real-time.

As described before, the network constraints can be divided into two categories, actual base-case network constraints and potential contingency-case network constraints. Each base-case network constraint contains three items: transmission element k under monitoring, initial active power flow P_{k0} in the base case, and long-term normal MW limit $LimitA_k$. Each contingency-case network constraint contains four items: contingency element c, transmission element k under monitoring, initial active power flow $P_{k,c,0}$ under contingency c, and short-term emergency MW limit $LimitC_{kc}$ under contingency c.

In reality, thermal limits for transmission elements are in the unit of MVA instead of MW. However, approximate MW limits are used for SCED and they can be derived by assuming that the reactive power flows do not change in the look-ahead period of SCED. Then, the branch normal limit $LimitA_k$ for base-case network constraint and

the emergency limit $LimitC_{kc}$ for contingency-case network constraint can be calculated by (5.1) and (5.2) respectively,

$$LimitA_k = \sqrt{RateA^2 - (\max(|Q_{k,from}|, |Q_{k,to}|))^2} \tag{5.1}$$

$$LimitC_{kc} = \sqrt{RateC^2 - (\max(|Q_{kc,from}|, |Q_{kc,to}|))^2} \tag{5.2}$$

where $Q_{k,from}$ and $Q_{k,to}$ denote the reactive power on line *k* flowing out of from-bus and to-bus in the base case respectively; $Q_{kc,from}$ and $Q_{kc,to}$ denote the reactive power on line *k* flowing out of from-bus and to-bus under contingency *c* respectively.

In case that contingency analysis is not available, branch emergency limit $LimitC_k$ under contingency can be approximately calculated by (5.3) which assumes reactive power flows do not change under contingency,

$$LimitC_k = \sqrt{RateC^2 - (\max(|Q_{k,from}|, |Q_{k,to}|))^2} \tag{5.3}$$

To reduce computational complexity, only a small subset of transmission elements will be monitored. Active network constraints can be determined by comparing the branch loading level with the tolerance Pct for the base case or the tolerance $PctC$ for the contingency cases. Tolerances Pct and $PctC$ are pre-defined percentages with a range between 0 and 100%. The branch loading level LL_k in the base case is defined in (5.4) while the branch loading level LL_{kc} under contingency *c* can be calculated with (5.5),

$$LL_k = \max(|S_{k,from}|, |S_{k,to}|) / RateA \tag{5.4}$$

$$LL_{kc} = \max(|S_{kc,from}|, |S_{kc,to}|) / RateC \tag{5.5}$$

where $S_{k,from}$ and $S_{k,to}$ denote the complex power on line *k* flowing out of from-bus and to-bus in the base case respectively; $S_{kc,from}$ and $S_{kc,to}$ denote the complex power on line *k* flowing out of from-bus and to-bus under contingency *c* respectively.

Therefore, a branch *k* will be monitored in the base case if its loading level LL_k is greater than Pct. Similarly, a branch *k* will be monitored under contingency *c* if the associated loading level LL_{kc} is greater than $PctC$. Those monitored branch constraints are referred to active network constraints. An active network constraint is referred to as a critical network constraint if the associated flow exceeds the branch capacity. A contingency is called active contingency if it causes one or multiple active network constraints. Similarly, a critical contingency is a contingency that would cause at least one critical network constraint.

If Pct is set to 1, only the actual congested and overloaded branches will be monitored in the base case. Similarly, if $PctC$ is set to 1, then only the potential congested and overloaded branches will be monitored under the associated contingencies.

The initial branch flow for base-case network constraints and contingency-case network constraints that are modeled in SCED are determined by (5.6) and (5.7) respectively,

$$P_{k0} = sign(P_{k,from}) \cdot \max(|P_{k,from}|, |P_{k,to}|) \tag{5.6}$$

$$P_{kc0} = sign(P_{kc,from}) \cdot \max(|P_{kc,from}|, |P_{kc,to}|) \tag{5.7}$$

where $P_{k,from}$ and $P_{k,to}$ denote the active power on line *k* flowing out of from-bus and to-bus in base-case respectively; $P_{kc,from}$ and $P_{kc,to}$ denote the active power on line *k* flowing out of from-bus and to-bus under contingency *c* respectively.

Representation of Transmission Losses

System losses in transmission network typically accounts for 2% to 4% of the total demand. It would be impractical if all losses are picked up by slack bus. Thus, losses should be precisely and properly modeled in SCED. Losses can either be modeled as virtual loads or be calculated with loss coefficients. In this work, transmission losses are not explicitly represented in the proposed SCED mathematical model; instead, virtual loads are used to represent the transmission losses.

Multiple methods as listed below are available to convert losses in an AC model into virtual loads in a DC model.

- assign losses to load buses,
- assign losses to generator buses,
- assign the loss on each branch to the actually receiving buses,
- assign the loss on each branch to the actually sending buses,
- assign the loss on each branch evenly to the from-bus and the to-bus.

In this work, the loss on each branch is evenly distributed to the two buses that are connected to that branch and modeled as virtual loads. In addition, the losses are assumed to remain the same. Note that, for the incremental PTDF based SCED models, there is no need to model losses as virtual loads since they are already implicitly represented in those models.

5.1.2 Procedure-B: SCED with CTS based RTCA

The proposed Procedure-A, which represents the industrial practice for RT SCED, is introduced in detail in Section 5.1.1. As demonstrated in Chapter 4, CTS is able to

enhance the system reliability by reducing violation under contingency. In this section, Procedure-B is proposed to enhance Procedure-A by considering the benefits that are provided by CTS. The proposed Procedure-B can substantially relieve network congestion and significantly reduce the congestion cost as compared to Procedure-A. To distinguish the regular SCED in Procedure-A, the SCED that considers the effect of CTS in Procedure-B is referred to as enhanced SCED.

The flowchart of the proposed Procedure-B is illustrated in Fig. 5.2. As shown in Fig. 5.2, Procedure-B consists of six steps, which are listed below,

Step 1) Monitor system status.

Step 2) Perform base-case power flow and RTCA.

Step 3) Perform CTS on critical contingencies only and identify beneficial switching actions for each critical contingency.

Step 4) Update the thermal limit in MW for critical network constraints.

Step 5) Run E-SCED and obtain a new set of dispatch points.

Step 6) Evaluate the E-SCED solution.

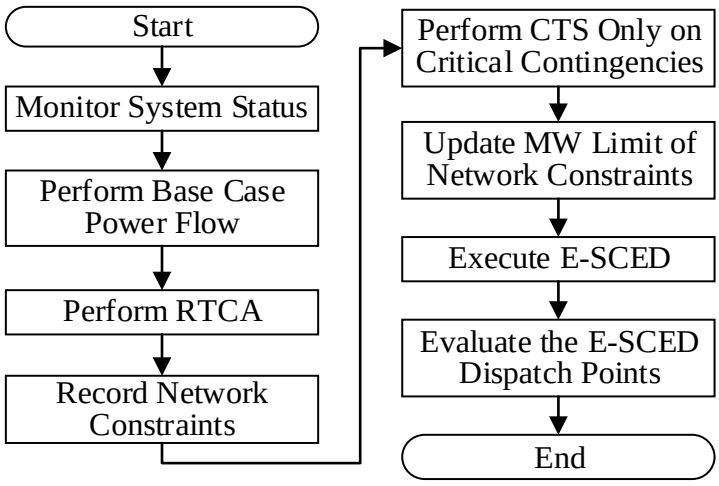

Fig. 5.2 Flowchart of the Proposed Procedure-B.

The first two steps of Procedure-B are the same as in Procedure-A. The third step of Procedure-B is to perform CTS on critical contingencies only and identify switching actions that can reduce post-contingency violations. Note that CTS is performed only on critical contingencies aiming to relieve critical network constraints, which is time-efficient as compared to that CTS is performed on all active contingencies. In Step 4), the limits of critical network constraints are updated with (5.8) and details are provided below.

For a critical contingency *c*, if the identified beneficial switching solutions can reduce the total violation and no single violation is worse off, then, the pseudo limit of the associated constraint can be calculated by the equation presented below,

$$LimitC_{kc} = \sqrt{(RateC + v_{kc}P_{kc,CTS})^2 - (\max(|Q_{kc,from}|, |Q_{kc,to}|))^2} \quad (5.8)$$

where v_{kc} denotes the violation on branch *k* under contingency *c* and $P_{kc,CTS}$ denotes the violation reduction in percent for branch *k* under contingency *c* with CTS and is calculated by (5.9),

$$P_{kc,CTS} = (v_{kc} - v_{kc,CTS})/v_{kc} \quad (5.9)$$

where $v_{kc,CTS}$ is the violation on branch *k* under contingency *c* with CTS action implemented.

In Step 5), E-SCED executes with the pseudo limits of critical network constraints and then a new set of dispatch points for dispatchable units are obtained. The last step of Procedure-B is to evaluate the E-SCED solutions. With the updated generation in the post-SCED stage, RTCA is performed on the same contingencies with Step 2) and it

will probably report violations as higher pseudo limits are used in E-SCED rather than the actual limits; however, those post-contingency violations are expected to occur on the same element under the same contingencies that are reported by RTCA in the pre-SCED stage. For the critical contingencies causing those post-contingency violations, the beneficial CTS solutions identified in Step 3) in the pre-SCED stage are also expected to reduce violations under the same contingencies in the post-SCED stage, which is demonstrated in Section 5.3.

5.2 SCED Mathematical Formulation

A SCED mathematical model is first proposed in this section, followed by several model variants. Based on availability of network flow information and different forms of network constraints, five SCED models are proposed in this dissertation. They are cold-start PTDF based SCED, warm-start PTDF based SCED, hot-start PTDF based SCED, cold-start *B-θ* based SCED, and hot-start *B-θ* based SCED.

The proposed SCED models co-optimize energy and reserve simultaneously while enforcing physical restrictions such as power balance constraints and security requirements such as reserve requirements.

Load shedding is included in both the base case and the contingency cases to handle the potential infeasibility and prevent the SCED software from terminating without reporting any information. Load shedding is modeled as slack variables in the power balance constraints.

It is worth mentioning that in the commercial RT SCED tools used by ISOs, all constraints are relaxed with slack variables; for different set of slack variables, the penalty factors for the associated penalty terms in objective function can be different as different types of constraints to be enforced have different priorities. Thus, the ISOs' commercial RT SCED tools will not terminate even in the worst case; instead, they can inform operators of what may be the sources causing SCED infeasibility and enable operators to manually adjust the system to avoid any potential damage.

5.2.1 Unit Cost Curve

ISOs including PJM, MISO, and NYISO typically require generators to submit incremental energy offer that is represented by MW quantity and price pairs [143]-[145]. For instance, both MISO and PJM accept up to 10 price-quantity segments. There are two types of energy offers: slope cost curve and block cost curve.

Fig. 5.3 shows an example that illustrates the unit block incremental cost curve. The lengths of the three segments are $P_{g,s1}$, $(P_{g,s2} - P_{g,s1})$, and $(P_{g,s3} - P_{g,s2})$ while the associated constant costs are C_1, C_2, and C_3 respectively. p_{g1}, p_{g2}, and p_{g3} denotes the net MW outputs associated with segment 1, 2, and 3 respectively. For the same generator, the optimal SCED solution will not schedule any power outputs on a segment if any other segment with a lower price is not entirely selected since the objective function is to minimize the total cost.

Fig. 5.4 illustrates the unit slope incremental cost curve. Obviously, the costs of the second segment and third segment are not constant, which would create non-linearity

when calculating the total cost. As non-linearity may create computational issues, linearization of the slope cost curve is required. The slope cost curve can be divided into several block sub-segments with the same length and, then, the total cost of a slope segment can be calculated by summing up those block sub-segments. Fig. 5.5 illustrates the linearization of a slope segment.

The procedure for linearizing a slope segment is presented below.

1) determine the number of sub-segments,

$$nSS = round(\frac{P_{g,s2} - P_{g,s1}}{\Delta bi}) \tag{5.10}$$

where nSS denotes the number of sub-segments for a slope segment; Δbi denotes the initially selected breadth of a sub-segment; and *round(x)* is a function that returns the integer number that is closest to *x*.

2) calculate the sub-segment breadth with (5.11),

$$\Delta s = (P_{g,s2} - P_{g,s1})/nSS \tag{5.11}$$

where Δs denotes the actual breadth of each sub-segment.

3) the cost for each sub-segment can be determined by (5.12).

$$C_i = C_1 + (i - 0.5)\frac{(P_{g,s2} - P_{g,s1})}{(C_2 - C_1)}\Delta s, \;\; i = 1..nSS \tag{5.12}$$

With the above procedure, a slope segment that is not flat can be converted into a series of small block segments. Therefore, a slope cost curve can be converted into a block cost curve, which enables the objective function to maintain linearity. It is worth noting that for both block cost curves and slope cost curves, the first segment is flat with zero slope and probably corresponds to the generator economic minimum $P_{g,s1}$ and the no-load cost C_1.

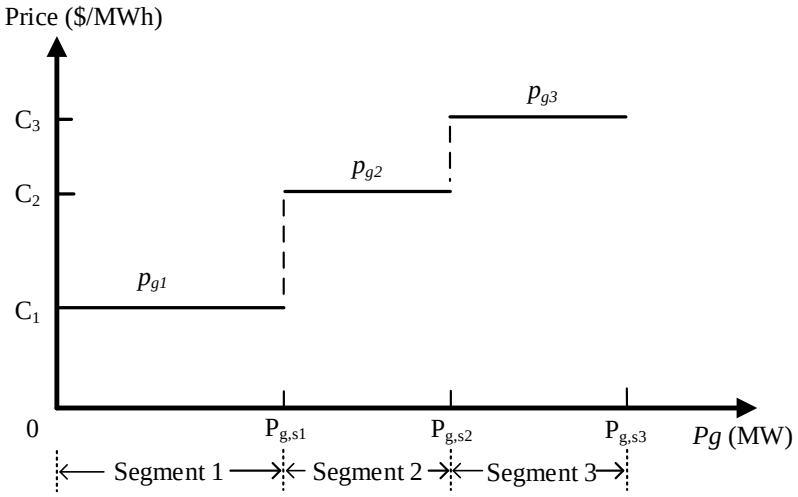

Fig. 5.3 Block Cost Curve of Generator *g*.

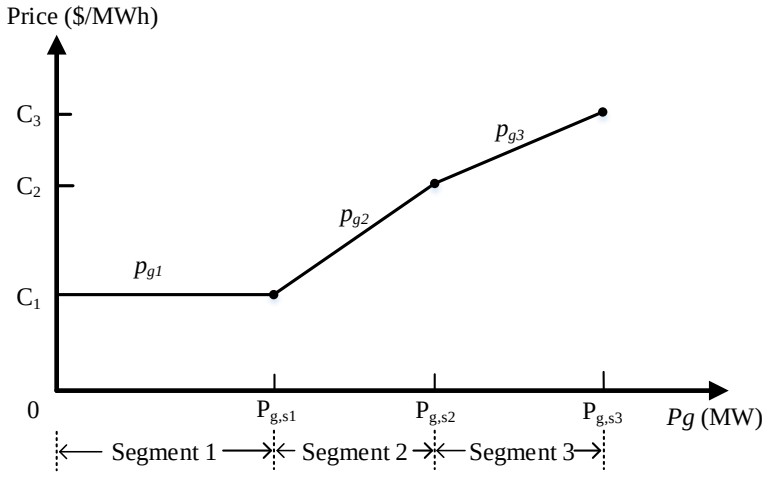

Fig. 5.4 Slope Cost Curve of Generator *g*.

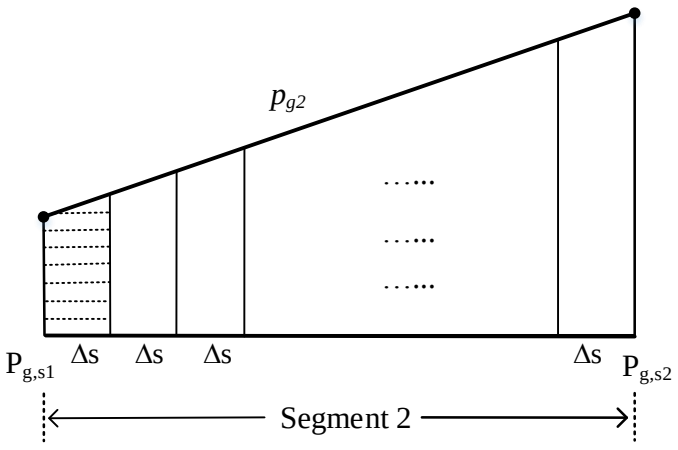

Fig. 5.5 Illustration of Linearization of a Slope Segment.

5.2.2 Objective Function

The proposed SCED models share the same objective function as existing industry practice, which is to minimize the total cost including operating energy cost and reserve cost. The objective function used in this work is shown below,

$$min \quad \sum_{g\in GD}\sum_{i=1}^{NS_g} p_{g,i}\cdot C_{g,i} + \sum_{g\in G} sr_g \cdot CSR_g + PF\_PD_{shed}\cdot(\sum_{d\in D} p_{d,shed} + \sum_{c\in C}\sum_{d\in D} p_{d,shed,c}) \tag{5.13}$$

Note that slope cost curves are converted into block cost curves before solving SCED.

5.2.3 Constraints

The constraints of a basic SCED can be expressed by (5.14)-(5.37). There are five sets of constraints: power balance constraints, load shedding constraints, generators constraints, reserve constraints, and network constraints. Those types of constraints are first introduced below and then several alternative constraints are presented.

Power Balance Constraints

One single system-wide power balance constraint per scenario is enough to model the power balance constraint for the PTDF based SCED formulation. System-wide power balance between generation and demand are enforced in (5.14) and (5.15) for the base case and the contingency cases respectively. For *B-θ* power flow model based formulation, node power balance constraints are used instead of one single system-wide constraint, which will be introduced later in this section.

$$\sum_{g\in G} p_g = \sum_{d\in D}(P_d - p_{d,shed}) \tag{5.14}$$

$$\sum_{g\in G} p_{g,c} = \sum_{d\in D}(P_d - p_{d,shed,c}) \ , \ c \in \mathrm{C} \tag{5.15}$$

Load Shedding Constraints

In a real power system, negative load may be used in the EMS to model fixed flows on the tie lines from energy market solutions. It is not reasonable to shed loads that are used to represent tie-line transfer flows with other neighboring systems. Similarly, it is not right to shed virtual loads that are used to represent losses. Thus, shedding load on negative loads and virtual loads is not allowed in this work, which is guaranteed by (5.16) and (5.17). For an actual positive demand, the shedded load cannot exceed the amount of that demand, which is guaranteed by (5.18) and (5.19).

$$p_{d,shed} = 0 \ , \ d \in \{\mathrm{DN}, \mathrm{DV}\} \tag{5.16}$$

$$p_{d,shed,c} = 0 \ , \ d \in \{\mathrm{DN}, \mathrm{DV}\}, \ c \in \mathrm{C} \tag{5.17}$$

$$0 \leq p_{d,shed} \leq P_d \ , \ d \in \{\mathrm{D}\} \backslash \{\mathrm{DN}, \mathrm{DV}\} \tag{5.18}$$

$$0 \leq p_{d,shed,c} \leq P_d \ , \ d \in \{\mathrm{D}\} \backslash \{\mathrm{DN}, \mathrm{DV}\}, \ c \in \mathrm{C} \tag{5.19}$$

Generator Constraints

Some generators such as self-scheduling units in practical power systems may not be available for dispatch to system operators. Therefore, those generators' outputs are fixed in RT SCED, which is expressed with (5.20) and (5.21).

Dispatchable generators typically offer stepwise incremental cost curves that consist of one or multiple pairs of segment prices and segment lengths. Equation (5.22) ensures that a generator's output equals the summation of the power outputs on all segments. Constraint (5.23) can guarantee that the power scheduled for each segment will not exceed the associated segment breadth.

Constraints (5.24) and (5.25) enforce the active power outputs of generators to be within their upper limits as well as lower limits for the base case and contingency cases respectively. Generators' energy ramping limit is modeled in (5.26) while generators' spinning ramping restriction is enforced by (5.27). Note that the ramping rates for energy re-dispatch and reserve deployment for the same unit may be different.

$$p_g = P_{g0} \ , \ g \in (G - GD) \tag{5.20}$$

$$p_{g,c} = P_{g0} \ , \ g \in (G - GD), \ c \in \mathrm{C} \tag{5.21}$$

$$p_g = \sum_{i=1}^{NS_g} p_{g,i} \ , \ g \in GD \tag{5.22}$$

$$0 \le p_{g,i} \le BS_{g,i} \ , \ g \in GD \tag{5.23}$$

$$P_{g,min} \le p_g \le P_{g,max} \ , \ g \in G \tag{5.24}$$

$$P_{g,min} \le p_{g,c} \le P_{g,max} \ , \ g \in G, \ c \in \mathrm{C} \tag{5.25}$$

$$-MRR_g \cdot T_{ED} \le p_g - P_{g0} \le MRR_g \cdot T_{ED} \ , \ g \in G \tag{5.26}$$

$$-SRR_g \cdot T_{SR} \le p_{g,c} - p_g \le SRR_g \cdot T_{SR} \ , \ g \in G, \ c \in \mathrm{C} \tag{5.27}$$

Reserve Constraints

The spinning reserve that an online unit can provide is subject to its ramping capability, which is expressed in (5.28). Constraint (5.29) guarantees that the sum of a unit's output and reserve cannot exceed its maximum limit. In other words, reserve is also restricted by unit's available capacity in addition to ramping limit. The "largest generator" rule is used for the reserve requirements as defined in (5.30), which ensures that there would be enough reserve to cover any of loss of a single generation.

$$0 \le sr_g \le SRR_g \cdot T_{SR} \ , \ \forall g \in G \tag{5.28}$$

$$p_g + sr_g \le P_{g,max} \ , \ \forall g \in G \tag{5.29}$$

$$\sum_{g \in G} sr_g \geq p_g + sr_g \ , \ \ \forall g \in G \tag{5.30}$$

Network Constraints

Though the largest generator contingency reserve requirement is modeled in SCED, there may still exist potential network violations due to congestion which limits reserve deliverability. Thus, it is necessary to model active network constraints in SCED. Branch thermal limits for the base case and contingency cases are enforced in (5.31) and (5.32) respectively. The branch monitor sets can be different for the base case and different contingency cases.

Due to concerns regarding voltage stability and transient stability, the total transfer capacity of the ties connecting two areas cannot exceed a specific limit which is referred to as interface limit or transfer limit. In SCED, the stability limit can be addressed by including constraints on the sum of active power flows on the branches that form the interface. The interface limit constraints are represented by (5.33) and (5.34) for the base case and contingency cases respectively. Note that the interface limit under contingency may be different with the limit in the base case especially when the contingency element is one of branches forming that interface.

Equations (5.35) and (5.36) that are used to calculate branch flows take the effects of generation re-dispatch, load shedding, and demand fluctuation into account. Note that (5.31) and (5.32) are only for branches in the monitor sets and (5.33) and (5.34) are only for critical interfaces; however, (5.35) and (5.36) are for both branches in the monitor sets and branches forming the active interfaces. The flow on contingency branch *c* is forced to be zero via (5.37).

$$-LimitA_k \le p_k \le LimitA_k \ , \ k \in KM(0) \tag{5.31}$$

$$-LimitC_k \le p_{k,c} \le LimitC_k \ , \ k \in \mathrm{KM(c)} \ , \ c \in \mathrm{C} \tag{5.32}$$

$$\sum_{k \in KI(i)} p_k \le Limit_i \ , \ i \in IM(0) \tag{5.33}$$

$$\sum_{k \in KI(i)} p_{k,c} \le Limit_{ic} \ , \ i \in IM(c), \ c \in \mathrm{C} \tag{5.34}$$

$$p_k = P_{k0} + \sum_{n \in N}(PTDF_{n,k} \cdot (\sum_{g \in G(n)}(p_g - P_{g0}) + \sum_{d \in D(n)}(p_{d,shed} + P_{d0} - P_d))) \ , \ k \in \{KM(0), IKM(0)\} \tag{5.35}$$

$$p_{k,c} = P_{k0} + LODF_{k,c} \cdot P_{c0} + \sum_{n \in N}(OTDF_{n,k,c} \cdot (\sum_{g \in G(n)}(p_{g,c} - P_{g0}) + \sum_{d \in D(n)}(p_{d,shed,c} + P_{d0} - P_d))) \ , \ k \in \{KM(c), IKM(c)\} \backslash \{c\}, \ c \in \mathrm{C} \tag{5.36}$$

$$p_{k,c} = 0 \ , \ k \in \{c\}, \ c \in \mathrm{C} \tag{5.37}$$

Alternative Constraints

Constraints (5.14)-(5.37) along with the objective function (5.13) form a basic SCED mathematical model. Enhancement can be made to this model. Some of those constraints can be replaced with alternative constraints as illustrated below.

Adding P_{g0} to each expression in inequality constraint (5.26) would reformulate it to (5.38), which shares the same form with (5.24). By simply taking the minimum of upper limits for p_g as the new upper limit and using the maximum of lower limits for p_g as the new lower limit, constraints (5.38) and (5.24) can be combined as (5.39). In other words, constraints (5.24) and (5.26) can be replaced by one single constraint (5.39), which would reduce the number of constraints and may increase the performance in terms of computational time.

$$P_{g0} - MRR_g \cdot T_{ED} \le p_g \le P_{g0} + MRR_g \cdot T_{ED} \ , \ g \in G \tag{5.38}$$

$$\max\{P_{g0} - MRR_g \cdot T_{ED},\ P_{g,min}\} \le p_g \le \min\{P_{g0} + MRR_g \cdot T_{ED},\ P_{g,max}\}, g \in G \quad (5.39)$$

When branch reactive power flow under contingency is available, $LimitC_{kc}$ can be calculated by (5.2) and should replace $LimitC_k$ in (5.32). Thus, (5.32) would be converted into the constraint shown below.

$$-LimitC_{k,c} \le p_{k,c} \le LimitC_{k,c}\ ,\ k \in \mathrm{KM(c)}\ ,\ c \in \mathrm{C} \quad (5.40)$$

Similarly, if the initial branch flow $P_{k,c,0}$ under contingency c is available from contingency analysis, the model would be more accurate by replacing $P_{k0} + LODF_{k,c}P_{c0}$ with $P_{k,c,0}$ in (5.36). Thus, (5.36) can be replaced by (5.41).

$$p_{k,c} = P_{k,c,0} + \sum_{n\in N}(OTDF_{n,k,c} \cdot (\sum_{g\in G(n)}(p_{g,c} - P_{g0}) + \sum_{d\in D(n)}(p_{d,shed,c} + P_{d0} - P_d)))\ ,\ k \in \{KM(c), IKM(c)\}\backslash\{c\},\ c \in \mathrm{C} \quad (5.41)$$

If the initial branch flow for both the base case and contingency case are not available, then, incremental PTDF based equations (5.35) and (5.36) can be replaced by cold-start PTDF based equations (5.42) and (5.43) respectively.

$$p_k = \sum_{n\in N}(PTDF_{n,k} \cdot (\sum_{g\in G(n)} p_g + \sum_{d\in D(n)}(p_{d,shed} - P_d))\ ,k \in \{KM(0), IKM(0)\} \quad (5.42)$$

$$p_{k,c} = \sum_{n\in N}(OTDF_{n,k,c} \cdot (\sum_{g\in G(n)} p_{g,c} + \sum_{d\in D(n)}(p_{d,shed,c} - P_d)))\ ,\ k \in \{KM(c), IKM(c)\}\backslash\{c\},\ c \in \mathrm{C} \quad (5.43)$$

Instead of using PTDF formulation, calculation of branch flow can use *B*-θ formulation, which are defined in (5.44) and (5.45). It is worth mentioning that all branch flows have to be calculated with *B*-θ formulation because there are mutual effects between voltage angle θ of all buses, while only the flows on branches of interests need

to be calculated with PTDF formulation. With *B*-θ formulation being used in SCED, system-wide power balance constraints (5.14) and (5.15) should be replaced with node power balance constraints (5.46) and (5.47) respectively.

$$p_k = (\delta_{n(k-)} - \delta_{n(k+)} + \alpha_k)/X_k \ , \ k \in K \tag{5.44}$$

$$p_{k,c} = (\delta_{n(k-),c} - \delta_{n(k+),c} + \alpha_k)/X_k \ , \ k \in K\backslash\{c\}, \ c \in \mathrm{C} \tag{5.45}$$

$$\sum_{g\in G(n)} p_g + \sum_{k\in K(n+)} p_k - \sum_{k\in K(n-)} p_k = \sum_{d\in D(n)}(P_d - p_{d,shed}), \ n \in N \tag{5.46}$$

$$\sum_{g\in G(n)} p_{g,c} + \sum_{k\in K(n+)} p_{k,c} - \sum_{k\in K(n-)} p_{k,c} = \sum_{d\in D(n)}(P_d - p_{d,shed,c}) \ , \ n \in N, \ c \in \mathrm{C} \tag{5.47}$$

5.2.4 Models

Based on the availability of network flow information and different power flow formulations, five different SCED models are proposed in this dissertation. They are listed below:

- Model 1: hot-start PTDF based SCED model,
- Model 2: warm-start PTDF based SCED model,
- Model 3: cold-start PTDF based SCED model,
- Model 4: hot-start *B*-θ based SCED model,
- Model 5: cold-start *B*-θ based SCED model.

The first three SCED models use PTDF power flow formulation while *B*-θ power flow formulation is used in the last two SCED models.

There are two types of SCED: corrective SCED (CSCED) and preventive SCED (PSCED). Generation re-dispatch is allowed for CSCED in the post-contingency sce-

narios; in other words, with CSCED model, the generation dispatch points under contingency are not necessary to be the same with the base-case generation schedule. However, the base-case generation schedule remains the same for all contingency cases with PSCED model. PSCED repositions online generators in advance to satisfy the operational requirements in both the base case and contingency cases. Therefore, PSCED is more conservative than CSCED, which would result in high variable operation cost. However, PSCED can provide a more secure and reliable solution than CSCED as the solution obtained from PSCED can withhold the loss of a single contingency without adjustment. Most, if not all, ISOs implement PSCED model rather than CSCED model due to security concerns.

Corrective SCED Models

The constraints described in Section 5.2.3 are general constraints for CSCED as variable $p_{g,c}$ is defined and used to represent unit generation under various contingency scenarios. The five proposed SCED models with corrective control strategy are described in Table 5.1. Those proposed SCED models share most of the constraints. For instance, the three SCED models that use PTDF formulation share the same system-wide power balance constraints while the two SCED models that use *B*-θ formulation share the same node power balance constraints.

The initial branch flow $P_{k,c,0}$ under contingency and the emergency limit $LimitC_{kc}$ that can be obtained from RTCA are available to Model 1, while Model 2 uses $P_{k,0}$ and line outage distribution factor (LODF) to calculate branch flow under contingency and uses $LimitC_k$ as the emergency limits of all contingency-case network constraints. A

cold-start branch flow calculation formulation is used in Model 3 rather than the incremental branch flow calculation formulations used in Model 1 and Model 2. SCED is built on the linearized DC power flow model; thus, apart from model error, the error of PTDF based branch flow calculation also depends on unit generation. Model 3 uses the entire generator output to calculate branch flow; however, incremental models only use the change in generator output, which is typically much smaller than the entire generator output, to calculate branch flow. Thus, the model precision of Model 3 would be less than Model 1 and Model 2. Model 4 and Model 5 are based on traditional *B-θ* power flow model. The difference between them is that Model 4 uses customized $LimitC_{kc}$ as the emergency limits for different contingency cases while Model 5 uses $LimitC_k$ as the emergency limit for all modeled active contingencies.

Table 5.1 Multiple Corrective SCED Models

	Shared set of constraints	Power balance constraints	Network constraints
CSCED Model 1	(5.16)-(5.23), (5.25), (5.27)-(5.31), (5.33), (5.34), (5.37), (5.39)	(5.14), (5.15)	(5.35), (5.40), (5.41)
CSCED Model 2			(5.32), (5.35), (5.36)
CSCED Model 3			(5.32), (5.42), (5.43)
CSCED Model 4		(5.46), (5.47)	(5.40), (5.44), (5.45)
CSCED Model 5			(5.32), (5.44), (5.45)

Preventive SCED Models

Corrective SCED allows the units' outputs under contingency to deviate from the base-case dispatch point, which would result in cheaper cost than preventive SCED. However, due to security and reliability concerns, preventive SCED is more popular in industry than corrective SCED. This section illustrates the mathematical model for SCED using preventive control strategy.

Given a CSCED model, a simple way to form a PSCED model is to add one more set of constraints (5.48), which force units' outputs under contingency to remain the same with units' outputs in the base case, into that CSCED model.

$$p_{g,c} = p_g \ , \ g \in G, \ c \in C \tag{5.48}$$

To construct a concise PSCED formulation, (5.48) can be simply substituted into the constraints that are involved with $p_{g,c}$. Thus, with adjustment, constraints (5.15), (5.36), (5.41), (5.43), and (5.47) can be transformed into the constraints below, (5.49) through (5.53), respectively. Moreover, with (5.48), constraints (5.21) and (5.25) will be equivalent to (5.20) and (5.24) respectively and constraint (5.27) will definitely hold; therefore, constraints (5.21), (5.25), and (5.27) should be removed in the PSCED model.

$$\sum_{d\in D} p_{d,shed} = \sum_{d\in D} p_{d,shed,c} \ , \ c \in \mathrm{C} \tag{5.49}$$

$$p_{k,c} = P_{k0} + LODF_{k,c}P_{c0} + \sum_{n\in N}(OTDF_{n,k,c}(\sum_{g\in G(n)}(p_g - P_{g0}) + \sum_{d\in D(n)}(p_{d,shed,c} + P_{d0} - P_d))) \ , \ k \in \{KM(c), IKM(c)\}\backslash\{c\}, \ c \in \mathrm{C} \tag{5.50}$$

$$p_{k,c} = P_{k,c,0} + \sum_{n\in N}(OTDF_{n,k,c}(\sum_{g\in G(n)}(p_g - P_{g0}) + \sum_{d\in D(n)}(p_{d,shed,c} + P_{d0} - P_d))) \ , \ k \in \{KM(c), IKM(c)\}\backslash\{c\}, \ c \in \mathrm{C} \tag{5.51}$$

$$p_{k,c} = \sum_{n\in N}(OTDF_{n,k,c}(\sum_{g\in G(n)} p_g + \sum_{d\in D(n)}(p_{d,shed,c} - P_d))) \ , \ k \in \{KM(c), IKM(c)\}\backslash\{c\}, \ c \in \mathrm{C} \tag{5.52}$$

$$\sum_{g\in G(n)} p_g + \sum_{k\in K(n+)} p_{k,c} - \sum_{k\in K(n-)} p_{k,c} = \sum_{d\in D(n)}(P_d - p_{d,shed,c}), n \in N, c \in \mathrm{C} \tag{5.53}$$

To further reduce the problem complexity, contingency-case load shedding variable $p_{d,shed,c}$ can be replaced by base-case load shedding variable $p_{d,shed}$. Thus, constraints (5.17), (5.19), and (5.49) can be ignore and constraints (5.50)-(5.53) can be converted to the constraints listed below, (5.54)-(5.57), respectively.

$$p_{k,c} = P_{k0} + LODF_{k,c}P_{c0} + \sum_{n\in N}(OTDF_{n,k,c}(\sum_{g\in G(n)}(p_g - P_{g0}) + \sum_{d\in D(n)}(p_{d,shed} + P_{d0} - P_d))),\ k \in \{KM(c), IKM(c)\}\backslash\{c\},\ c \in \mathrm{C} \quad (5.54)$$

$$p_{k,c} = P_{k,c,0} + \sum_{n\in N}(OTDF_{n,k,c}(\sum_{g\in G(n)}(p_g - P_{g0}) + \sum_{d\in D(n)}(p_{d,shed} + P_{d0} - P_d))),\ k \in \{KM(c), IKM(c)\}\backslash\{c\},\ c \in \mathrm{C} \quad (5.55)$$

$$p_{k,c} = \sum_{n\in N}(OTDF_{n,k,c}(\sum_{g\in G(n)} p_g + \sum_{d\in D(n)}(p_{d,shed} - P_d))),\ k \in \{KM(c), IKM(c)\}\backslash\{c\},\ c \in \mathrm{C} \quad (5.56)$$

$$\sum_{g\in G(n)} p_g + \sum_{k\in K(n+)} p_{k,c} - \sum_{k\in K(n-)} p_{k,c} = \sum_{d\in D(n)}(P_d - p_{d,shed}),\ n \in N,\ c \in \mathrm{C} \quad (5.57)$$

Table 5.2 Multiple Preventive SCED Models

	Shared set of constraints	Power balance constraints	Network constraints
PSCED Model 1	(5.16), (5.18), (5.20), (5.22), (5.23), (5.28)-(5.31), (5.33), (5.34), (5.37) (5.39)	(5.14)	(5.35), (5.40), (5.55)
PSCED Model 2			(5.32), (5.35), (5.54)
PSCED Model 3			(5.32), (5.42), (5.56)
PSCED Model 4		(5.46), (5.57)	(5.40), (5.44), (5.45)
PSCED Model 5			(5.32), (5.44), (5.45)

Similar to the proposed CSCED models, the proposed SCED models with preventive control strategy are described in Table 5.2. The differences between the proposed PSCED models are the availability of network flow information and different branch flow calculation formulations, which are consistent with the differences between the proposed CSCED models.

5.2.5 Market Implication

In addition to providing updated real-time dispatch solutions, SCED is also used to determine real-time energy market solutions including LMP. As the proposed E-SCED takes advantage of transmission network flexibility by using pseudo limit rather than actual limit used by a traditional SCED, it is important to analyze the effect of utilization of pseudo limit on market results. Thus, LMP, load payment, generator revenue, generator cost, generator rent, congestion cost, and congestion revenue are introduced and analyzed in this work.

Locational marginal pricing is a market mechanism that is used to clear wholesale energy markets that are managed by ISOs. A locational marginal price at a specific bus reflects the least cost of supplying the next increment load at that bus while meeting all physical and reliability constraints. LMP consists of three components: energy component, congestion component, and loss component. If a system had a network with infinite capacity and no losses, all LMPs would be the same over the entire system. However, in reality, losses cannot be avoided and network congestion issue typically exists. In this work, losses are represented by virtual loads for SCED models 3-5 and are implicitly incorporated in the initial branch flows for SCED models 1-2; thus, the loss component is ignored in this work. The nodal LMP for PSCED model 1 can be calculated by the following equation,

$$LMP_n = LMP_s + LMP_{cg,n}\ ,\ n \in N \tag{5.58}$$

where $LMP_{cg,n}$ denotes the congestion component of the LMP at bus *n*, which can be calculated below,

$$LMP_{cg,n} = \sum_{k\in KM(0)} PTDF_{n,k}(F_k^+ - F_k^-) + \sum_{c\in C}\sum_{k\in KM(c)} OTDF_{n,k,c}\left(F_{k,c}^+ - F_{k,c}^-\right) + \sum_{i\in IM(0)}\sum_{k\in KI(i)} PTDF_{n,k}(F_i^+ - F_i^-) + \sum_{c\in C}\sum_{i\in IM(0)}\sum_{k\in KI(i)} OTDF_{n,k,c}\left(F_{i,c}^+ - F_{i,c}^-\right), n \in N \quad (5.59)$$

Proof of (5.58)

This proof is only for deriving the nodal LMP equation (5.58); thus, for simplicity, the constraints and variables that are not of interest are ignored, as well as the objective function. As strong duality theory is used to prove (5.58), the constraints for a simplified but sufficient primal problem are listed below.

$$\sum_{n\in N} PI_n = 0 \qquad (LMP_s) \quad (5.60)$$

$$\sum_{g\in G(n)} p_g + \sum_{d\in D(n)} p_{d,shed} - PI_n = \sum_{d\in D(n)} P_d \ , n \in N \qquad (LMP_n) \quad (5.61)$$

$$P_{k0} + \sum_{n\in N}(PTDF_{n,k}(PI_n - PI_{n,0})) \le LimitA_k \ , k \in KM(0) \qquad (F_k^+) \quad (5.62)$$

$$-P_{k0} - \sum_{n\in N}(PTDF_{n,k}(PI_n - PI_{n,0})) \le LimitA_k \ , k \in KM(0) \qquad (F_k^-) \quad (5.63)$$

$$P_{k,c,0} + \sum_{n\in N}(OTDF_{n,k}(PI_n - PI_{n,0})) \le LimitC_{kc} \ , k \in KM(c) \qquad (F_{k,c}^+) \quad (5.64)$$

$$-P_{k,c,0} - \sum_{n\in N}(OTDF_{n,k}(PI_n - PI_{n,0})) \le LimitC_{kc} \ , k \in KM(c) \qquad (F_{k,c}^-) \quad (5.65)$$

$$\sum_{k\in KI(i)}(P_{k0} + \sum_{n\in N}(PTDF_{n,k}(PI_n - PI_{n,0})) \le Limit_i, i \in IM(0) \qquad (F_i^+) \quad (5.66)$$

$$-\sum_{k\in KI(i)}(P_{k0} + \sum_{n\in N}(PTDF_{n,k}(PI_n - PI_{n,0})) \le Limit_i, \ i \in IM(0) \qquad (F_i^-) \quad (5.67)$$

$$\sum_{k\in KI(i)}(P_{k,c,0} + \sum_{n\in N}(OTDF_{n,k}(PI_n - PI_{n,0})) \le Limit_{ic}, \ i \in IM(c) \qquad (F_{i,c}^+) \quad (5.68)$$

$$-\sum_{k\in KI(i)}(P_{k,c,0} + \sum_{n\in N}(OTDF_{n,k}(PI_n - PI_{n,0})) \le Limit_{ic}, \ i \in IM(c) \qquad (F_{i,c}^-) \quad (5.69)$$

Constraint (5.60) ensures the system-wide power balance while constraint (5.61) is for nodal power balance. Constraint (5.60) is redundant for *B-θ* based SCED (SCED model 4 - SCED model 5) while constraint (5.61) is not needed for PTDF based SCED

(SCED model 1 - SCED model 3); however, they are listed in this model just for deriving the relationship between nodal LMP and system LMP. Constraints (5.62)-(5.65) show that the system is subject to branch thermal limit. Moreover, power systems are also restricted by interface limits, which is guaranteed by (5.66)-(5.69). Variables LMP_s, LMP_n, F_k^+, F_k^- $F_{k,c}^+$, $F_{k,c}^-$, F_i^+, F_i^-, $F_{i,c}^+$, and $F_{i,c}^-$ are the dual variables that are associated with these constraints of the primal problem.

Note that variable PI_n denotes power net injection at bus *n*, which can either positive or non-positive; then, it is unconstrained in the primal problem. Therefore, the associated constraints in the dual problem are the equality constraints as expressed in (5.70),

$$LMP_n - LMP_s + \sum_{k\in KM(0)} PTDF_{n,k}(F_k^+ - F_k^-) + \sum_{c\in C}\sum_{k\in KM(c)} OTDF_{n,k,c}\left(F_{k,c}^+ - F_{k,c}^-\right) + \sum_{i\in IM(0)}\sum_{k\in KI(i)} PTDF_{n,k}(F_i^+ - F_i^-) + \sum_{c\in C}\sum_{i\in IM(0)}\sum_{k\in KI(i)} OTDF_{n,k,c}\left(F_{i,c}^+ - F_{i,c}^-\right) = 0,\ n \in N \quad (5.70)$$

where LMP_s and LMP_n are unconstrained; F_k^+, F_k^- $F_{k,c}^+$, $F_{k,c}^-$, F_i^+, F_i^-, $F_{i,c}^+$, and $F_{i,c}^-$ are non-positive. Then, (5.58) can be obtained by reformatting (5.70).

Average LMP is proposed to analyze the effect of modeling CTS implicitly in SCED on LMP. Average LMP over the entire system is defined in (5.71). Similarly, average congestion LMP is defined in (5.72).

$$AvgLMP = \sum_{n\in N} LMP_n\ ,\ n \in N \quad (5.71)$$

$$AvgLMP_{cg} = \sum_{n\in N} LMP_{cg,n}\ \ ,\ n \in N \quad (5.72)$$

Load payment is calculated by (5.73) and generator revenue is determined by (5.74). Equation (5.75) calculates the generator cost which is part of the objective function. Generator rent is calculated by (5.76). Note that in this work, the generator rent only accounts energy and does not include reserve rent. Congestion revenue, which is used to fund the financial transmission rights markets, is the difference between generator revenue and load payment, as calculated by (5.77).

$$LdPaymt = \sum_{n\in N}(LMP_n(\sum_{d\in D(n)} P_d)) \tag{5.73}$$

$$GenRvn = \sum_{n\in N}(LMP_n(\sum_{g\in G(n)} p_g)) \tag{5.74}$$

$$GenCost = \sum_{g\in GD}\sum_{i=1}^{NS_g} p_{g,i}C_{g,i} \tag{5.75}$$

$$GenRent = GenRvn - GenCost \tag{5.76}$$

$$CngstRvn = GenRvn - GenCost \tag{5.77}$$

In addition to congestion revenue, congestion cost is also proposed to measure the degree of network congestion. Congestion cost is defined as (5.78),

$$CngstCost = TotalCost1 - TotalCost2 \tag{5.78}$$

where $TotalCost1$ denotes the optimal objective value of either an E-SCED or a SCED and $TotalCost2$ denotes the optimal objective value obtained by solving the same E-SCED or SCED but without any network constraints.

Thus, the congestion cost reduction CCR_{CTS} achieved by E-SCED as compared to a traditional SCED can be calculated with (5.79).

$$CCR_{CTS} = CngstCost_{E-SCED} - CngstCost_{SCED} \tag{5.79}$$

5.3 Case Studies

In this section, the Cascadia system [140] is used to verify the proposed Procedure-A and Procedure-B, as well as the proposed SCED models. This test case contains 179 buses, 40 online generators, and 245 branches. The total in-service load is 7324 MW while the total online generation capacity is 9323 MW.

5.3.1 Procedure-A: SCED with RTCA

To fully evaluate the proposed Procedure-A, base-case power flow is first performed; then, RTCA is conducted on a contingency list consisting of all non-radial branches.

There is no violation observed in the base case. Fig. 5.6 shows the initial system condition of a key portion of the Cascadia system where contains two critical contingency-element and the beneficial switching branches.

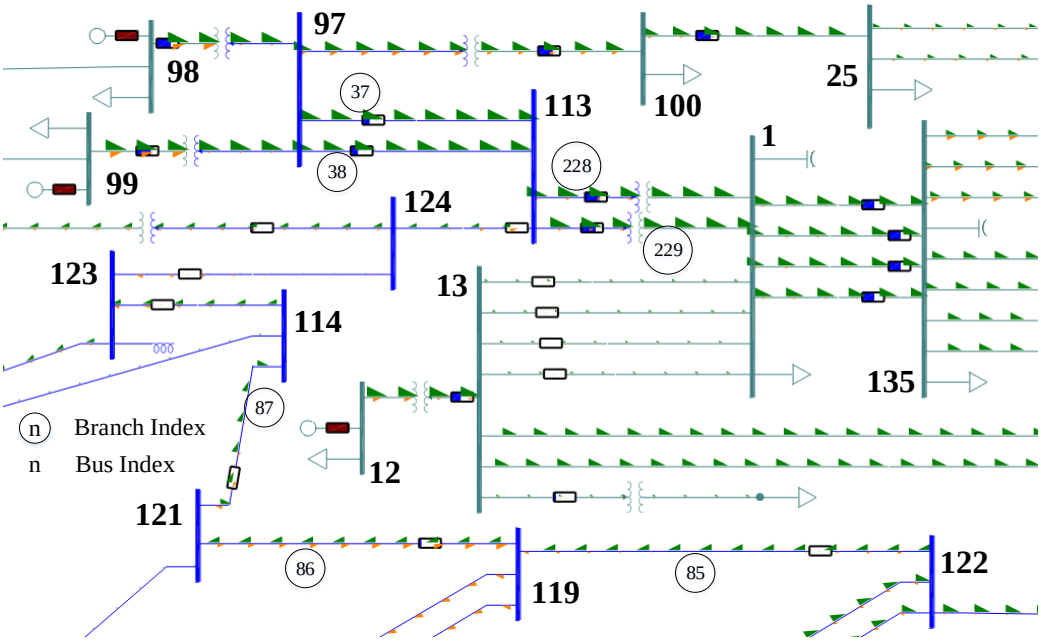

Fig. 5.6 System Condition of a Portion of the Cascadia System in the Base Case.

The RTCA results on the Cascadia system are listed in Table 5.3. Two out of 150 contingencies cause violations and, thus, they are considered to be critical contingencies. Those two critical contingencies, which are branch 228 and branch 229 respectively, are two parallel branches. When one of them is out of service, the other branch will be overload by 241.6 MVA or 18.69% beyond the emergency rating. Fig. 5.7 shows branch 229 is overloaded under the outage of branch 228. As those two critical contingencies are equivalent and cause the same consequences, only the results for the contingency on branch 228 will be presented for the rest of this section.

Table 5.3 Results of RTCA on the Cascadia System

Contingency Branch	Monitor Branch	Branch Flow (MVA)	Emergency Rating (MVA)	Violation (MVA)	Violation in Percent
228	229	1534.1	1292.5	241.6	18.69%
229	228	1534.1	1292.5	241.6	18.69%

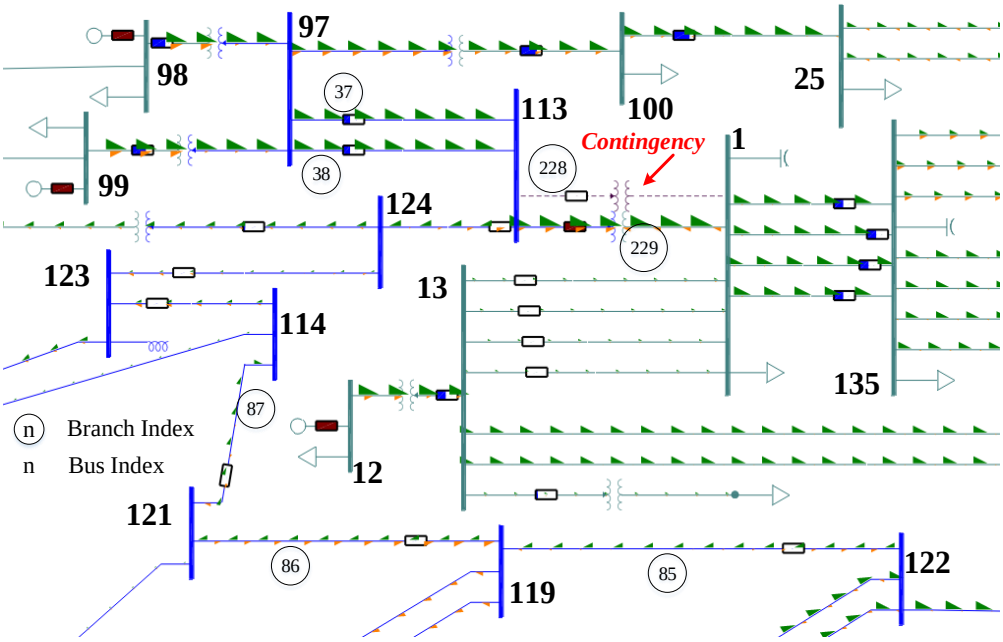

Fig. 5.7 System Condition of a Portion of the Cascadia System under the Outage of Branch 228.

As existing SCED application in industry uses preventive control strategy rather than corrective control strategy, only the proposed PSCED models presented in Table 5.2 are studied in this section. In this study, Pct and $PctC$ are set to 50% and 90% respectively unless they are explicitly described. The proposed SCED models share most of the constraints and the difference between them is the form of network constraints. In this report, Gurobi [146] is used as the optimization solver to solve SCED.

Table 5.4 presents the cost results with different SCED models. Cold-start PTDF power flow formulation based Model 3 and cold-start B-θ power flow formulation based Model 5 are essentially equivalent and they share the same lowest total cost among all SCED models. As shown in Table 5.5, the solution times for solving different SCED models are very similar.

It is essential to evaluate the SCED solution in an AC setting since the DC power flow model used in SCED is an approximation and the accuracy cannot be guaranteed. Thus, the SCED solution, mainly the generators' active power output setting points, is fed back into the base-case power flow simulation and N-1 contingency analysis. The results for both SCED application and Post-SCED contingency analysis are shown in Table 5.6.

Table 5.4 Cost for Different PSCED Models on the Cascadia System

	Total cost ($/h)	Energy cost ($/h)	Reserve cost ($/h)
SCED Model 1	50169.0	42943.3	7225.7
SCED Model 2	50011.8	42930.7	7081.1
SCED Model 3	49862.1	42903.7	6958.4
SCED Model 4	49903.8	42920.4	6983.3
SCED Model 5	49862.1	42903.7	6958.4

Table 5.5 Computational Time for Solving Different PSCED Models on the Cascadia System

	Total time (s)	Presolve time (s)	LP solver time (s)
SCED Model 1	0.09	0.01	0.01
SCED Model 2	0.11	0.01	0.01
SCED Model 3	0.11	0.01	0.01
SCED Model 4	0.14	0.01	0.02
SCED Model 5	0.17	0.01	0.02

Table 5.6 Results of SCED and Post-SCED *N*-1 check with Different PSCED Models on Cascadia

	SCED			Post-SCED *N*-1 check			
	Limit (MW)	Flow (MW)	Dual ($/MWh)	Rating (MVA)	Flow (MVA)	Violation (MVA)	Over Loading
SCED Model 1	1284.0	1284.0	-10.49	1292.5	1294.0	1.5	0.11%
SCED Model 2	1291.7	1291.	-9.76		1310.6	18.0	1.40%
SCED Model 3	1291.7	1291.7	-2.44		1329.7	37.2	2.88%
SCED Model 4	1284.0	1284.0	-9.76		1322.4	29.8	2.31%
SCED Model 5	1291.7	1291.7	-2.44		1329.7	37.2	2.88%

Obviously, the generation re-dispatch solution obtained from SCED Model 1 out-performs any other models in the AC based *N*-1 check (contingency analysis) in the post-SCED stage. With the dispatch points obtained from SCED Model 1, the flow violation on branch 229 under contingency 228 is reduced from 241.6 MVA down to only 1.5 MVA, corresponding to an overloading of 0.11% beyond the emergency limit, which is negligible; moreover, there is no other post-contingency violation or base-case violation.

Model 2 has the second best performance. In this model, LODF is used to calculate the initial post-contingency branch flow. The solution of SCED Model 2 causes 18.0 MVA violation, which is 16.5 MVA violation more than Model 1, under the same contingency 228. The extra 16.5 MVA overload comes from two sources: 1) DC model based LODF cannot accurately calculate the post-contingency branch flow, and 2) the branch emergency limit calculated by (5.2) is less precise than (5.3).

As expected, cold-start PTDF based Model 3 and cold-start B-θ based Model 5 share the least performance and result in 37.2 MVA post-contingency violation on branch 229 under contingency 228. Model 4 has a better performance than Model 5 since the branch emergency limit used in Model 4 is more accurate than Model 5.

Though Model 1 results in the highest total cost as shown in Table 5.4, it provides the best performance in the accurate AC setting. On the contrary, the dispatch points obtained by other SCED models would cause severe violations. In other words, Model 2 though Model 5 provide a cheaper solution at the cost of system security, which would violate the security standards and put the system in a dangerous situation. Thus, Model 1 is preferred than other models and the rest analysis of this work will use Model 1 only.

Note that the dual variable of the network constraint on branch 229 under contingency 228 with Model 1 is 10.49 $/MWh, which implies that the total cost will be reduced by 10.49 $/h if the emergency limit of branch 229 increases by 1 MW.

As network constraints can largely affect the SCED performance especially for large-scale real power systems, the sensitivity of thresholds Pct and $PctC$ on the SCED performance is investigated and the results for system performance, cost, and computational time are presented in Table 5.7, Table 5.8, and Table 5.9 respectively. It is interesting to observe that the system performance with different thresholds for selecting network constraints are the same, as well as the SCED cost.

Table 5.7 Results with Different *Pct* and *PctC* on the Cascadia System

Pct	*PctC*	SCED Model 1			*N*-1 check			
		Limit (MW)	Flow (MW)	Dual ($/MWh)	Rating (MVA)	Flow (MVA)	Violation (MVA)	Over Loading
1%	1%	1284.0	1284.0	-10.49	1292.5	1294.0	1.5	0.11%
50%	50%		1284.0	-10.49		1294.0	1.5	0.11%
80%	80%		1284.0	-10.49		1294.0	1.5	0.11%
100%	100%		1284.0	-10.49		1294.0	1.5	0.11%

Table 5.8 SCED Cost with Different *Pct and PctC* on the Cascadia System

Pct	*PctC*	SCED Model 1		
		Total cost ($/hr)	Energy cost ($/h)	Reserve cost ($/h)
1%	1%	50169.0	42943.3	7225.7
50%	50%	50169.0	42943.3	7225.7
80%	80%	50169.0	42943.3	7225.7
100%	100%	50169.0	42943.3	7225.7

Table 5.9 Computational Time for Solving SCED with Different *Pct* and *PctC* on the Cascadia System

Pct	*PctC*	SCED Model 1		
		Total time (s)	Presolve time (s)	LP solver time (s)
1%	1%	5.27	1.05	1.63
50%	50%	1.60	0.23	0.34
80%	80%	0.12	0.01	0.02
100%	100%	0.06	0.00	0.01

As shown in Table 5.9, the case with both Pct and $PctC$ being set to 100% takes much less time than other cases while obtaining exactly the same solutions. This is consistent with industrial practice. For a real power system, the initial dispatch point for RT SCED is not far away from the optimal solution, which is the key why only modeling a very small subset of critical network constraints can maintain the system security.

5.3.2 Procedure-B: SCED with CTS-based RTCA

Procedure-B is an enhanced version of Procedure-A by taking CTS into consideration. To focus on the potential benefits that would be provided by CTS, the duplicate results shared by both procedures will not be presented again in this section.

In Procedure-B, RTCA with CTS is implemented rather than just a traditional RTCA. Table 5.10 shows the results of CTS for contingency 228. The top five best switching actions that provide Pareto improvement can reduce the post-contingency violation by 30.78%, 30.78%, 29.01%, 20.11%, and 19.85% respectively. Fig. 5.8 shows the system condition with branch 37 switching out of service for relieving the overload that is caused by outage of branch 228. Though the overload on branch 229 still exists, it can be reduced by 74.4 MVA with the top CTS solution.

Table 5.10 Results of RTCA with CTS on the Cascadia System

Contingency branch	Original violation (MVA)	CTS ranking	CTS branch	Pareto improvement flag	Violation reduction (MVA)	Violation reduction in percent
228	241.6	1st Best	37	Yes	74.4	30.78%
		2nd Best	38	Yes	74.4	30.78%
		3rd Best	85	Yes	70.1	29.01%
		4th Best	86	Yes	48.6	20.11%
		5th Best	87	Yes	48.0	19.85%

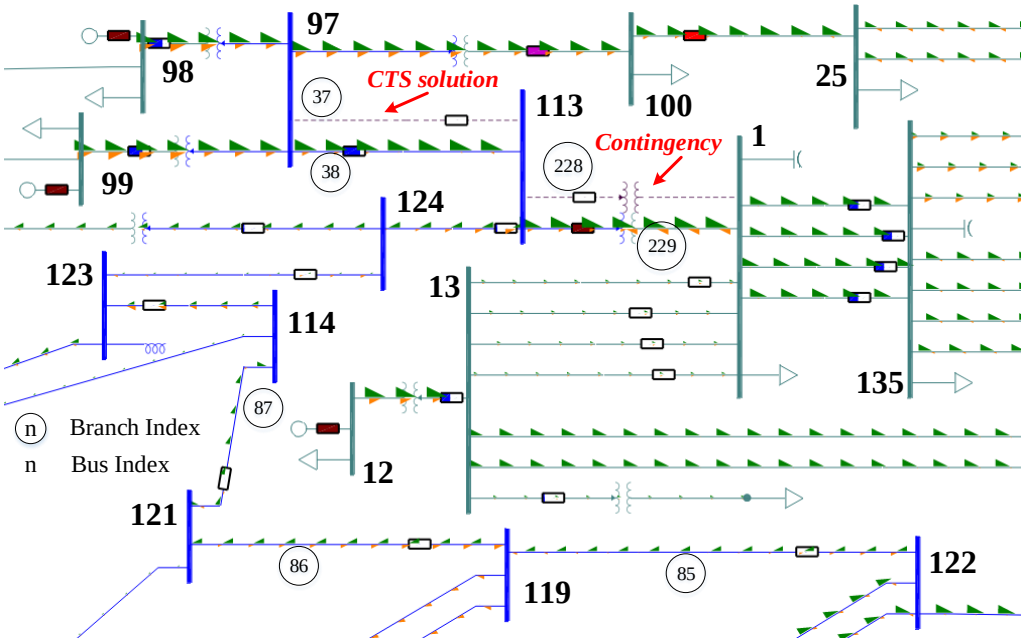

Fig. 5.8 System Condition of a Portion of the Cascadia System in the Post-Switching Situation (CTS Branch 37) under the Outage of Branch 228.

Table 5.11 lists the emergency limits of branch 229 in the SCED applications with and without CTS. Without consideration of CTS, the actual emergency limit for SCED is 1284.0 MW calculated by (5.2). However, considering the violation reduction benefit provided by CTS, pseudo emergency limits, which can be calculated by (5.8) and are higher than the actual emergency limits, are used to replace actual emergency limits in E-SCED. E-SCED1, E-SCED2, E-SCED3, E-SCED4, and E-SCED5 in Table 5.11 considers different pseudo emergency limits that are associated with the 1st, 2nd, 3rd, 4th, and 5th best switching actions respectively.

With the best switching solution, the associated pseudo emergency limit of branch 229 under contingency 228 for SCED is 1358.8 MW, which is 74.4 MW higher than the actual emergency limit. In addition, the emergency limit of branch 229 for E-SCED can increase by 48 MW even with the 5th best switching action.

Table 5.11 Emergency Limits of Branch 229 under Contingency 228 with and without CTS on the Cascadia System

	CTS ranking	CTS branch	Actual emergency limit (in MW) w/o CTS	Pseudo emergency limit (in MW) w. CTS
SCED	NA	NA	1284.0	NA
E-SCED1	1st Best	37	NA	1358.8
E-SCED2	2nd Best	38		1358.8
E-SCED3	3rd Best	85		1354.5
E-SCED4	4th Best	86		1332.9
E-SCED5	5th Best	87		1332.3

NA denotes "not applicable".

To be consistent with previous analysis, Pct and $PctC$ are set to be 50% and 90% respectively for E-SCED that considers CTS. Table 5.12 shows the results of a traditional SCED without CTS, E-SCEDs with different CTS actions, and a relaxed SCED without any network constraint.

Table 5.12 Results of Various SCED Models on the Cascadia System

			SCED Model 1						
			Branch 229 under contingency 228			Total cost ($/h)	Congestion cost ($/h)	Congestion cost reduction w. CTS	Total solution time (s)
			Limit (MW)	Flow (MW)	Dual ($/MWh)				
E-SCED1	with CTS	1st Best	1358.8	1358.8	-1.23	49797.9	34.5	91.49%	0.11
E-SCED2		2nd Best	1358.8	1358.8	-1.23	49797.9	34.5	91.49%	0.11
E-SCED3		3rd Best	1354.5	1354.5	-1.37	49803.6	40.2	90.09%	0.12
E-SCED4		4th Best	1332.9	1332.9	-1.82	49834.6	71.2	82.45%	0.12
E-SCED5		5th Best	1332.3	1332.3	-1.82	49835.8	71.6	82.35%	0.12
SCED	w/o. CTS		1284.0	1284.0	-10.49	50169.0	405.6	NA	0.09
Relaxed SCED	With no network constraint		NA			49763.4	0.0	NA	0.04

NA denotes "not applicable".

A binding branch constraint may prevent the cheap units from producing more power, which is the cause of congestion cost and unnecessary high total cost. The results of a SCED without consideration of network constraints are used as the benchmark to gauge the effect of CTS on SCED. By comparing the total cost of a traditional SCED

and the total cost of a SCED without any network constraints, the congestion cost of the traditional SCED without CTS can be calculated and it is 405.6 $/h.

It is intuitive that the congestion cost would drop with a higher limit of the bottleneck branch, which is illustrated in Table 5.12. The congestion cost of E-SCED can be reduced by 91.49% to 82.35% with the top five identified switching solutions. Fig. 5.9 presents the congestion cost associated with the traditional SCED and different E-SCED models on the Cascadia system. With the top five identified CTS solutions being considered in E-SCEDs respectively, the congestion cost is reduced from 405.6 $/h to a much smaller value ranging from 34.5 $/h to 71.6 $/h.

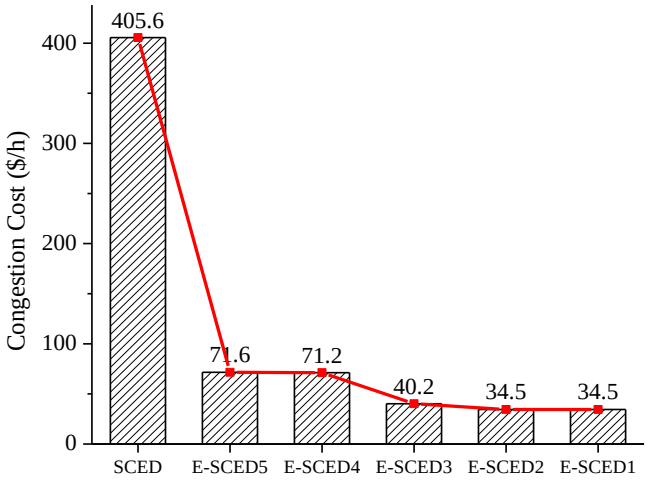

Fig. 5.9 Congestion Costs of the Traditional SCED and Various E-SCEDs on the Cascadia System.

It is interesting that the top switching action can reduce the congestion cost by 91.49% while it can only reduce the post-contingency violation by 30.78%. By implementing one single switching action, the congestion cost reduction in percent for SCED with CTS is much higher than post-contingency violation reduction in percent for

RTCA with CTS. One possible reason is that the marginal cost reduction with 1 MW increase on branch limit may drop as the associated branch limit becomes higher.

Relieving the binding branch constraint by increasing the branch limit would first allow the cheapest available unit to ramp up and force the most expensive unit to reduce its output. After that, if that branch is still binding, further increasing the branch limit may allow second cheapest available units to ramp up and reduce the outputs of the second most expensive units, which would still reduce the total cost but the cost reduction for each MW relieved in the branch limit would decline.

The above conclusion can also be made from the viewpoint of flowgate pricing, the dual variable of network constraint. With the actual emergency limit 1284.0 MW of branch 229, the associated dual variable is -10.49 $/h, which implies that the total cost will drop by 10.49 $/h if the emergency limit of branch 229 increase by 1 MW from 1284.0 MW. However, when the pseudo emergency limit 1332.3 MW is used, the associated dual variable becomes -1.82 $/h, which implies that the total cost will only drop by 1.82 $/h if the emergency limit of branch 229 increase by 1 MW from 1332.3 MW. Thus, as the branch limit increases, the marginal total cost reduction may drop, which implies that small post-contingency violation reduction in percent with CTS may result in high cost reduction in percent for SCED.

Though it has been demonstrated that congestion cost can be significantly reduced with CTS by using the pseudo emergency limits in SCED, the violation reduction performance of CTS in the post-SCED stage should also be examined as the system condition changes.

In the pre-SCED stage, the post-contingency violation reductions would be different by implementing different switching actions and, thus, the associated pseudo limits calculated by (5.8) would also be different in the SCED stage, which may result in different SCED solutions. The results of traditional RTCA in the post-SCED stage, with different CTS or pseudo limits considered in SCED, are shown in Table 5.13. The results in this table are for branch 229 under contingency 228. As expected, the post-contingency violation increases with higher ranked beneficial switching action considered in SCED.

Table 5.13 Results of the Post-SCED RTCA with Different CTS Considered in SCED on Cascadia

CTS	Actual Emergency Rating (MVA)	Flow (MVA)	Violation (MVA)	Over Loading
1st Best	1292.5	1376.5	84.0	6.50%
2nd Best				
3rd Best		1371.6	79.0	6.11%
4th Best		1346.6	54.1	4.18%
5th Best		1345.8	53.3	4.12%

Table 5.14 shows the results of RTCA with CTS in the post-SCED stage. The SCED solution used for Table 5.14 corresponds to the 1st best CTS solution identified in the pre-SCED stage on the Cascadia system. The results in this table are for branch 229 under contingency 228. Before CTS, contingency 228 causes a violation of 84 MVA on branch 229 as shown in Table 5.13. However, that violation can be eliminated with CTS. All five beneficial CTS actions identified in the pre-SCED stage are investigated in the post-SCED stage. In this case, the top two switching actions that are identified in the pre-SCED situation can reduce the post-contingency violation by about 85% while the other three switching actions can all fully eliminate the violation.

Table 5.14 Results of RTCA with CTS in the Post-SCED Stage with the SCED Solution Corresponding to the 1st Best CTS Solution Identified in the Pre-SCED Stage on the Cascadia System

CTS	Flow (MVA)	Flow change caused by CTS (MVA)	Percent violation beyond limit	Violation (MVA)	Violation reduction (MVA)	Violation reduction in percent
1st Best	1304.9	-71.5	0.96%	12.4	71.5	85.20%
2nd Best	1304.9	-71.5	0.96%	12.4	71.5	85.20%
3rd Best	1235.6	-140.9	0.0%	-56.9	84.0	100%
4th Best	1285.8	-90.7	0.0%	-6.7	84.0	100%
5th Best	1280.2	-96.3	0.0%	-12.3	84.0	100%

Though the amounts of violation reduction with CTS in the post-SCED scenario are different with the pre-SCED scenario, all CTS actions identified in the pre-SCED scenario can reduce the flow on the overloaded branch. This demonstrates that CTS is able to provide benefits even when the system condition has changed.

The results for considering the benefits provided by the 2nd best CTS action in SCED would be the same with 1st best CTS action considered, since the 1st best CTS branch and the 2nd best CTS branch are equivalent as they are in parallel and share the same parameters.

Table 5.15, Table 5.16, and Table 5.17 show the results of RTCA with CTS in the post-SCED stage, corresponding to different generator dispatch points obtained from the SCEDs that considers the 3rd, 4th, and 5th best CTS solutions respectively. If the pseudo emergency limit associated with the 3rd best CTS action is used in SCED, RTCA simulated in the post-SCED stage results in an overload of 79 MVA on branch 229 under contingency 228; however, three of the five CTS actions can fully eliminate that post-contingency violation while the other two CTS solutions can reduce overload by

more than 90%. For E-SCED with the 4th or 5th best CTS action, all five CTS actions can fully eliminate the post-contingency overload.

Table 5.15 Results of RTCA with CTS in the Post-SCED Stage with the SCED Solution Corresponding to the 3rd Best CTS Solution Identified in the Pre-SCED Stage on the Cascadia System

CTS	Flow (MVA)	Flow change caused by CTS (MVA)	Percent violation beyond limit	Violation (MVA)	Violation reduction (MVA)	Violation reduction in percent
1st Best	1300.0	-71.5	0.58%	7.5	71.5	90.53%
2nd Best	1300.0	-71.5	0.58%	7.5	71.5	90.53%
3rd Best	1228.5	-143.1	0.0%	-64.1	79.0	100%
4th Best	1282.2	-89.3	0.0%	-10.3	79.0	100%
5th Best	1277.0	-94.5	0.0%	-15.5	79.0	100%

Table 5.16 Results of RTCA with CTS in the Post-SCED Stage with the SCED Solution Corresponding to the 4th best CTS Solution Identified in the Pre-SCED Stage on the Cascadia System

CTS	Flow (MVA)	Flow change caused by CTS (MVA)	Percent violation beyond limit	Violation (MVA)	Violation reduction (MVA)	Violation reduction in percent
1st Best	1275.3	-71.3	0.0%	-17.2	54.1	100%
2nd Best	1275.3	-71.3	0.0%	-17.2	54.1	100%
3rd Best	1195.2	-151.4	0.0%	-97.3	54.1	100%
4th Best	1263.8	-82.8	0.0%	-28.7	54.1	100%
5th Best	1260.8	-85.8	0.0%	-31.7	54.1	100%

Table 5.17 Results of RTCA with CTS in the Post-SCED Stage with the SCED Solution Corresponding to the 5th Best CTS Solution Identified in the Pre-SCED Stage on the Cascadia System

CTS	Flow (MVA)	Flow change caused by CTS (MVA)	Percent violation beyond limit	Violation (MVA)	Violation reduction (MVA)	Violation reduction in percent
1st Best	1274.5	-71.4	0.0%	-18	53.3	100%
2nd Best	1274.5	-71.4	0.0%	-18	53.3	100%
3rd Best	1194.4	-151.5	0.0%	-98.1	53.3	100%
4th Best	1263.1	-82.8	0.0%	-29.4	53.3	100%
5th Best	1260.2	-85.7	0.0%	-32.3	53.3	100%

With lower branch limits used for the network constraints in SCED, branches would have more security margins in the post-SCED stage. As the congestion cost reduction does not vary much with different CTS solutions considered in SCED, using

the pseudo limit associated with the 3rd best switching actions can provide both economic benefits and significant post-contingency violation reductions.

Market solutions of the traditional SCED and the proposed E-SCEDs are shown in Table 5.18. When the flexibility in transmission network is taken into account, the load payment drops significantly, as well as the generator revenue, generator rent, and congestion revenue. It is observed that the amount of load payment reduction is much more than the amount of generator rent reduction. Fig. 5.10 and Fig. 5.11 show the load payment and congestion revenue respectively, for various SCED and E-SCEDs on the Cascadia system. Apparently, with higher pseudo limit used in E-SCED, the system-wide load payment and congestion revenue substantially decreases, which implies that E-SCED can improve the market efficiency in comparison with a traditional SCED.

Table 5.18 Market Results with SCED and Various E-SCED on the Cascadia System

	Load Payment ($/h)	Generator Revenue ($/h)	Generator Cost ($/h)	Generator Rent ($/h)	Congestion Revenue ($/h)
E-SCED1	58158.48	57290.96	42839.47	14451.49	867.52
E-SCED2	58158.48	57290.96	42839.47	14451.49	867.52
E-SCED3	58112.06	57056.21	42845.19	14211.02	1055.85
E-SCED4	58977.22	57363.58	42876.2	14487.38	1613.64
E-SCED5	58977.22	57364.73	42877.34	14487.39	1612.49
SCED	74865.79	62553.62	42943.34	19610.28	12312.17

The nodal LMP including the energy component and congestion component is shown in Table 5.19. The energy LMP of each bus is the same across the entire system and is also equal to the LMP at the slack bus. The average LMPs and the average congestion LMPs for various E-SCED are very close, since even the fifth best CTS solution can relieve the system congestion by 82%. However, in comparison with the traditional

SCED, the average LMP is reduce by about 5% while the average congestion LMP is reduced by 82% to 88%, which is consistent with the degree of congestion cost reduction as shown in Table 5.12.

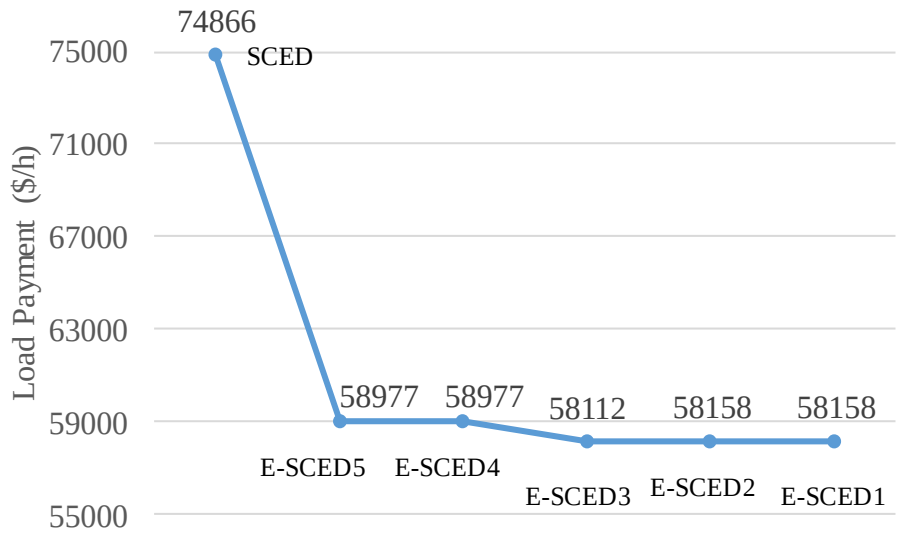

Fig. 5.10 Load Payment for Various SCED and E-SCEDs on the Cascadia System.

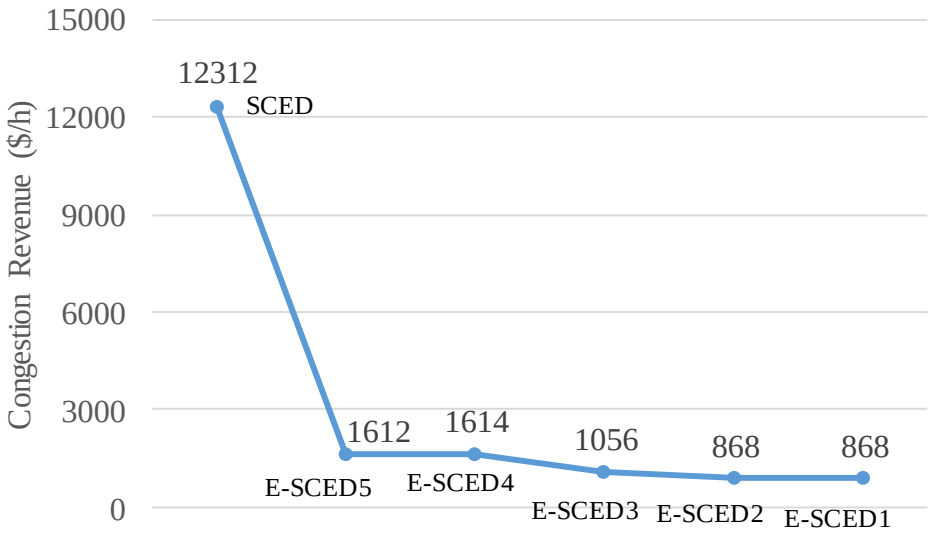

Fig. 5.11 Congestion Revenue for Various SCED and E-SCEDs on the Cascadia System.

Table 5.19 Average LMP with SCED and Various E-SCEDs on the Cascadia System

	Average LMP ($/MWh)	Average Congestion LMP ($/MWh)	Energy LMP ($/MWh)
E-SCED1	7.685	0.063	7.622
E-SCED2	7.685	0.063	7.622
E-SCED3	7.649	0.071	7.578
E-SCED4	7.672	0.094	7.578
E-SCED5	7.672	0.095	7.578
SCED	8.037	0.542	7.494

5.4 Conclusions

In Chapter 4, it is demonstrated that corrective transmission switching can significantly reduce or even fully eliminate post-contingency violations, which is believed to reduce the need for expensive reliability-motivated generation re-dispatch and can be translated into significant saving [147]. Thus, two procedures are proposed in this chapter to investigate the potential cost saving with CTS: 1) the proposed Procedure-A represents existing industrial practice; 2) the proposed Procedure-B can fully utilize the benefits provided by CTS in the RT SCED application. Built upon existing SCED tools, the change required to implement the proposed Procedure-B and the proposed E-SCED model is only to replace the actual limits with pseudo limits for branch limit constraints in SCED, which requires minimal effort for the industry to adopt the proposed Procedure-B.

Numerical simulations have demonstrated that the post-contingency violation reduction with CTS can translate into significant congestion cost reduction for RT SCED. The marginal cost reduction with 1 MW increase in the limit of a bottleneck branch may drop as the associated branch limit increases. Even with a conservative CTS solution, for instance, using the branch pseudo limit that is associated with the 3rd best CTS

solution in SCED, the 29% reduction in post-contingency violation is translated into 90% reduction in congestion cost in RT SCED. The case studies also demonstrate the performance of CTS-based RTCA in the post-SCED stage. It is concluded that congestion cost can be significantly reduced with the consideration of CTS.

6. FALSE DATA INJECTION CYBER-ATTACK DETECTION

State estimation estimates the system condition in real-time and provides a starting point for other EMS applications including RTCA and RT SCED. Failure of state estimation may cause very severe consequences. The measurements collected by state estimation may involve random errors, which can be identified and removed by bad data detection. However, malicious cyber-attacks can inject false measurements that can bypass traditional bad data detection and result in an incorrectly estimated system condition [105]-[123]. This indicates that power system state estimation is subject to false data injection cyber-attacks. In addition, a biased system condition may mislead operators to take unnecessary or improper actions that reduce the reliability and damage the system. For instance, recent efforts [109]-[114] show that FDI cyber-attacks can cause unobservable branch overloads in real-time. Thus, developing a detection approach that can efficiently detect FDI attacks is vital for reliability enhancements and secure operations of electric power systems. The goal of FDID is to improve system reliability by detecting FDI cyber-attacks and enhancing state estimation.

6.1 Concept

6.1.1 State Estimation

State estimation is run continuously to estimate the system status in real-time, including bus voltages and line flows. The measurement model for state estimation can be represented by (6.1). In (6.1), $h(x)$ describes the relationship between state variable x and measurements z, while e denotes the measurement error vector.

$$z = h(x) + e \tag{6.1}$$

For DC state estimation, the relationship between state variable x and measurements z is linear and $h(x)$ can be replaced by Hx, where H is a constant Jacobian matrix; then, (6.1) can be replaced by (6.2) for DC state estimation. Variable x in (6.2) denotes the bus voltage angle vector. This chapter focuses on the DC measurement model, which is a linearization of (6.1).

$$z = Hx + e \tag{6.2}$$

6.1.2 FDI Cyber-Attack

To launch an unobservable FDI cyber-attack, the injected false measurements should meet (6.3) that represents the measurement model under attack. In (6.3), $\tilde{x}$ denotes the state variable under attack and $\tilde{z}$ denotes false measurements. Equation (6.4) defines the relationship between the cyber state variable under attack and the actual state variable; variable c in (6.4) is referred to as the attack vector.

$$\tilde{z} = H\tilde{x} + e \tag{6.3}$$

$$\tilde{x} = x + c \tag{6.4}$$

If the attacker has access to only a part of the system, then the measurements outside the attack area will remain the same. Similarly, for the buses that are located outside the attack area, the associated elements in the attack vector c are zeros. For simplicity, it is assumed in this work that the attacker has access to the entire system.

Fig. 6.1 shows the time line that is used to illustrate FDI cyber-attacks. There are two dispatch intervals. The assumptions made in this work are listed below:

- the attacker injects false data or measurements at $t = 0^{-}$, right before SE and SCED execute at $t = 0$,

- the generation at $t = -T_{ED}^{-}$ is optimal, which implies the generation in the first SCED period remain the same,
- system operators have accurate information at $t = -T_{ED}$,
- the load in the second SCED dispatch interval remains constant, or the forecasting load at the end of the second SCED interval is the same with the load at the beginning of the second SCED interval,
- SE executes repeatedly with the same frequency of SCED execution,
- Loads at the same bus are combined into a single aggregate load.

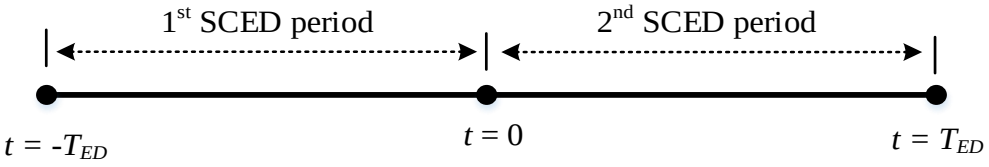

Fig. 6.1 Time Line for Illustrating FDI Cyber-Attack

In [110], a bi-level optimization model is proposed to determine the attack vector and false load vector that can cause the most severe loading condition on a target transmission and may result in physical flow violation. Heuristics for this bi-level model are proposed in [111]; a modified version of one of those heuristic models is presented below,

$$maximize\ \ sign(P_{l,0^-})(p_l - \tilde{p}_l) \tag{6.5}$$

subject to

$$p_k = (\theta_{n(k-)} - \theta_{n(k+)})/X_k\ ,\ k \in K \tag{6.6}$$

$$\tilde{p}_k = (\tilde{\theta}_{n(k-)} - \tilde{\theta}_{n(k+)})/X_k\ ,\ k \in K \tag{6.7}$$

$$\tilde{\theta}_n = \theta_n + c_n\ ,\ n \in N \tag{6.8}$$

$$\Delta\tilde{p}_d = \sum_{k\in K(n(d)-)}(p_k - \tilde{p}_k) - \sum_{k\in K(n(d)+)}(p_k - \tilde{p}_k),\ d \in D \tag{6.9}$$

$$-L_S P_d \le \Delta\tilde{p}_d \le L_S P_d\ ,\ d \in D \tag{6.10}$$

$$-c_n \le s_n\ ,\ n \in N \tag{6.11}$$

$$c_n \le s_n\ ,\ n \in N \tag{6.12}$$

$$\sum_n s_n \le N_1 \tag{6.13}$$

where $P_{l,0^-}$ denotes the actual flow on the target branch l at $t = 0^-$; p_k and $\tilde{p}_k$ denote the expected actual flow and cyber flow on branch k at $t = T_{ED}$ respectively; θ_n and $\tilde{\theta}_n$ denote the expected phase angle and cyber phase angle of bus n at $t = T_{ED}$ respectively; $\Delta\tilde{p}_d$ denotes the malicious deviation of load d; and L_S denotes the load shift factor.

The objective of this model is to maximize the difference between post-attack physical and cyber power flows on a pre-specified target branch l. Equations (6.6) and (6.7) calculate the post-attack physical branch flows and cyber branch flows respectively. Equation (6.8) shows the relationship between physical bus angles and cyber bus angles. Equation (6.9) calculates the malicious load deviation vector, while (6.10) ensures that the load shift is within the limit. The summation of the absolute change in state variables is restricted by (6.11)-(6.13), which is equivalent to an l_1-norm constraint; where N_1 is the limit of that l_1-norm constraint.

The above model can be further simplified by introducing a new variable Δp_k that denotes the difference between the post-attack physical and cyber power flows. The simplified FDI cyber-attack model is formulated below.

$$maximize\ \ sign(P_{l,0^-})\Delta p_l \tag{6.14}$$

subject to (6.10), (6.11), (6.12), (6.13), and

$$\Delta p_k = (-c_{n(k-)} + c_{n(k+)})/X_k\,,\ k \in K \tag{6.15}$$

$$\Delta \tilde{p}_d = \sum_{k \in K(n(d)-)} (\Delta p_k) - \sum_{k \in K(n(d)+)} (\Delta p_k)\,,\ d \in D \tag{6.16}$$

where,

$$\Delta p_l = p_l - \tilde{p}_l \tag{6.17}$$

Note that this simplified B-$\Delta\theta$ FDI cyber-attack model, consisting of (6.10)-(6.17), is mathematically equivalent to the third heuristic algorithm presented in [111]. The proposed B-$\Delta\theta$ FDI cyber-attack model is implemented to provide data for the FDID studies in this dissertation.

6.2 FDID Metrics

Two categories of metrics are proposed in this dissertation to detect potential FDI cyber-attacks on a specific branch. They are the malicious load deviation index (MLDI) and the branch overload risk index (BORI). MLDI can recognize load change patterns and identify malicious load deviation, while BORI monitors suspicious changes in branch flows. MLDI and BORI are metrics for determining whether a specific branch is an attack target. Systematic metrics and methodology are discussed in Section 6.3.

An FDI cyber-attack alert system is also proposed in this dissertation. This system has four different alert levels that are defined as *Danger*, *Warning*, *Monitor*, and *Normal*. The alert level can be determined by the proposed FDID metrics.

6.2.1 MLDI

As described in the previous chapter, PTDF is a matrix of sensitivity factors that measures the incremental change in branch flow due to a change in power transferring

between a slack bus and a non-slack bus. Thus, given a branch, the loads that have a significant impact on that branch should be monitored. It would be unusual if the changes in all the loads that are critical to a branch *k* contribute to decreasing the flow on branch *k*. Therefore, based on this observation, a malicious load deviation index is proposed to detect potential FDI cyber-attacks. Given a branch *k*, $MLDI_k$ can be calculated by (6.18),

$$MLDI_k = sign(P_{k-}) \frac{\sum_{d \in D(k)} Indctr_{d,k}}{ND_k} \tag{6.18}$$

where

$$Indictr_{d,k} = \begin{cases} -sign\left(PTDF_{n(d),k}\right) , & if \frac{P_{d0,ISO} - P_{d-}}{P_{d-}} \leq -5\% \\ 0 , & if -5\% < \frac{P_{d0,ISO} - P_{d-}}{P_{d-}} < 5\% \\ sign(PTDF_{n(d),k}) , & if \frac{P_{d0,ISO} - P_{d-}}{P_{d-}} \geq 5\% \end{cases} \tag{6.19}$$

and,

$$ND_k = \sum_{d \in D(k)} 1 \tag{6.20}$$

where *D(k)* denotes a set of loads that are critical to branch *k*. If the absolute value of $PTDF_{n(d),k}$ is not less than 1%, then, load *d* is defined to be critical to branch *k*.

Though $MLDI_k$ is in the range of [-1, 1] theoretically, $MLDI_k$ is typically close to zero if the load fluctuates randomly. A positive value indicates that the load change might reduce the flow on branch *k*. A very high positive value may imply the load fluctuation is abnormal and the probably of branch *k* being targeted by an FDI attack is high.

Metric $MLDI_k$ only considers the number of load buses that are critical to a branch, but fails to take load magnitude and PTDF values into account. To consider those two

factors, an enhanced malicious load deviation index (EMLDI) is proposed in this work. Similar to $MLDI_k$, $EMLDI_k$ is defined by (6.21),

$$EMLDI_k = sign(P_{k-}) \sum_{d \in D(k)} (If_{d,k} Indictr_{d,k}) \quad (6.21)$$

where,

$$If_{d,k} = \frac{|(P_{d0,ISO} - P_{d-}) \cdot PTDF_{n(d),k}|}{\sum_{d \in D(k)} |(P_{d0,ISO} - P_{d-}) \cdot PTDF_{n(d),k}|} \quad (6.22)$$

$EMLDI_k$ shares the same range and indication with $MLDI_k$. The difference is that the effects of load magnitude and PTDF values are not considered for $MLDI_k$ but are captured by $EMLDI_k$. Thus, given a potential target branch *k*, $EMLDI_k$ may be a better indicator to determine whether there is an attack targeting that branch.

The alert level criteria for $MLDI_k$ and $EMLDI_k$ are the same and defined in Table 6.1. With the proposed metrics and alert system, it is not very hard to identify whether a specified branch is under attack. As $EMLDI_k$ considers more factors than $MLDI_k$, the alert level for branch *k* should be determined by $EMLDI_k$. In this work, ALM_k denotes the alert level associated with $MLDI_k$ while ALE_k denotes the alert level associated with $EMLDI_k$.

Table 6.1 Alert Level Criteria based on $MLDI_k$ or $EMLDI_k$

Alert level	$MLDI_k$ or $EMLDI_k$
Danger	>50%
Warning	>35%
Monitor	>20%
Normal	<20%

6.2.2 BORI

The first category of FDID metrics monitors load change and identifies potential attacks while the second category of FDID metrics monitors flow changes and identifies

potential overloads. As introduced above, in order to execute an unobservable FDI cyber-attack that would overload a line, the attacker needs to change the measurements including load measurements that are sent to the system operators. In the cyber world, the attacker can deliberately reduce the flow on a congested line or a heavily loaded line by shifting loads. This would mislead operators to believe that there is extra available capacity on the target branch; then, operators may re-dispatch generation to take advantage of that extra available capacity and reduce the total cost. However, in the real world, there is no such extra available capacity and physical overloads may occur. Thus, based on this type of flow change pattern, this work proposes a branch overload risk index to detect FDI cyber-attacks.

Considering the attacker may or may not take the effect of generation re-dispatch into account, two similar but different metrics, BORI1 and BORI2, are proposed in this dissertation. BORI1 only considers the flow changes during the previous interval while BORI2 takes the SCED results into account. BORI1 and BORI2 are defined in (6.23) and (6.24) respectively.

$$BORI1_k = sign(P_{k-})(P_{k-} - P_{k0,ISO} + P_{k-})/LimitA_k \tag{6.23}$$

$$BORI2_k = sign(P_{k-})(P_{k-} - P_{k0,ISO} + P_{k+,SCED})/LimitA_k \tag{6.24}$$

A comprehensive metric $BORI_k$ is proposed to combine those two metrics belonging to the second category of FDID metrics. As shown in (6.25), $BORI_k$ is defined to be the larger between $BORI1_k$ and $BORI2_k$.

$$BORI_k = max(BORI1_k, BORI2_k) \tag{6.25}$$

The alert level criterion for $BORI_k$ is defined in Table 6.2. In this work, ALB_k denotes the alert level associated with $BORI_k$. $BORI_k$ and ALB_k enable operators to determine whether a branch is under attack from the viewpoint of flow violations.

Table 6.2 Alert Level Criteria based on $BORI_k$

Alert level	$BORI_k$
Danger	>115%
Warning	>110%
Monitor	>105%
Normal	<105%

6.3 Two-stage FDID Approach

Metrics MLDI and BORI presented in Section 6.2 are used to detect potential FDI attacks on a specific branch rather than monitor the system as a whole. Thus, a systematic approach is desired. In this section, a two-stage FDID approach, consisting the FDI attack awareness stage and the target branch identification stage, is proposed to detect potential FDI cyber-attacks. The first stage is to determine whether the system is under FDI cyber-attack and the second stage would identify the target branch.

6.3.1 Stage 1: FDI Attack Awareness

As introduced in Section 6.2, MLDI and BORI are proposed to detect whether an FDI cyber-attack is launched for a specific branch. Since system operators have limited information regarding which branch the attacker would target, it is necessary to calculate the metrics for all branches. However, given that a practical power system typically has a large number of branches, even random load fluctuations may cause large $MLDI_k$, $EMLDI_k$, and $BORI_k$ values for a few branches, which may mislead system operators

to believe that the load fluctuation is abnormal and the system is under attack. Therefore, a system-wide malicious load deviation index (SMLDI) is proposed to resolve this issue. SMLDI is defined in the equation shown below,

$$SMLDI = \frac{\sum_{k \in KA} MLDI_k}{\sum_{k \in KA} 1} \tag{6.26}$$

where *KA* is a set of ten branches that have the top ten $MLDI_k$ values. If the number of load buses that have significant effects on branch *k* is too small, then the associated $MLDI_k$ cannot be used for malicious load deviation recognition and branch *k* will not be included in the set *KA*. In this work, branches that have less than five critical load buses will not be considered as a candidate element of set *KA*.

In this stage, SMLDI is used as the only metric to determine whether the system is under attack. Similar to the alert level designed for a target line, a system-wide FDI alert level is defined in Table 6.3. A system would be considered to be FDI cyber-attack free if the associated alert level is marked as *Normal* or *Monitor* in stage 1. Only the cases that have either *Warning* or *Danger* alert flags will be sent to stage 2 for FDI target branch identification.

Table 6.3 Alert Level Criteria based on $SMLDI$

Alert level	$SMLDI$
Danger	>50%
Warning	>35%
Monitor	>20%
Normal	<20%

6.3.2 Stage 2: Target Branch Identification

It is vital to determine whether the system is under malicious FDI cyber-attack in stage 1. It is also very important to identify which branch is the attacker's target so that

system operators can take immediate actions to handle the detected FDI attack. Thus, the goal of stage 2 is to identify the target branch.

As presented above, $EMLDI_k$ detects FDI attacks targeting branch k from the viewpoint of suspicious load deviation while $BORI_k$ detects FDI attacks targeting branch k from the viewpoint of potential flow violation. Both of the metrics are considered in this stage. The alert levels associated with $EMLDI_k$ and $BORI_k$ can be combined into a single comprehensive FDI attack alert level. The combination of the two alert levels is defined in Table 6.4. This comprehensive alert level, denoted by ALC_k, is used as the alert level for identifying the target branch.

Table 6.4 Comprehensive Alert Level Combined from Two Separate Alert Levels

Alert level	Alert level			
	Normal	Monitor	Warning	Danger
Normal	*Normal*	*Monitor*	*Monitor*	*Warning*
Monitor	*Monitor*	*Monitor*	*Warning*	*Warning*
Warning	*Monitor*	*Warning*	*Warning*	*Danger*
Danger	*Warning*	*Warning*	*Danger*	*Danger*

Though the proposed alert system can provide a qualitative analysis, it is also very important to analyze the FDI attack quantitatively. Thus, a comprehensive FDI attack index (CI) that considers both load deviation patterns and potential branch overloads is proposed in this work. CI_k is defined in (6.27). Thus, the branch that has the biggest CI_k is considered to be the most suspicious target branch; moreover, the CI_k rank can serve as a metric that indicates the possibility of branch k being the target branch.

$$CI_k = EMLDI_k \, BORI_k \tag{6.27}$$

Therefore, the proposed comprehensive index CI_k and the proposed comprehensive alert level ALC_k are used to identify the target branch in stage 2. In this work, the

branches that are marked as *Danger* or have a CI_k ranking in the top three are considered to be the most suspicious target branches.

6.4 Case Studies

The IEEE 118-bus test system is used in this work to investigate the proposed B-$\Delta\theta$ FDI cyber-attack model presented in Section 6.1.2. Then, this test case is further used to examine the proposed two-stage FDID approach, as well as the proposed FDI cyber-attack alert system. This case contains 118 buses, 186 branches, and 19 online units. The initial total load at $t = -T_{ED}$ is 4,242 MW. Out of 118 buses, 99 buses are load buses or have non-zero loads.

6.4.1 FDI Results

In this section, to study the effectiveness of the proposed B-$\Delta\theta$ FDI cyber-attack model, numerical simulations are conducted with different system scenarios including constant load scenarios and random load fluctuation scenarios in the first dispatch interval, from $t = -T_{ED}$ to $t = 0$. The effects of different load shift factors and l_1-norm constraint limits on the physical consequences of an FDI attack are also analyzed in this section.

By assuming the load profile does not change in the first dispatch interval, the maximum power flows on branch 111 and branch 118 with different FDI attack settings are presented in Fig. 6.2 and Fig. 6.3 respectively. The blue curve with diamond markers in Fig. 6.2 corresponds to the FDI results with a load shift factor of 5% and it becomes flat quickly. The reason is that the load shift constraint is binding when N_1 is 6 and further relaxing the l_1-norm constraint will not change the FDI results.

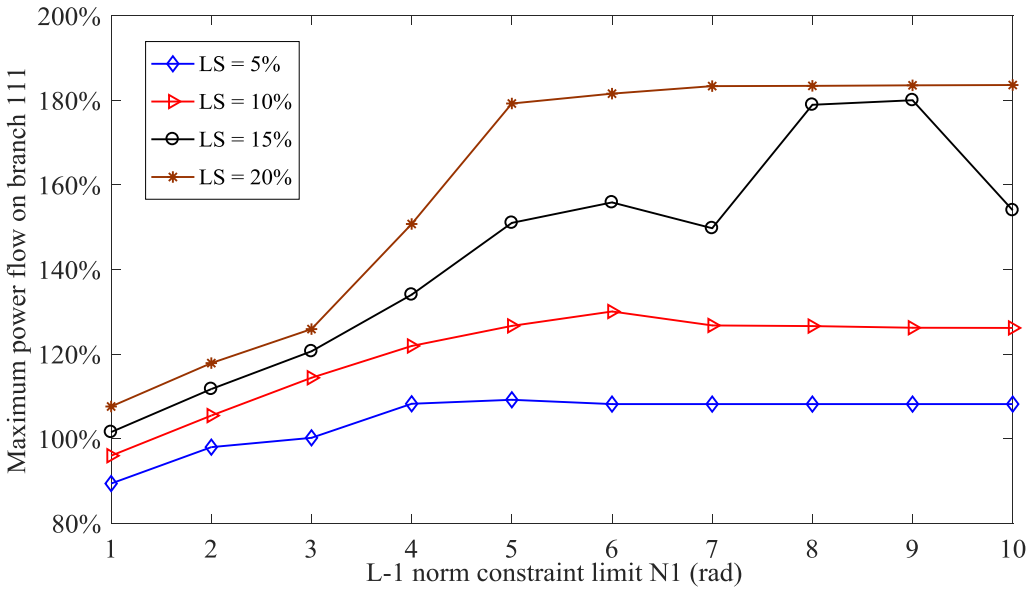

Fig. 6.2 Maximum Power Flow on Line 111 with Various Load Shift Factors and l_1-Norm Constraint Limits.

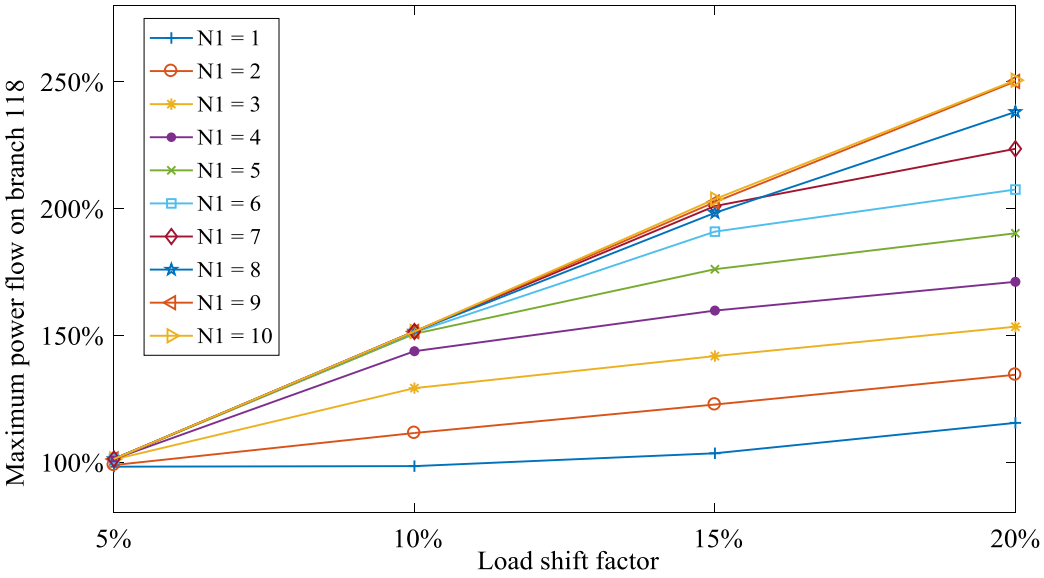

Fig. 6.3 Maximum Power Flow on Line 118 with Various Load Shift Factors and l_1-Norm Constraint Limits.

Since the B-$\Delta\theta$ FDI model proposed in this work is a fast heuristic rather than an exact approach, the maximum flows shown in Fig. 6.2 and Fig. 6.3 do not strictly increase as the load shift factor or l_1-norm constraint limit increases. However, with a more flexible condition, the attacker can typically cause more severe flow violations.

In reality, loads fluctuate all the time. Thus, it is important to analyze the effects of random load fluctuations on FDI cyber-attacks. It is assumed that the load fluctuation follows the normal distribution with a mean of μ (a percentage) and a standard deviation σ (a percentage), which is denoted by $N(\mu, \sigma)$. The process of generating a load fluctuation vector following $N(\mu, \sigma)$ is presented below:

1) generate a vector v that follows standard normal distribution,
2) apply a cutoff value 1.96 to this vector v,
3) adjust v with equation: $v = v\sigma + \mu$,
4) create a load fluctuation vector: $\Delta p_d = P_{d-}v$.

Note that since loads do not fluctuate significantly in the short-term, step 2) ensures that the random load fluctuation does not have a long tail distribution.

For the FDI simulations conducted in this section, the random load fluctuation follows $N(0, 3\%)$. For each FDI attack simulated, the load profile is updated with a different randomly generated load fluctuation vector. The results of FDI attacks with load fluctuations are presented in Fig. 6.4 and Fig. 6.5. Fig. 6.4 shows the results of an FDI attack targeting branch 111 while Fig. 6.5 shows the results of an FDI attack targeting branch 118. The curves in Fig. 6.4 and Fig. 6.5 look very similar to the corresponding curves in Fig. 6.2 and Fig. 6.3 respectively. Random load fluctuations may either relieve

the violation or contribute to the violation to a limited extent. Fig. 6.4 and Fig. 6.5 show that an FDI cyber-attack can still result in a flow violation on the target branch even with random load fluctuations.

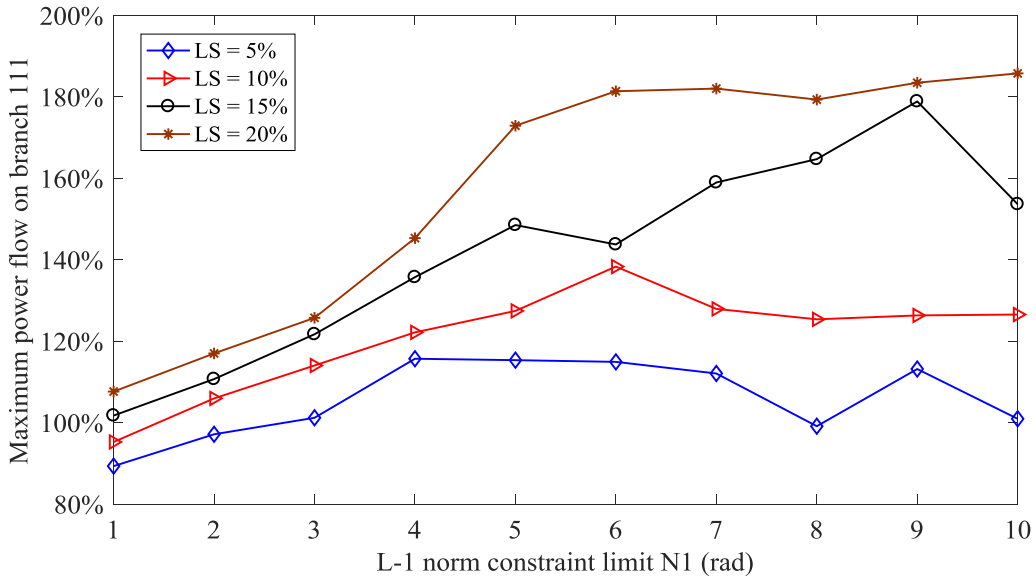

Fig. 6.4 Maximum Power Flow on Line 111 with Random Load Fluctuation.

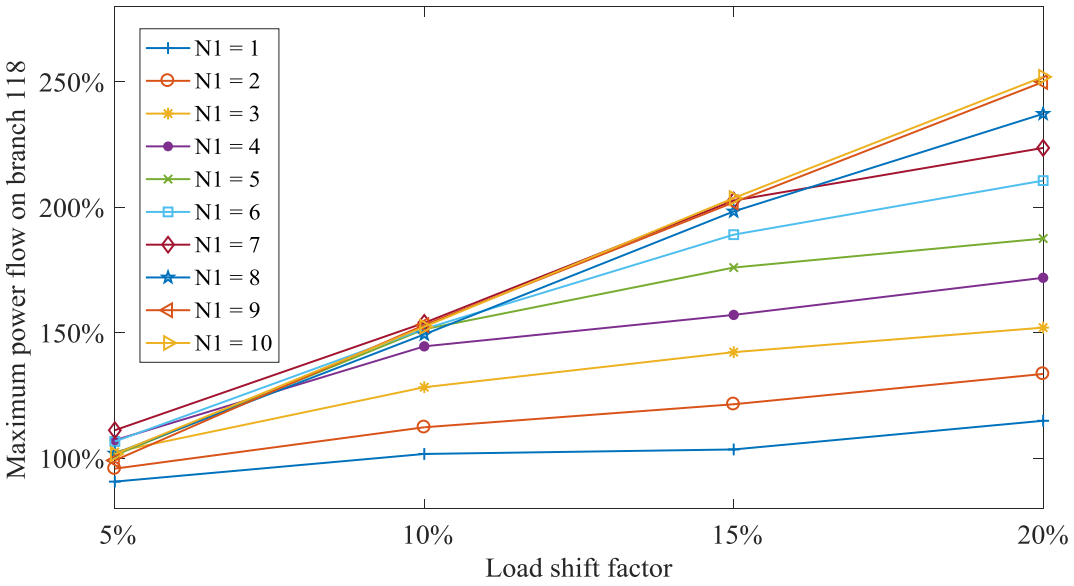

Fig. 6.5 Maximum Power Flow on Line 118 with Random Load Fluctuation.

6.4.2 FDID Results

Stage 1: FDI Attack Awareness

As introduced above, the proposed FDID strategy consists of two stages. Stage 1 determines whether the system is under an FDI cyber-attack by analyzing the load profile changes. It is important to detect FDI attacks. Furthermore, it is also vital to bypass random load fluctuations. The goal of stage 1 is to have a low false alarm probability as well as a low false dismissal probability.

Two sets of load deviation vectors, including the FDI malicious load deviation vectors and random load fluctuation vectors, are tested in this stage. The load deviation vector denotes the difference between the loads at the beginning of the second dispatch interval ($t = 0$) and the loads profile at the beginning of the first dispatch interval ($t = -T_{ED}$). The first set of malicious load deviation vectors can be obtained from the 160 different FDI attacks performed in Section 6.4.1. The second set of normal load fluctuation vectors is created with four different normal distributions: $N(0, 3\%)$, $N(0, 5\%)$, $N(-1\%, 3\%)$, and $N(1\%, 3\%)$. Twenty independent vectors are generated for each normal distribution. Thus, the second set has a total of 80 normal load fluctuation vectors.

The SMLDI values for those 240 load change vectors are calculated in stage 1. The results for the 160 FDI malicious load deviation vectors and 80 random load fluctuation vectors are presented in Table 6.5 and Table 6.6 respectively. The SMLDI values for the random load fluctuation vectors are very small and the averages are close to zero. As for the FDI malicious load deviation vectors, the associated SMLDI values are much bigger and the average values are around 70%. This indicates that FDI cyber-attacks

can be successfully detected with the proposed metric SMLDI and random load fluctuations can successfully bypass this two-stage FDID approach.

Fig. 6.6 shows a scatter plot of the SMLDI values for all the random load fluctuations and FDI cyber-attacks simulated in this work. The blue squares correspond to the random load fluctuation vectors while the red triangles correspond to the FDI malicious load deviation vectors. As shown in Fig. 6.6, the SMLDI values for the random load fluctuation vectors are all below 35% and, thus, the associated alert levels are either *Normal* or *Monitor*. The alert levels for most random vectors are *Normal*. As for the FDI malicious load deviation vectors, the associated SMLDI values are all above the warning tolerance and the alert levels for most FDI attack load deviation vectors are *Danger*. Therefore, it is demonstrated that the proposed metric SMLDI can efficiently detect FDI cyber-attacks and would not mistakenly identify a random load fluctuation as an FDI attack. In other words, the results presented in Fig. 6.6 demonstrate the proposed two-stage FDID approach has a very low false alarm rate as well as a very low false dismissal rate.

The first 80 system scenarios in Fig. 6.6 correspond to random load fluctuations with four different normal distributions. They are listed as the order of $N(0, 3\%)$, $N(0, 5\%)$, $N(-1\%, 3\%)$, and $N(1\%, 3\%)$. Each normal distribution has 20 scenarios. By comparing the random load fluctuations generated with different normal distribution functions, it is observed that the mean of load fluctuation does not affect the metric while higher standard deviations may result in higher SMLDI values. This is consistent with

the statistics presented in Table 6.6. This implies that the false alarm rate for the proposed approach may increase as the magnitude of load deviation increases. It is worth noting that loads typically do not deviate too much in a short time frame.

Fig. 6.7 illustrates the SMLDI values that are associated with various FDI attacks targeting branch 118 with random load fluctuations that follow $N(0, 3\%)$ in the first dispatch interval. The red dotted line is the boundary between the alert levels *Monitor* and *Warning*. Those SMLDI values are well above the *Warning* alert tolerance of 35%, especially for the cases that have more flexible constraints. It is very straightforward and efficient to identify whether the system is under malicious FDI cyber-attack with the proposed metric SMLDI.

Table 6.5 SMLDI Values for FDI Malicious Load Deviation Vectors

	Attack on branch 118		Attack on branch 111	
	Constant load	$N(0, 3\%)$	Constant load	$N(0, 3\%)$
max	97.8%	97.8%	97.8%	97.5%
min	48.8%	39.9%	35.7%	38.7%
median	62.9%	68.5%	62.9%	63.8%
average	72.1%	74.5%	68.6%	70.7%
std	16.8%	19.0%	19.4%	20.3%

Table 6.6 SMLDI Values for Random Load Fluctuation Vector

	Normal load fluctuation only			
	$N(0, 3\%)$	$N(0, 5\%)$	$N(-1\%, 3\%)$	$N(1\%, 3\%)$
max	23.1%	28.0%	23.5%	20.9%
min	3.2%	13.8%	5.5%	7.5%
median	11.8%	22.8%	12.0%	12.5%
average	12.2%	21.7%	12.4%	13.2%
std	4.4%	3.7%	4.7%	3.7%

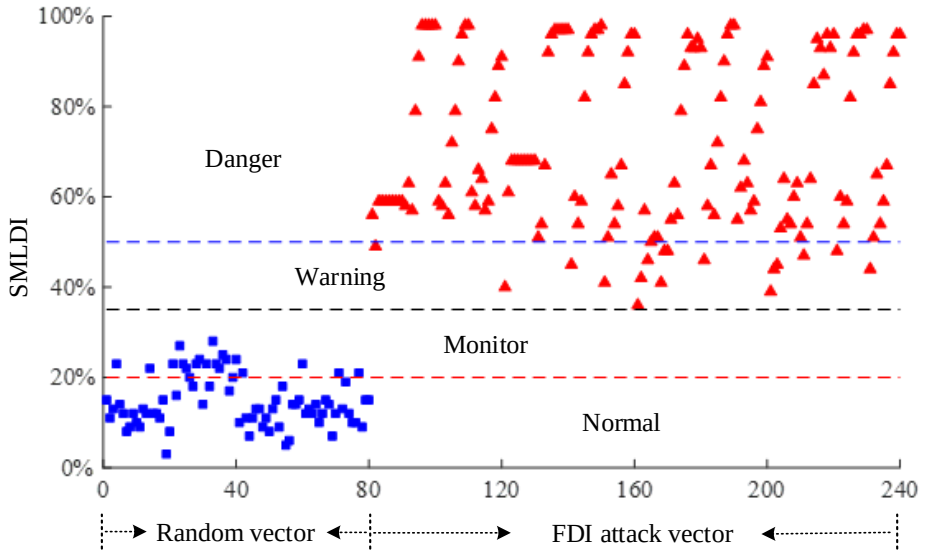

Fig. 6.6 SMLDI Values for Random Load Fluctuations and FDI Cyber-Attacks.

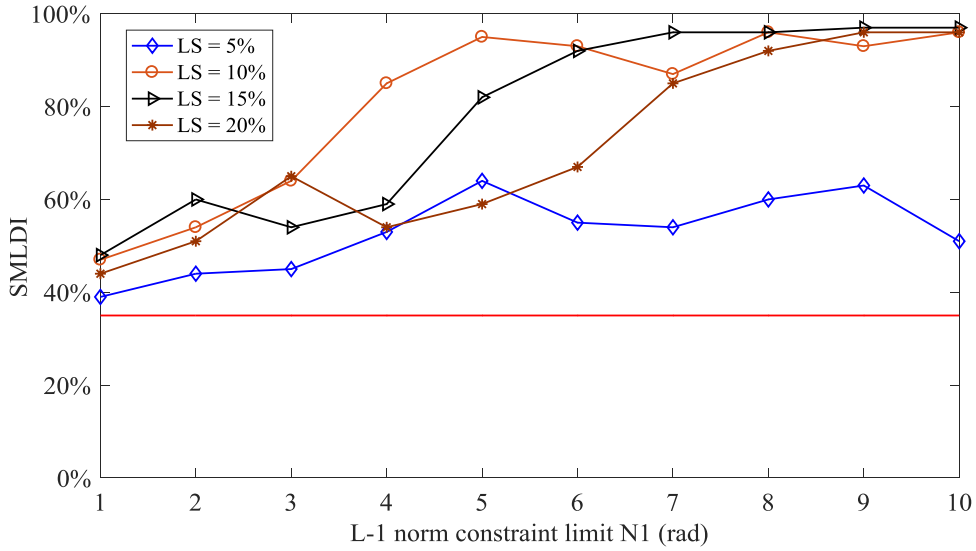

Fig. 6.7 SMLDI of FDI Attacks for Target Branch 118 with $N(0, 3\%)$ Random Load Fluctuation.

Stage 2: Target Branch Identification

In this stage, only the cases that are identified to be under FDI cyber-attack will be examined. Thus, only those 160 FDI attack scenarios are sent to the target branch identification routine.

Table 6.7 shows the results of target line identification for FDI attacks on branch 111 with a load shift factor of 10% and no random load fluctuations in the first dispatch

interval. Out of the ten system scenarios, the metric CI_k of branch 111 ranks first for the nine scenarios and ranks second for the remaining one scenario. There are eight scenarios for which branches marked as *Danger* exist; branch 111 is the only one that is marked as *Danger* for those eight scenarios. Therefore, both the proposed comprehensive FDID index and the proposed comprehensive alert level indicate that branch 111 is the most suspicious target branch. Table 6.8 shows the results of target line identification for FDI attacks on branch 111 with a load shift factor of 10% and a random load fluctuation that follows $N(0, 3\%)$. The difference between the two sets of simulations associated with Table 6.7 and Table 6.8 respectively is that the simulations corresponding to Table 6.7 do not involve random load fluctuations. Therefore, the results shown in Table 6.8 are more realistic. However, the conclusions drawn from Table 6.8 are similar to Table 6.7. This indicates that the proposed method is effective even when the normal load fluctuation is modeled.

Table 6.7 Target Line Identification Results for FDI Attacks on Line 111 with a Load Shift Factor of 10% and No Random Load Fluctuation in the First Dispatch Interval

	CI_{111}	Rank of CI_{111}	ALC_{111}	ALE_{111}	ALB_{111}	Number of lines marked *Danger*	List of suspicious target lines
$N_1 = 1$	0.46	2	*Monitor*	*Warning*	*Normal*	0	145, 111, 150
$N_1 = 2$	0.66	1	*Warning*	*Danger*	*Monitor*	0	111, 129, 145
$N_1 = 3$	0.90	1	*Danger*	*Danger*	*Warning*	1	111, 129, 181
$N_1 = 4$	1.13	1	*Danger*	*Danger*	*Danger*	1	111, 119, 141
$N_1 = 5$	1.26	1	*Danger*	*Danger*	*Danger*	1	111, 97, 141
$N_1 = 6$	1.30	1	*Danger*	*Danger*	*Danger*	1	111, 97, 186
$N_1 = 7$	1.27	1	*Danger*	*Danger*	*Danger*	1	111, 97, 186
$N_1 = 8$	1.27	1	*Danger*	*Danger*	*Danger*	1	111, 97, 186
$N_1 = 9$	1.26	1	*Danger*	*Danger*	*Danger*	1	111, 97, 186
$N_1 = 10$	1.26	1	*Danger*	*Danger*	*Danger*	1	111, 97, 186

Table 6.9 presents the FDID results on various FDI attacks. As shown in Table 6.9, the target branches are correctly identified for 96.9% or 155 scenarios out of the 160 FDI cyber-attacks. The target branch is marked as *Danger* for over 90% of the FDI attacks on branch 118. The percentage of the cases that the target line for the FDI attacks on line 111 is marked as *Danger* is relatively low. The reason is that the overloads on line 111 for some attacks, including most FDI attacks with a load shift factor of 5%, are not very significant and do not reach the *Warning* alert threshold. However, the associated comprehensive FDI attack index CI of line 111 ranks first for most cases. For all FDID tests on the 160 FDI attacks, the FDID comprehensive index CI of the target line ranks very high and almost all of the FDID comprehensive indices rank either first or second.

Table 6.8 Target Line Identification Results for FDI Attacks on Line 111 with a Load Shift Factor of 10% and $N(0, 3\%)$ Load Random Fluctuation in the First Dispatch Interval

	CI_{111}	Rank of CI_{111}	ALC_{111}	ALE_{111}	ALB_{111}	Number of lines marked *Danger*	List of suspicious target lines
$N_1 = 1$	0.45	2	*Monitor*	*Warning*	*Normal*	0	145, 111, 150
$N_1 = 2$	0.68	1	*Warning*	*Danger*	*Monitor*	0	111, 129, 145
$N_1 = 3$	0.91	1	*Danger*	*Danger*	*Danger*	1	111, 129, 181
$N_1 = 4$	1.07	1	*Danger*	*Danger*	*Danger*	1	111, 119, 141
$N_1 = 5$	1.21	1	*Danger*	*Danger*	*Danger*	1	111, 97, 141
$N_1 = 6$	1.37	1	*Danger*	*Danger*	*Danger*	2	111, 97, 186
$N_1 = 7$	1.19	1	*Danger*	*Danger*	*Danger*	1	111, 97, 186
$N_1 = 8$	1.29	1	*Danger*	*Danger*	*Danger*	2	111, 97, 186
$N_1 = 9$	1.23	1	*Danger*	*Danger*	*Danger*	1	111, 97, 186
$N_1 = 10$	1.20	1	*Danger*	*Danger*	*Danger*	1	111, 97, 141

Table 6.9 Results of FDID on Various FDI Attacks

	Attack on line 118		Attack on line 111		Total
	Constant load	$N(0, 3\%)$	Constant load	$N(0, 3\%)$	
Average CI_k rank of the target line	1.58	1.55	1.13	1.33	1.39
Percent of scenarios for which the target line is identified	92.5%	100%	100%	95.0%	96.9%
Percent of scenarios for which the target line is marked as *Danger*	92.5%	92.5%	65%	77.5%	81.9%
Number of scenarios simulated	40	40	40	40	160

6.5 Conclusions

Recent work in the literature has demonstrated that power systems are subject to unobservable FDI cyber-attacks in real-time. Attackers can cause flow violations that are neither observed nor detected by conventional state estimation. Therefore, it is very important to develop a strategy that can quickly detect such malicious FDI cyber-attacks in real-time.

An FDI model is first proposed in this dissertation in order to examine the effects of FDI attacks on system reliability. Then, a two-stage strategy is proposed to detect FDI attacks. Two categories of metrics, MLDI and BORI, are proposed and used in this two-stage approach to determine whether the change in system condition is abnormal. MLDI recognizes malicious load changes while BORI identifies suspicious flow changes. In stage 1, the proposed system-wide MLDI is used to determine whether the system is under attack. If the system is deemed to be under attack, stage 2 will launch and the proposed alert system and comprehensive FDID index will be used to identify the attack target branch.

Simulation results show that FDI cyber-attacks can cause physical flow violations and, then, demonstrates the effectiveness of the proposed FDID metrics, FDI cyber-

attack alert system, and two-stage FDID approach. The proposed two-stage FDID approach successfully detects all 160 FDI attacks that are simulated in this work and correctly identifies the target branch for about 97% of the cases. In addition, random load fluctuations will not activate the FDID alert system. Numerical simulations conducted on 80 different random load fluctuation vectors show that none of the random load fluctuation scenarios are mistakenly identified as malicious load deviations. To conclude, normal load fluctuations will not activate the proposed FDI alert system, while the proposed two-stage FDID approach can efficiently detect FDI attacks and the target branch. In other words, the false alarm rate and false dismissal rate for the proposed two-stage FDID approach are very low.

7. CONCLUSIONS

Transmission components are traditionally modeled as static assets in power system real-time operations. Although previous studies have demonstrated transmission switching can provide a variety of benefits, they are based on a DC framework and are verified with small test systems. Directly modeling transmission switching in RTCA and RT SCED will cause a serious computational burden and substantially increase the solution time, which is impractical for real-time applications. Therefore, this dissertation proposes CTS to utilize the flexibility in transmission networks in a practical way. The reliability benefits and economic benefits provided by CTS are investigated on large-scale power systems on an AC framework. The proposed CTS can reduce post-contingency violations as an inexpensive corrective strategy and reduce congestion cost by relieving critical network constraints.

If an unexpected critical contingency is not handled properly, it may result in a serious emergency and cause blackouts. RTCA identifies critical contingencies and the associated violations. With RTCA, pre-planned strategies can be made in advance to deal with potential critical contingencies. One widely used strategy is to re-dispatch generation to eliminate potential post-contingency violations. However, reliability-motivated generation re-dispatch is typically very expensive.

In this dissertation, CTS is proposed as another technique to handle potential post-contingency violations. Over 1.5 million contingencies are simulated on three large-scale practical power systems (TVA, ERCOT, and PJM) to evaluate the effectiveness of CTS with respect to post-contingency violation reduction. Numerical simulations

using the full AC power flow model show that each system is subject to critical contingencies and the proposed CTS algorithms can effectively reduce potential post-contingency violations. For instance, the average flow violation reduction achieved with CTS is around 60% for the PJM system. The percent of contingencies for which the associated violations can be fully eliminated by CTS is greater than 25% while the percent of contingencies where there is no beneficial CTS solution is less than 10%.

It is verified that CTS can provide operators with an alternative corrective strategy to relieve both flow violations and voltage violations caused by critical contingencies. Multiple beneficial switching actions are available, which provide operators with choices. Substantial post-contingency violation reduction can be achieved with the proposed heuristic algorithms that can achieve very similar results with complete enumeration but are much faster. Parallel computing can further reduce the solution time. Pareto improvement is proposed to investigate the impact of CTS on individual element. The benefits achieved with and without enforcing Pareto improvement are very similar; in other words, most identified CTS solutions can reduce post-contingency violations at an aggregate level while creating no additional violations on any individual element.

Incorporating CTS in RTCA can substantially improve system reliability. In existing EMS, RTCA provides RT SCED with a list of network constraints. As CTS can efficiently reduce or even eliminate post-contingency violations, the network constraints sent to RT SCED can be relaxed, which reduce the need for reliability-motivated generation re-dispatch. Simulation results on the Cascadia system illustrate significant (about 90%) cost reduction can be achieved when modeling CTS in RT SCED.

Two procedures are proposed in this dissertation to connect RTCA and RT SCED. Procedure-A represents the traditional procedure used in industry. In Procedure-A, the potential post-contingency violations are sent to RT SCED, as well as the actual base-case violations. RT SCED determines the optimal dispatch solution that has the least cost while all violations are eliminated and reliability requirements are met. Although the solution provided by RT SCED is on a DC model basis, it is fully evaluated on an AC framework and the effectiveness of Procedure-A is demonstrated. Multiple SCED models with different forms of network constraints are investigated and the hot-start PTDF model based SCED is shown to have the best performance.

Procedure-B, an enhanced version of Procedure-A, is proposed to integrate CTS into existing real-time operational modules in EMS. Procedure-B can capture the reliability benefits of CTS in RT SCED. With the proposed concept of pseudo limit, the transition from Procedure-A to more advanced Procedure-B requires minimal change, which is the replacement of actual limits with pseudo limits for the contingency-case network constraints in RT SCED. Numerical simulations show that substantial congestion cost reduction can be achieved by considering CTS in RT SCED; The beneficial CTS actions identified in the pre-SCED stage can also reduce the violations caused by the same contingency in the post-SCED stage even if the system condition may have changed significantly.

Full utilization of the network flexibility could benefit power systems significantly. Transmission switching has gained ISOs' considerable attention in various areas in power systems since CTS can add flexibility in power system real-time operations. The

cost to implement CTS is low since the required hardware is already available in the field of existing power systems. In this dissertation, it is demonstrated that CTS is able to provide reliability benefits in regard to post-contingency violation reduction as well as economic benefits with respect to congestion cost reduction. Moreover, the proposed mechanism of integrating CTS into EMS including RTCA and RT SCED will require minimal change; in other words, CTS can be considered as an add-on module for existing EMS. Thus, with the proposed mechanism, it is not very difficult for the industry to adopt CTS for real-time operations.

The traditional bad data detection function of state estimation can effectively identify large measurement errors and outliers that would dramatically drift the estimated system status away from the actual system status. It ensures the impact of random measurement noises on state estimation is minimal. However, malicious FDI cyber-attacks can inject false measurements that are designed to meet the physical laws and bypass bad data detection. Thus, state estimation under FDI attack would provide an inaccurate base case for other EMS applications. This would mislead system operators to adjust the generation improperly, which may cause unobservable flow violations. Numerical simulations show that FDI cyber-attacks can cause severe flow violations in real-time. Therefore, it is very important to identify FDI cyber-attack effectively.

Several metrics are proposed to monitor abnormal load deviations and flow changes. An FDI cyber-attack alert system is proposed to identify FDI attacks. It is very unlikely that a system is under FDI attack if the corresponding alert level is marked as *Normal* or *Monitor*. However, the system can be considered to be under FDI attack

when the alert flag is marked as *Warning* or *Danger*. Based on the proposed metrics and alert system, a systematic two-stage FDID approach is proposed to detect malicious FDI cyber-attacks. The first stage determines whether a system is under attack. For the cases that are deemed to be under attack, they will be sent to the target branch identification routine in the second stage. Case studies demonstrate the effectiveness of the proposed two-stage FDID approach. The proposed approach successfully detects all 160 FDI attacks and identifies the target correctly for about 97% of the cases. The false alarm rate is zero as none of the normal load fluctuations activate the proposed alert system.

In conclusion, this dissertation proposes a two-stage FDID approach that can effectively detect FDI cyber-attacks and secure state estimation. After state estimation determines the system status in real-time, RTCA would execute and identify the potential network violations that would be converted into network constraints for RT SCED. Traditional RTCA and RT SCED treat the transmission network as a static network and are not able to capture the flexibility in the transmission network. In this dissertation, corrective transmission switching is proposed to enable operators to utilize the flexibility in the transmission network. Incorporating CTS into RTCA and RT SCED can enhance system reliability and reduce the total cost. The proposed approaches are demonstrated with the cases that are tested in this dissertation, while it is worth noting that they can be applied to other systems as well.

8. FUTURE WORK

The effects of CTS on RTCA and RT SCED are examined in this dissertation. Heuristics are proposed to create the ranked switching list and identify the beneficial switching solutions in real-time. Case studies show that CTS can efficiently reduce post-contingency violations. With the reliability benefits provided by CTS, higher limits are available for contingency-case network constraints in RT SCED, which substantially reduce congestion cost.

The reliability benefits of employing CTS in RTCA are tested on the TVA, ERCOT, and PJM systems. Numerical simulations verify the effectiveness of CTS. The results are promising and convincing as the test cases are large-scale practical power systems with real EMS data. The proposed heuristics that can quickly identify beneficial switching solutions include two vicinity-based local search algorithms (CBCE and CBVE) and two different data mining methods (RDM and EDM). In addition, sensitivity factors, mainly LODF, may be a good indicator to identify the beneficial CTS solutions for flow violation reduction. Thus, potential future work is to investigate LODF based heuristic algorithm for identifying the candidate CTS list. Since NERC requires power systems to be *N*-1 reliable, another potential future work is to ensure the system is *N*-1 reliable in the post-switching situation.

With the availability of CTS as a corrective control scheme, higher short-term branch limits can be used in RT SCED, which reduces congestion cost significantly. Numerical simulations on the Cascadia system demonstrate the effectiveness of CTS in terms of congestion cost reduction. Though RT SCED is based on DC power flow

model, AC feasibility of the RT SCED solutions is verified by performing AC power flow, AC contingency analysis, and AC transmission switching simulations in the post-SCED stage. This work is tested on the Cascadia system, which is an artificial 179-bus system. Therefore, in order to demonstrate the robustness and effectiveness of the proposed strategy for integrating CTS into RT SCED, potential future work is to investigate this strategy on large-scale realistic power systems.

False data injection cyber-attacks can compromise measurements that are sent to the control center and result in biased state estimation solutions. This could further mislead operators to take improper adjustments and cause physical flow violations, which would jeopardize system security. Thus, it is key to detecting FDI cyber-attacks efficiently. This dissertation implements an FDI heuristic method to show the physical consequences of an FDI attack and proposes a two-stage FDID approach to identify potential FDI attacks. Case studies demonstrate that FDI attack can overload the target branch and that the proposed FDID approach can efficiently detect FDI attacks. It is worth noting that: 1) the simplified DC model is used rather than the full AC model; 2) it is assumed that attackers have access to the entire system; and 3) the test case is the IEEE 118-bus system that is small-scale and artificial. Therefore, future work may extend this work to AC framework with a more realistic assumption that attackers have limited access to only a single area rather than access to the entire system; numerical simulations on large-scale practical power systems are also desired.

REFERENCES

[1]. U.S. Department of Energy, "Large Power Transformers and the U.S. Electric Grid - Infrastructure Security and Energy Restoration Office of Electricity Delivery and Energy Reliability," [Online]. Available at: http://energy.gov/sites/prod/files/Large%20Power%20Transformer%20Study%20-%20June%202012_0.pdf

[2]. Federal Energy Regulatory Commission, "Grid 2030 - A National Vision for Electricity's Second 100 Years," [Online]. Available at: http://www.ferc.gov/eventcalendar/files/20050608125055-grid-2030.pdf

[3]. U.S. Energy Information Administration, "Annual Energy Outlook 2014 with projections to 2040," [Online]. Available at: http://www.eia.gov/forecasts/archive/aeo14/

[4]. Federal Energy Regulatory Commission, [Online]. Available at: http://www.ferc.gov/default.asp

[5]. North American Electric Reliability Corporation (NERC), [Online]. Available at: http://www.nerc.com/Pages/default.aspx

[6]. Federal Energy Regulatory Commission, Regional Transmission Organizations (RTO)/Independent System Operators (ISO), [Online]. Available at: http://www.ferc.gov/industries/electric/indus-act/rto.asp

[7]. Allen J. Wood and Bruce F. Wollenberg, "Power Generation, Operation and Control," *2nd Ed, John Wiley & Sons*, USA, 1996.

[8]. Allen J. Wood, Bruce F. Wollenberg, and Gerald B. Sheblé, "Power Generation, Operation and Control," *3rd Ed, John Wiley & Sons*, USA, 2012.

[9]. Brian Stott and Ongun Alsac, "Fast Decoupled Load Flow," *IEEE Transactions on Power Apparatus and Systems*, vol. PAS-93, no. 3, pp. 859–869, May 1974.

[10]. DSATools, PSAT Manual, [Online]. Available at: http://www.dsatools.com/

[11]. Yingying Qi, Di Shi, and Daniel Tylavsky, "Impact of Assumptions on DC Power Flow Model Accuracy," *IEEE North American Power Symposium (NAPS)*, Champaign, IL, USA, Sep. 2012.

[12]. Brian Stott, Jorge Jardim, and Ongun Alsac, "DC Power Flow Revisited," *IEEE Transactions on Power Systems*, vol. 24, no. 3, pp.1290-1300, Aug. 2009.

[13]. Paul A. Trodden, Waqquas A. Bukhsh, Andreas Grothey, and Ken I. M. McKinnon, "Optimization-based Islanding of Power Networks Using Piecewise Linear AC Power Flow." *IEEE Transactions on Power Systems*, vol. 29, no. 3, pp. 1212-1220, May 2014.

[14]. Carleton Coffrin and Pascal V. Hentenryck, "A Linear-programming Approximation of AC Power Flows," *INFORMS Journal on Computing*, vol. 26, no.4, pp. 718-734, May 2014.

[15]. Midcontinent ISO, Reliability Assurance, [Online]. Available at: https://www.misoenergy.org/WhatWeDo/Pages/Reliability.aspx

[16]. Midcontinent ISO, MISO's Existing Methods for Managing Voltage and Plans to Improve Voltage Profiles, Apr. 2012, [Online]. Available at: http://www.ferc.gov/CalendarFiles/20120503131554-MISO.pdf

[17]. John Baranowski and Dan French, "Operational Use of Contingency Analysis at PJM," *IEEE PES General Meeting*, San Diego, CA, USA, Jul. 2012.

[18]. PJM, LMP Model Information, Contingencies, [Online]. Available at: http://www.pjm.com/markets-and-operations/energy/lmp-model-info.aspx

[19]. Chad Thompson, Kenneth McIntyre, Sarma (NDR) Nuthalapati, Freddy Garcia, and Elias A. Villanueva, "Real-time Contingency Analysis Methods to Mitigate Congestion in the ERCOT Region," *IEEE PES General Meeting*, Calgary, AB, Canada, Jul. 2009.

[20]. Freddy Garcia, Sarma (NDR) Nuthalapati, Venkata Kanduri, Greeshma Nissankala, Karthik Gopinath, Jithender Polusani, Tim Mortensen, and Isabel Flores, "ERCOT Control Center Experience in Using Real-Time Contingency Analysis in the New Nodal Market," *IEEE PES General Meeting*, San Diego, CA, USA, Jul. 2012.

[21]. Nancy Traweek, "CAISO Real Time Tools, Visualization and Situational Awareness", WECC Meeting, May 2017, [Online]. Available at: https://www.wecc.biz/Administrative/05%20-%20Traweek%20System%20Awareness.pdf

[22]. NYISO, Manual 12 - Transmission and Dispatching Operations Manual, version 3.9, Oct. 2017, [Online]. Available at:

http://www.nyiso.com/public/webdocs/markets_operations/documents/Manuals_and_Guides/Manuals/Operations/trans_disp.pdf

[23]. ISO New England, Introduction to ISO New England System Operations, [Online]. Available at: https://www.iso-ne.com/static-assets/documents/2014/08/iso101-t2-op-score.pdf

[24]. ISO New England, Contingency Analysis, revision number 7, May 2017, [Online]. Available at: https://www.iso-ne.com/static-assets/documents/rules_proceds/operating/sysop/cr_ops/crop_34007.pdf

[25]. Kory W. Hedman, Shmuel S. Oren, and Richard P. O'Neill, "A Review of Transmission Switching and Network Topology Optimization," *IEEE PES General Meeting*, Detroit, MI, USA, Jul. 2011.

[26]. Akshay S. Korad, Pranavamoorthy Balasubramanian, and Kory W. Hedman, "Robust Corrective Topology Control," Handbook of Clean Energy Systems, *John Wiley & Sons*, Jul. 2015.

[27]. Kory W. Hedman, Michael C. Ferris, Richard P. O'Neill, Emily B. Fisher, and Shmuel S. Oren, "Co-optimization of Generation Unit Commitment and Transmission Switching with N-1 Reliability," *IEEE Transactions on Power Systems*, vol. 25, no.2, pp. 1052-1063, May 2010.

[28]. Amin Khodaei and Mohammad Shahidehpour, "Transmission Switching in Security-constrained Unit Commitment," *IEEE Transactions on Power Systems*, vol. 25, no. 4, pp. 1937-1945, Nov. 2010.

[29]. Mojdeh Abdi-Khorsand and Kory W. Hedman, "Day-ahead Corrective Transmission Topology Control," *IEEE PES General Meeting*, Washington D.C., USA, Jul. 2014.

[30]. Emily B. Fisher, Richard P. O'Neill, and Michael C. Ferris, "Optimal Transmission Switching," *IEEE Transactions on Power Systems*, vol. 23, no. 3, pp. 1346-1355, Aug. 2008.

[31]. Kory W. Hedman, Richard P. O'Neill, Emily B. Fisher, and Shmuel S. Oren, "Optimal Transmission Switching- Sensitivity Analysis and Extensions," *IEEE Transactions on Power Systems*, vol. 23, no. 3, pp. 1469-1479, Aug. 2008.

[32]. Kory W. Hedman, Richard P. O'Neil, Emily B. Fisher, and Shmuel S. Oren, "Optimal Transmission Switching with Contingency Analysis," *IEEE Transactions on Power Systems*, vol. 24, no. 3, pp. 1577-1586, Aug. 2009.

[33]. Pablo A. Ruiz, Aleksandr Rudkevich, Michael C. Caramanis, Evgenyi Goldis, Elli Ntakou, and C. Russ Philbrick, "Reduced MIP Formulation for Transmission Topology Control," *IEEE 50th Annual Allerton Conference on Communication, Control, and Computing (Allerton)*, pp. 1073-1079, Monticello, IL, USA, Oct. 2012.

[34]. Mostafa Sahraei-Ardakani, Akshay S. Korad, Kory W. Hedman, Paula Lipka, and Shmuel S. Oren, "Performance of AC and DC based Transmission Switching Heuristics on a Large-scale Polish System," *IEEE PES General Meeting*, Washington D.C., USA, Jul. 2014.

[35]. Pablo A. Ruiz, Justin M. Foster, Aleksandr Rudkevich, and Michael C. Caramanis, "On Fast Transmission Topology Control Heuristics," *IEEE PES General Meeting*, Detroit, MI, USA, Jul. 2011.

[36]. Pablo A. Ruiz, Justin M. Foster, Aleksandr Rudkevich, and Michael C. Caramanis, "Tractable Transmission Topology Control Using Sensitivity Analysis," *IEEE Transactions on Power Systems*, vol. 27, no. 3, pp. 1550-1559, 2012.

[37]. J. David Fuller, Raynier Ramasra, and Amanda Cha, "Fast Heuristics for Transmission-line Switching," *IEEE Transactions on Power Systems*, vol. 27, no. 3 pp. 1377-1386, Aug. 2012.

[38]. Milad Soroush and J. David Fuller, "Accuracies of Optimal Transmission Switching Heuristics based on DCOPF and ACOPF," *IEEE Transactions on Power Systems*, vol. 29, no. 2, pp. 924-932, Mar. 2014.

[39]. Kwok W. Cheung, "Economic Evaluation of Transmission Outages and Switching for Market and System Operations," *IEEE PES General Meeting*, Detroit, MI, USA, Jul. 2011.

[40]. Richard P. O'Neill, Kory W. Hedman, Eric A. Krall, Anthony Papavasiliou, and Shmuel S. Oren, "Economic Analysis of the N-1 Reliable Unit Commitment and Transmission Switching Problem Using Duality Concepts," *Energy System*, vol. 1, no. 2, pp. 165-195, May 2010.

[41]. Emily B. Fisher, Kory W. Hedman, Richard P. O'Neill, Michael C. Ferris, and Shmuel S. Oren, "Optimal Transmission Switching in Electric Network for Improve Economic Operations," *INFRADAY Conference*, 2008.

[42]. Kory W. Hedman, Richard P. O'Neill, Emily B. Fisher, and Shmuel S. Oren, "Smart Flexible Just-in-time Transmission and Flowgate Bidding," *IEEE Transactions on Power Systems*, vol. 26, no. 1, pp. 93-102, Feb. 2011.

[43]. Amin Khodaei, Mohammad Shahidehpour, and Saeed Kamalinia, "Transmission Switching in Expansion Planning," *IEEE Transactions on Power Systems*, vol. 25, no. 3, pp. 1722-1733, Aug. 2010.

[44]. Adolfo R. Escobedo, Erick Moreno-Centeno, and Kory W. Hedman, "Topology Control for Load Shed Recovery," *IEEE Transactions on Power Systems*, vol. 29, no. 2, pp. 908-916, Mar. 2014.

[45]. PJM State of the Market, Report, 2013, [Online]. Available at: http://www.monitoringanalytics.com/reports/PJM_State_of_the_Market/2013.shtml.

[46]. Hamed Ahmadi, Mojtaba Khanabadi, and Hassan Ghasemi, "Transmission System Reconfiguration for Congestion Management Ensuring Transient and Voltage Stability," *13th International Conference on Environment and Electrical Engineering (EEEIC)*, pp. 22 - 26, Wrocław, Poland, Nov. 2013.

[47]. Gianpietro Granelli, Mario Montagna, Fabio Zanellini, Paola Bresesti, Riccardo Vailati, and Mario Innorta, "Optimal Network Reconfiguration for Congestion Management by Deterministic and Genetic Algorithms," *Electric Power Systems Research*, vol. 76, no. 6-7, pp. 549-556, Apr. 2006.

[48]. PJM, Switching Solutions, [Online]. Available at: http://www.pjm.com/markets-and-operations/etools/oasis/system-information/switching-solutions.aspx

[49]. Akshay S. Korad and Kory W. Hedman, "Robust Corrective Topology Control for System Reliability," *IEEE Transactions on Power Systems*, vol. 28, no. 4, pp. 4042-4051, Nov. 2013.

[50]. Manoel F.de Medeiros Júnior, Arrhenius V. da Costa Oliveira, and Marcus V. Costa de Oliveira, "Impact of Corrective Switching in Wind Farms Operation," *International Conference on Renewable Energies and Power Quality (ICREPQ'13)*, Bilbao, Spain, Mar. 2013.

[51]. Wei Shao and Vijay Vittal, "Corrective Switching Algorithm for Relieving Overloads and Voltage Violations," *IEEE Transactions on Power Systems*, vol. 20, no. 4, pp. 1877-1885, Nov. 2005.

[52]. Pranavamoorthy Balasubramanian and Kory W. Hedman, "Real-Time Corrective Switching in Response to Simultaneous Contingencies," *Journal of Energy Engineering*, vol. 141, Special Issue: Smart Grid and Emerging Technology Integration, Feb. 2014.

[53]. Abdulhalem A. Mazi, Bruce F Wollenberg, and M. Harry Hesse, "Corrective Control of Power System Flows by Line and Bus-bar Switching," *IEEE Transactions on Power Systems*, vol. 1, no. 3, pp. 258–265, Aug. 1986.

[54]. Anastasios Bakirtzis and A. P. Sakis Meliopoulos, "Incorporation of Switching Operations in Power System Corrective Control Computations," *IEEE Transactions on Power Systems*, vol. 2, no. 3, pp. 669–676, Aug. 1987.

[55]. Elham B. Makram, Katherine P. Thornton, and Homer E. Brown, "Selection of Lines to be Switched to Eliminate Overload Lines using a Z-matrix Method," *IEEE Transactions on Power Systems*, vol. 4, no. 2, pp. 653–661, May 1989.

[56]. California ISO, Minimum Effective Threshold Report, 2010, [Online]. Available at:
http://www.caiso.com/274c/274ce77df630.pdf

[57]. ISO New England, Operating Procedure No. 19 - Transmission Operations, Revision 8, Jun. 2015, [Online]. Available at:
http://www.iso-ne.com/rules_proceds/operating/isone/op19/op19_rto_final.pdf

[58]. PJM, Manual 3 - Transmission Operations, Section 5 - Index and Operating Procedures for PJM RTO Operation, Revision 37, Jun. 2010. [Online]. Available at:
http://www.pjm.com/~/media/training/nerc-certifications/m03v37-transmission-operations.ashx

[59]. NERC, "Standard TPL-002-0b - System Performance Following Loss of a Single Bulk Electric System Element," [Online]. Available at:
http://www.nerc.com/files/TPL-002-0b.pdf

[60]. Yonghong Chen and Juan Li, "Comparison of Security Constrained Economic Dispatch Formulations to Incorporate Reliability Standards on Demand Response Resources into Midwest ISO Co-optimized Energy and Ancillary Service Market," *Electric Power Systems Research*, vol. 81, no. 9, pp. 1786-1795, Sep. 2011.

[61]. United States Department of Energy, "Economic Dispatch of Electric Generation Capacity", Feb. 2007, [Online]. Available at:

http://energy.gov/oe/downloads/economic-dispatch-electric-generation-capacity

[62]. Abdullah Urkmez and Nurettin Cetinkaya, "Determining Spot Price and Economic Dispatch in Deregulated Power Systems," *Mathematical and Computational Applications*, vol. 15, no. 1, pp. 25-33, Jan. 2010.

[63]. California ISO, Technical Bulletin, "Market Optimization Details", Jun. 2009, [Online]. Available at: http://www.caiso.com/23cf/23cfe2c91d880.pdf

[64]. Salkuti Surender Reddy, Pradeep. R. Bijwe, and Abhijit R. Abhyankar, "Real-time Economic Dispatch Considering Renewable Power Generation Variability and Uncertainty over Scheduling Period," *IEEE Systems Journal*, vol. 9, no. 4, pp. 1440-1451, Dec. 2015.

[65]. Yingzhong Gu and Le Xie, "Stochastic Look-Ahead Economic Dispatch With Variable Generation Resources," *IEEE Transactions on Power Systems*, vol. 32, no. 1, pp. 17-29, Jan. 2017.

[66]. Harsha Gangammanavar, Suvrajeet Sen, and Victor M. Zavala, "Stochastic Optimization of Sub-hourly Economic Dispatch with Wind Energy," *IEEE Transactions on Power Systems*, vol. 31, no. 2, pp. 949-959, Mar. 2016.

[67]. Giulio Binetti, Ali Davoudi, Frank L. Lewis, David Naso, and Biagio Turchiano, "Distributed Consensus-based Economic Dispatch with Transmission Losses," *IEEE Transactions on Power Systems*, vol. 29, no. 4, pp. 1711-1720, Jul. 2014.

[68]. Vincenzo Loia and Alfredo Vaccaro, "Decentralized Economic Dispatch in Smart Grids by Self-organizing Dynamic Agents," *IEEE Transactions on Systems, Man, and Cybernetics: Systems*, vol. 44, no. 4, pp. 397-408, Apr. 2014.

[69]. Wael T. Elsayed and Ehab F. El-Saadany, "A Fully Decentralized Approach for Solving the Economic Dispatch Problem," *IEEE Transactions on Power Systems*, vol. 30, no. 4, pp. 2179-2189, Jul. 2015.

[70]. Xiaowen Lai, Le Xie, Qing Xia, Haiwang Zhong, and Chongqing Kang, "Decentralized Multi-area Economic Dispatch via Dynamic Multiplier-based Lagrangian Relaxation," *IEEE Transactions on Power Systems*, vol. 30, no. 6, pp. 3225-3233, Nov. 2015.

[71]. Raghuraman Mudumbai, Soura Dasgupta, and Brian B. Cho, "Distributed Control for Optimal Economic Dispatch of a Network of Heterogeneous Power

Generators," *IEEE Transactions on Power Systems*, vol. 27, no. 4, pp. 1750-1760, Nov. 2012.

[72]. Na Li, Changhong Zhao, and Lijun Chen, "Connecting Automatic Generation Control and Economic Dispatch from an Optimization View," *IEEE Transactions on Control of Network Systems*, vol. 3, no. 3, pp. 254-264, Sep. 2016.

[73]. Erik Ela and Mark O'Malley, "Studying the Variability and Uncertainty Impacts of Variable Generation at Multiple Timescales," *IEEE Transactions on Power Systems*, vol. 27, no. 3, pp. 1324-1333, Aug. 2012.

[74]. Moritz Paulus and Frieder Borggrefe, "The Potential of Demand-side Management in Energy-intensive Industries for Electricity Markets in Germany," *Applied Energy*, vol. 88, no. 2, pp. 432-441, Apr. 2011.

[75]. Duncan S. Callaway and Ian A. Hiskens, "Achieving Controllability of Electric Loads," *Proceedings of the IEEE*, vol. 99, no. 1, pp. 184-199, Jan. 2011.

[76]. Ookie Ma, Nasr Alkadi, Peter Cappers, Paul Cappers, Paul Denholm, Junqiao Dudley, Sasank Goli, Marissa Hummon, Sila Kiliccote, Jason MacDonald, Nance Matson, Daniel Olsen, Cody Rose, Michael D. Sohn, Michael Starke, Brendan Kirby, and Mark O'Malley, "Demand Response for Ancillary Services," *IEEE Transactions on Smart Grid*, vol. 4, no. 4, pp. 1988-1995, Dec. 2013.

[77]. Mary B. Cain, Richard P. O'Neill, and Anya Castillo, "History of Optimal Power Flow and Formulations," *US Federal Energy Regulatory Commission Technical Report*, pp. 1-36, Dec. 2012.

[78]. J. Carpentier, "Contribution to the Economic Dispatch Problem," *Bulletin de la Societe Francoise des Electriciens*, vol. 3, no. 8, pp. 431– 447, 1962, in French.

[79]. PJM, Intermediate Term Security Constrained Economic Dispatch (IT SCED) Engine Overview, [Online]. Available at: http://www.pjm.com/~/media/markets-ops/energy/real-time/it-sced-forecasted-lmps/it-sced-overview.ashx

[80]. PJM, Asanga Perera, PJM Marginal Zone Participation Factor Calculation Method & Applicability to Relevant Calculation, [Online]. Available at: https://www.pjm.com/~/media/documents/agreements/miso-pjm-joa-marginal-zone-participatoin-factor-methodology-and-applicability-document.ashx

[81]. PJM, Manual 11 "Energy & Ancillary Services Market Operations" revision 86, Feb. 2017, [Online]. Available at:

http://www.pjm.com/~/media/documents/manuals/m11.ashx

[82]. PJM, Manual 12 “Balancing Operations” revision 36, Feb. 2017, [Online]. Available at: http://www.pjm.com/~/media/documents/manuals/m12.ashx

[83]. PJM, Module LS 8 of Interconnection Training Program, “Security Constrained Economic Dispatch System (SCED)”, 2011, [Online]. Available at: http://www.pjm.com/~/media/training/nerc-certifications/ls8-SCED.ashx

[84]. Midcontinent ISO, Business Practices Manual No. 002 revision 16, “Energy and Operating Reserve Markets”, Oct. 2016, [Online]. Available at: https://www.misoenergy.org/_layouts/MISO/ECM/Redirect.aspx?ID=19178

[85]. Midcontinent ISO, Business Practices Manual No. 002 revision 16, “Energy and Operating Reserve Markets, Attachment A - Market Optimization Techniques”, Mar. 2016, [Online]. Available at: https://www.misoenergy.org/_layouts/MISO/ECM/Redirect.aspx?ID=19178

[86]. ISO New England, “Dispatch using RTUC and UDS”, revision 10, Mar. 2017, [Online]. Available at: https://www.iso-ne.com/static-assets/documents/2014/12/crop_35005.pdf

[87]. Pacific Northwest National Laboratory, document prepared for U.S. Department of Energy, “Analysis of ISO NE Balancing Requirements: Uncertainty-based Secure Ranges for ISO New England Dynamic Interchange Adjustments”, Jan. 2013, [Online]. Available at: http://www.pnnl.gov/main/publications/external/technical_reports/PNNL-22222.pdf

[88]. ISO New England, “Reserve Requirement Adjustments”, revision 12, Sep. 2016, [Online]. Available at: https://www.iso-ne.com/static-assets/documents/rules_proceds/operating/sysop/cr_ops/crop_35003.pdf

[89]. ISO New England, Feng Zhao and Matthew White, Technical Session #7 “Real-Time Price Formation: Fast-Start Pricing - A Survey”, Nov. 2014, [Online]. Available at: https://www.iso-ne.com/static-assets/documents/2014/11/price_information_technical_session7.pdf

[90]. ISO New England, “Posturing”, revision 7, Mar. 2017, [Online]. Available at: https://www.iso-ne.com/static-assets/documents/rules_proceds/operating/sysop/cr_ops/crop_25001.pdf

[91]. New York ISO, Manual 12, "Transmission and Dispatching Operations Manual", Oct. 2016, [Online]. Available at: http://www.nyiso.com/public/webdocs/markets_operations/documents/Manuals_and_Guides/Manuals/Operations/trans_disp.pdf

[92]. New York ISO, A536: Real-Time Scheduling, "Real-Time Commitment (RTC) and Real-Time Dispatch (RTD) - Concept of Operation", [Online]. Available at: http://www.nyiso.com/public/webdocs/markets_operations/committees/bic_mswg/meeting_materials/2003-06-16/a536_coo_scheduling_030616_redline.pdf

[93]. California ISO, "Business Practice Manual for Managing Full Network Model" version 11, Jan. 2017, [Online]. Available at: https://bpmcm.caiso.com/Pages/BPMDetails.aspx?BPM=Managing%20Full%20Network%20Model

[94]. California ISO, "Business Practice Manual for Market Instruments" version 44, Apr. 2017, [Online]. Available at: https://bpmcm.caiso.com/Pages/BPMDetails.aspx?BPM=Market%20Instruments

[95]. California ISO, "Business Practice Manual for Market Operations" version 52, May 2017, [Online]. Available at: https://bpmcm.caiso.com/Pages/BPMDetails.aspx?BPM=Market%20Operations

[96]. California ISO, Technical Bulletin 2009-06-05, "Market Optimization Details", Revised Nov. 2009, [Online]. Available at: http://www.caiso.com/23cf/23cfe2c91d880.pdf

[97]. ERCOT, "Real-Time or Security Constrained Economic Dispatch (SCED)", [Online]. Available at: http://www.ercot.org/about/wc/rt.html

[98]. Hailong Hui, Chien-Ning Yu, Resmi Surendran, Feng Gao, Sainath Moorty, and Xiangjun Xu, "Look Ahead to the Unforeseen: ERCOT's Nonbinding Look-ahead SCED Study," *IEEE PES General Meeting*, Vancouver, BC, Canada, pp. 1-5, Jul. 2013.

[99]. Xiangjun Xu and Richard Howard, "Ramp Rate Modeling for ERCOT Look Ahead SCED," *IEEE* PES *General Meeting*, Vancouver, BC, Canada, pp. 1-5, Jul. 2013.

[100]. ERCOT, “ERCOT Market Education - Basic Training Program”, [Online]. Available at:
http://www.ercot.com/content/wcm/training_courses/52/BTP201M6_03242015.pdf

[101]. ERCOT, “ERCOT Business Practices - ERCOT and QSE Operations Practices During the Operating Hour” version 5.7, May 2014, [Online]. Available at:
http://www.ercot.com/content/mktrules/bpm/ERCOT%20And%20QSE%20Operations%20Practices%20During%20The%20Operating%20Hour.doc

[102]. ERCOT, “ERCOT Concept Paper for Real-Time Market Improvements - Co-optimization of Energy and Ancillary Services & Multi-Interval Real-Time Market” version 0.1, Sep. 2014, [Online]. Available at:
http://www.ercot.com/content/meetings/tac/keydocs/2014/0925/11.%20Co_optimization_Multi-interval_DRAFT_09192014.r1.doc

[103]. ERCOT, ERCOT Market Education, “Basic Training Program - Module 6: Real-Time Operations”, [Online]. Available at:
http://www.ercot.com/content/wcm/training_courses/52/BTP201M6_03242015.pdf

[104]. ERCOT, “Real-Time Transmission Congestion Management & Market Effects”, [Online]. Available at:
http://www.ercot.com/content/wcm/training_courses/109626/Constraint_Management.pptx

[105]. Yao Liu, Peng Ning, and Michael K. Reiter, “False Data Injection Attacks Against State Estimation in Electric Power Grids,” *Proceedings of the 16th ACM conference on Computer and communications security (CCS ‘09)*, Chicago, IL, USA, pp. 21-32, Nov. 2009.

[106]. Yao Liu, Peng Ning, and Michael K. Reiter, “False Data Injection Attacks Against State Estimation in Electric Power Grids,” *ACM Transactions on Information and System Security (TISSEC)*, vol. 14, no. 1, Article 13, pp. 13:1-13:33, May 2011.

[107]. Oliver Kosut, Liyan Jia, Robert J. Thomas, and Lang Tong, “Malicious Data Attacks on the Smart Grid,” *IEEE Transactions on Smart Grid*, vol. 2, no. 4, pp. 645-658, Dec. 2011.

[108]. Gabriela Hug and Joseph Andrew Giampapa, "Vulnerability Assessment of AC State Estimation with Respect to False Data Injection Cyber-Attacks," *IEEE Transactions on Smart Grid*, vol. 3, no. 3, pp. 1362-1370, Aug. 2012.

[109]. Jingwen Liang, Oliver Kosut, and Lalitha Sankar, "Cyber Attacks on AC State Estimation: Unobservability and Physical Consequences," *IEEE PES General Meeting Conference & Exposition*, Washington D.C., USA, pp. 1-5, Jul. 2014.

[110]. Jingwen Liang, Lalitha Sankar, and Oliver Kosut, "Vulnerability Analysis and Consequences of False Data Injection Attack on Power System State Estimation," *IEEE Transactions on Power Systems*, vol. 31, no. 5, pp. 3864-3872, Sep. 2016.

[111]. Zhigang Chu, Jiazi Zhang, Oliver Kosut, and Lalitha Sankar, "Evaluating Power System Vulnerability to False Data Injection Attacks via Scalable Optimization," *2016 IEEE International Conference on Smart Grid Communications (SmartGridComm)*, pp. 1-6, Nov. 2016.

[112]. Zhigang Chu, Jiazi Zhang, Oliver Kosut, and Lalitha Sankar, "Vulnerability Assessment of Large-scale Power Systems to False Data Injection Attacks," *arXiv preprint arXiv: 1705.04218*, May. 2017.

[113]. Jiazi Zhang, Zhigang Chu, Lalitha Sankar, and Oliver Kosut, "False Data Injection Attacks on Power System State Estimation with Limited Information," *IEEE Power and Energy Society General Meeting*, Boston, MA, USA, Jul. 2016.

[114]. Jiazi Zhang, Zhigang Chu, Lalitha Sankar, and Oliver Kosut, "Can Attackers with Limited Information Exploit Historical Data to Mount Successful False Data Injection Attacks on Power Systems?" *arXiv preprint arXiv: 1703.07500*, Mar. 2017.

[115]. Jiazi Zhang and Lalitha Sankar, "Implementation of Unobservable State-preserving Topology Attacks," *IEEE North American Power Symposium (NAPS)*, Charlotte, NC, USA, Oct. 2015.

[116]. Jiazi Zhang and Lalitha Sankar, "Physical System Consequences of Unobservable State-and-Topology Cyber-Physical Attacks," *IEEE Transactions on Smart Grid*, vol. 7, no. 4, Jul. 2016.

[117]. Rakesh B. Bobba, Katherine M. Rogers, Qiyan Wang, Himanshu Khurana, Klara Nahrstedt, and Thomas J. Overbye, "Detecting False Data Injection Attacks on DC State Estimation," *In Proceedings of the First Workshop on Secure Control Systems*, 2010.

[118]. Yi Huang, Mohammad Esmalifalak, Huy Nguyen, Rong Zheng, Zhu Han, Husheng Li, and Lingyang Song, "Bad Data Injection in Smart Grid: Attack and Defense Mechanisms," *IEEE Communications Magazine*, vol. 51, no. 1, pp. 27-33, Jan. 2013.

[119]. Lanchao Liu, Mohammad Esmalifalak, Qifeng Ding, Valentine A. Emesih, and Zhu Han, "Detecting False Data Injection Attacks on Power Grid by Sparse Optimization," *IEEE Transactions on Smart Grid*, vol. 5, no. 2, pp. 612-621, Mar. 2014.

[120]. Po-Yu Chen, Shusen Yang, Julie A. McCann, Jie Lin, and Xinyu Yang, "Detection of False Data Injection Attacks in Smart-grid Systems," *IEEE Communications Magazine*, vol. 53, no. 2, pp. 206-213, Feb. 2015.

[121]. Gu Chaojun, Panida Jirutitijaroen, and Mehul Motani, "Detecting False Data Injection Attacks in AC State Estimation," *IEEE Transactions on Smart Grid*, vol. 6, no. 5, pp. 2476-2483, Sep. 2015.

[122]. Shang Li, Yasin Yılmaz, and Xiaodong Wang, "Quickest Detection of False Data Injection Attack in Wide-area Smart Grids," *IEEE Transactions on Smart Grid*, vol. 6, no. 6, pp. 2725-2735, Nov. 2015.

[123]. Ruilong Deng, Gaoxi Xiao, and Rongxing Lu, "Defending Against False Data Injection Attacks on Power System State Estimation," *IEEE Transactions on Industrial Informatics*, vol. 13, no. 1, pp. 198-207, Feb. 2017.

[124]. Jun Wang, Bormin Huang, Allen Huang, and Mitchell D. Goldberg, "Parallel Computation of the Weather Research and Forecast (WRF) WDM5 Cloud Microphysics on a Many-core GPU," *IEEE 17th International Conference on Parallel and Distributed Systems (ICPADS)*, Tainan, pp. 1032-1037, Dec. 2011.

[125]. Lawrence Livermore National Laboratory, POSIX Threads Programming, [Online]. Available at:
https://computing.llnl.gov/tutorials/pthreads

[126]. Lawrence Livermore National Laboratory, Message Passing Interface (MPI), [Online]. Available at:
https://computing.llnl.gov/tutorials/mpi

[127]. Aamir Shafi, Bryan Carpenter, and Mark Baker, "Nested Parallelism for Multi-core HPC Systems Using Java," *Journal of Parallel and Distributed Computing*, vol. 69, no. 6, pp. 532-545, Jun. 2009.

[128]. MPJ Express, [Online]. Available at: http://mpj-express.org

[129]. CUDA C Programming Guide Version 6.0, [Online]. Available at: http://docs.nvidia.com/cuda/cuda-c-programming-guide/#axzz3NoIvme1z

[130]. GCC Wiki, Coarray, [Online]. Available at: https://gcc.gnu.org/wiki/Coarray

[131]. Gene M. Amdahl, "Validity of the Single Processor Approach to Achieving Large Scale Computing Capabilities," *Proceedings of the Spring Joint Computer Conference*, pp. 483-485, Apr. 1967.

[132]. Jong-Yul Kim, Kyeong-Jun Mun, Hyung-Su Kim, and June Ho Park, "Optimal Power System Operation Using Parallel Processing System and PSO Algorithm," *International Journal of Electrical Power & Energy Systems*, vol. 33, no. 8, pp. 1457-1461, Oct. 2011.

[133]. Ying Li, Yijia Cao, Zhaoyan Liu, Yi Liu, and Quanyuan Jiang, "Dynamic Optimal Reactive Power Dispatch based on Parallel Particle Swarm Optimization Algorithm," *Computers & Mathematics with Applications*, vol. 57, no. 11-12, pp. 1835-1842, Jun. 2009.

[134]. Quanyuan Jiang, Boran Zhou, and Mingze Zhang, "Parallel Augment Lagrangian Relaxation Method for Transient Stability Constrained Unit Commitment," *IEEE Transactions on Power Systems*, vol. 28, no. 2, pp. 1140-1148, May 2013.

[135]. Guangchao Geng and Quanyuan Jiang, "A Two-level Parallel Decomposition Approach for Transient Stability Constrained Optimal Power Flow," *IEEE Transactions on Power Systems*, vol. 27, no. 4, pp. 2063-2073, Nov. 2012.

[136]. Guangchao Geng, Venkataramana Ajjarapu, and Quanyuan Jiang, "A Hybrid Dynamic Optimization Approach for Stability Constrained Optimal Power Flow," *IEEE Transactions on Power Systems*, vol. 29, no. 5, pp. 2138-2149, Sep. 2014.

[137]. Jianzhong Tong, "Performance metrics for PJM on-line TSA application," *IEEE PES General Meeting*, Denver, CO, USA, pp. 1-21, Jul. 2015.

[138]. Jianzhong Tong, "Direct Methods - BCU in Transient Stability Screening," Jul. 2016, [Online]. Available at: http://resourcecenter.ieee-pes.org/product/-/download/partnumber/PESSLI1287

[139]. Anthony Papavasiliou, Shmuel S. Oren, Zhu Yang, Pranavmoorthy Balasubramanian, and Kory W. Hedman, "An Application of High Performance Computing to Transmission Switching," *IEEE Bulk Power System Dynamics and Control-IX Optimization, Security and Control of the Emerging Power Grid (IREP), 2013 IREP Symposium*, Rethymno, Greece, Aug. 2013.

[140]. IncSys, PowerData Corporation. OpenPA, "Java classes sub-project for Open Power Apps", First version, 2013, [Online]. Available at: https://github.com/powerdata/com.powerdata.openpa

[141]. Xingpeng Li, Pranavamoorthy Balasubramanian, Mojdeh Abdi-Khorsand, Akshay S. Korad, and Kory W. Hedman, "Effect of Topology Control on System Reliability: TVA Test Case," *CIGRE Grid of the Future Symposium*, Houston, TX, USA, Oct. 2014.

[142]. Lawrence Livermore National Laboratory, Machine Catalog, Cab, [Online]. Available at: http://computation.llnl.gov/computers/cab

[143]. PJM eMKT User Guide, effective Jul. 2015, [Online]. Available at: https://www.pjm.com/~/media/etools/emkt/ts-userguide.ashx

[144]. NYISO, Manual 11 - "Day-Ahead Scheduling Manual" version 4.5, Jun. 2017, [Online]. Available: http://www.nyiso.com/public/webdocs/markets_operations/documents/Manuals_and_Guides/Manuals/Operations/dayahd_schd_mnl.pdf

[145]. MISO, MISO Overview Training Level 101, Apr. 2012, [Online]. Available at: https://www.misoenergy.org/Library/Repository/Meeting%20Material/Stakeholder/Training%20Materials/100%20Level%20Training/Level%20100%20-%20MISO%20Overview.pdf

[146]. Gurobi Optimization, Gurobi Optimizer Reference Manual. [Online]. Available: http://www.gurobi.com.

[147]. Xingpeng Li, Pranavamoorthy Balasubramanian, Mostafa Sahraei-Ardakani, Mojdeh Abdi-Khorsand, Kory W. Hedman, and Robin Podmore, "Real-Time Contingency Analysis with Correct Transmission Switching," *IEEE Transactions on Power Systems*, early access, Oct. 2016.